Functions of GluN2D-containing NMDA receptors in dopamine neurons of the substantia nigra pars compacta

Paul George Morris

St. Edmund's College, Cambridge

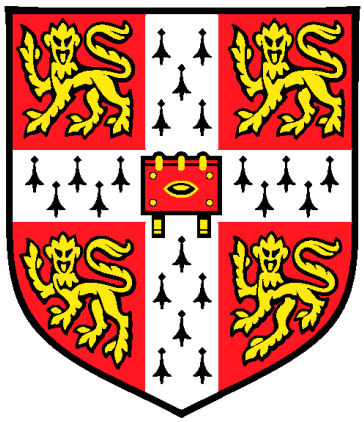

Department of Physiology, Development and Neuroscience

This thesis is submitted for the degree of Doctor of Philosophy

January 2018

Functions of GluN2D-containing NMDA receptors in dopamine neurons of the substantia nigra pars compacta

Paul George Morris

Abstract

Dopamine (DA) neurons of the substantia nigra pars compacta (SNc) have a key role in regulation of voluntary movement control. Their death is a hallmark of Parkinson's disease (PD), a neurodegenerative illness characterised by inhibited motor control, including muscle rigidity and tremor. Excitatory input to SNc-DA neurons is primarily from the subthalamic nucleus (STN), and in PD these afferents display a higher frequency firing, as well as increased burst firing, which could cause increased excitatory activity in SNc-DA neurons, in turn potentially activating regulatory processes.

NMDA receptors (NMDARs) are widely expressed receptors for the excitatory neurotransmitter glutamate, and are essential for learning and memory due to their ability to act as synaptic coincidence detectors. In SNc-DA neurons, NMDARs have a putative triheteromeric subunit arrangement of GluN1 plus GluN2B and/or GluN2D. Wild type (WT) mice, and those lacking the gene for the GluN2D subunit (*Grin2D*-null), were used to explore the role of the GluN2D subunit in various aspects of DA neuronal function and dysfunction using whole cell patch clamp electrophysiology, viability assaying, and immunofluorescence. Constitutive expression of synaptic NMDARs was assessed in SNc-DA neurons at several ages by recording the ratio of AMPA receptor EPSC to NMDAR-EPSC, which revealed a nonlinear developmental alteration in this ratio but no genotype-related difference, indicating similar overall expression of functional NMDARs at the synapse in *Grin2D*-null mice. Pharmacological intervention using subunit-specific inhibitors ifenprodil and DQP-1105 on elicited NMDAR-EPSCs was also explored, with results suggesting a developmental shift from primarily GluN2B to GluN2B/D. Activity dependent regulation was then assessed by high frequency burst stimulation of glutamatergic afferents: in comparison to controls, significant downregulation of NMDARs was observed in SNc-DA neurons from WT mice, though no differences were observed based on genotype, indicating that the GluN2D subunit

is not essential for it to occur. This regulatory function may be a neuroprotective or homeostatic response.

Ambient extracellular glutamate elicits tonic NMDAR activity in SNc-DA neurons, which may be important for maintaining basal levels of activity: the role of GluN2D was assessed by recording baseline currents and recording the deflection caused by application of the competitive NMDAR antagonist D-AP5. There was a significantly larger NMDAR-mediated current in WT in comparison to *Grin2D*-null mice, indicating that GluN2D-containing NMDARs have a role in binding ambient glutamate. Application of tetrodotoxin had no effect on the amplitude of the current, suggesting it is not of action potential-dependent origin. Dysfunction of glutamate uptake could be a secondary pathophysiological occurrence in the SNc, leading to higher levels of ambient glutamate: the effect of this was explored by application of the competitive glutamate transporter blocker TBOA. Under these conditions, glutamate-mediated currents significantly increased in SNc-DA neurons, and indeed the NMDAR-mediated portion of this current was significantly higher in WT mice in comparison to *Grin2D*-null.

Interestingly, dose-response data obtained from bath application of NMDA showed significantly larger currents in *Grin2D*-null animals in comparison to WT, but only at the upper part of the response curve (~1-10 mM), which may indicate a capability for larger conductance in *Grin2D*-null animals at only the highest levels NMDA/glutamate saturation due to the replacement of GluN2D with GluN2B within the receptor. The presence of GluN2D may therefore be neuroprotective, by attenuating peak current flow in response to very high agonist concentrations in SNc-DA neurons.

Lastly, GluN2D has been found to decrease NMDAR open probability under hypoxic conditions, potentially conferring resistance to hypoxia / ischemia related excitotoxicity. Therefore, low (15% O_2 / 80% N_2 / 5% CO_2) vs high (95% O_2 / 5% CO_2) oxygen conditions were used along with immunofluorescent propidium iodide cell death assaying and immunofluorescent labeling for DA neurons in order to compare levels of DA neuronal death in the SNc based on oxygen status and genotype. Whilst there was a significant submaximal effect based on O_2 status, genotype did not confer a practical resistance under these conditions.

In summary, NMDARs have diverse roles in SNc-DA neurons which may both serve to maintain normal function and protect the cell against potentially pathological conditions.

Contents

List of Figures

List of Abbreviations

A/N: AMPAR / NMDAR EPSC (see below) ratio

AD: Alzheimer's disease

AMPA: α-amino-3-hydroxy-5-methyl-4-isoxazolepropionic acid

AMPAR: α-amino-3-hydroxy-5-methyl-4-isoxazolepropionic acid receptor

ANOVA: Analysis of variance

ATD: Amino-terminal domain

ATP: Adenosine 5′-triphosphate magnesium salt

BAPTA: 1,2-Bis(2-aminophenoxy)ethane-N,N,N',N'-tetraacetic acid

CaMK: Calcium/calmodulin-dependent protein kinases (CaMKI/II)

CNS: Central nervous system

CREB: cAMP-responsive element binding protein

DA: Dopamine / dopaminergic

DAP5: D-(-)-2-Amino-5-phosphonopentanoic acid

DBS: Deep brain stimulation

DNQX: 6,7-dinitroquinoxaline-2,3-dione

"DQP" (DQP-1105): 5-(4-Bromophenyl)-3-(1,2-dihydro-6-methyl-2-oxo-4-phenyl-3-quinolinyl)-4,5-dihydro-γ-oxo-1H-pyrazole-1-butanoic acid

EGTA: Ethylene-bis(oxyethylenenitrilo)tetraacetic acid

EPSC: Excitatory postsynaptic potential

GABA: γ-aminobutyric acid

GluT: Glutamate transporter

GP: Globus pallidus

GPe: Globus pallidus pars externa

GPi: Globus pallidus pars interna

GTP: Guanosine 5′-triphosphate

HCN: Hyperpolarization-activated cyclic nucleotide–gated

HEPES: 4-(2-hydroxyethyl)-1-piperazineethanesulfonic acid

HFS: High-frequency stimulation

I_{NaP}: Persistent inward sodium current

IP: Induction protocol

LBD: Ligand-binding domain

LTP: Long term potentiation

LTD: Long term depression

LY: LY 341495; (2S)-2-Amino-2-[(1S,2S)-2-carboxycycloprop-1-yl]-3-(xanth-9-yl) propanoic acid

mGluR: Metabotropic glutamate receptor

MPTP: 1-methyl-4-phenyl-1, 2, 3, 6-tetrahydropyridine

NMDA: N-methyl-D-aspartic acid

NMDAR: N-methyl-D-aspartic acid receptor

MΩ: Megaohm

MT: Medial terminal nucleus of the accessory optic tract

OCD: Obsessive-compulsive disorder

OGD: Oxygen and glucose depravation

P: Postnatal day

pA: Picoamp, or picoamps

PBS: Phosphate-buffered saline

PCP: Phencyclidine

PD: Parkinson’s disease

PI: Propidium iodide

PK: Protein kinase (A/B/C)

PPDA: Piperazine-2,3-dicarboxylic acid

PPN: Pedunculopontine nucleus

PPR: Paired pulse ratio

PSD: Postsynaptic density

SN: Substantia nigra

SNc: Substantia nigra pars compacta

SNr: Substantia nigra pars reticulata

STN: Subthalamic nucleus

TBOA: DL-*threo*-β-Benzyloxyaspartate

TBS: Tris-buffered saline

TBS-T: TBS-Tween-20

TCP: Thienylcyclohexylpiperidine

TH: Tyrosine hyrdoxylase

TMD: Transmembrane domain

TTX: Tetrodotoxin

$\mathbf{V_{Izero}}$: zero-current potential

VTA: Ventral tegmental area

WT: Wild type

DECLARATION

This thesis is the result of my own work, with the exception of around half of the ifenprodil synaptic pharmacology dataset (section 3.1.2) which was carried out by Dr. Sue Jones. This thesis includes nothing which is the outcome of work carried out in collaboration except as declared in the Preface and specified in the text. It is not substantially the same as any that I have submitted, or, is being concurrently submitted for a degree or diploma or other qualification at the University of Cambridge or any other University or similar institution except as declared in the Preface and specified in the text. I further state that no substantial part of my dissertation has already been submitted, or, is being concurrently submitted for any such degree, diploma or other qualification at the University of Cambridge or any other University or similar institution except as declared in the Preface and specified in the text

This thesis does not exceed the prescribed word limit for the relevant Degree Committee.

ACKNOWLEDGEMENTS

I would like to firstly express my eternal love and thanks to my wonderful mum Sally, who passed away in the summer of 2015, just two and a half years following her ALS diagnosis. This thesis is dedicated to her. I also can't overstate my love and appreciation for my dad Trevor, who has been unbelievably supportive and kind hearted throughout what was a long and terrifying period for us all.

I would like to state my great appreciation for my supervisor Dr Sue Jones, who helped me hugely when starting on the difficult path into the world of electrophysiology. Her continued support and feedback has been extremely helpful during this project. Thank you also to both Dr Hugh Robinson and Dr Hugh Matthews for their insight and guidance; and indeed to Dr Ewan Smith and Dr Zoé Husson, from whom I first learned about hypoxia assaying and who were incredibly helpful in offering support in this area.

I also have to state my appreciation to my great friends; Jack Curtis, for always being a highly entertaining source of both inspiration and light hearted pessimism; and Angie Wild, for her unwavering optimism and friendship and for always giving me hope when I needed it.

Thank you to Jane, who supported and encouraged me to begin this PhD.

Finally, thank you to the BBSRC, to the department, and to the University for making this work possible.

CHAPTER 1

INTRODUCTION

1 Introduction

The *N*-methyl-D-aspartate (NMDA) receptor (NMDAR) is one of three major types of ionotropic glutamate receptor (iGluR), the others being the α-amino-3-hydroxy-5-methyl-4-isoxazolepropionic acid receptor (AMPARs) and the kainate receptor. iGluRs are cation-permeable, responsible for the majority of excitatory neurotransmission in the central nervous system, and are activated by binding of the amino acid L-glutamate. They are differentiated by their sensitivities to various ligands and ions, and their gating properties (Davies and Watkins 1982; Evans et al. 1982; Traynelis et al. 2010).

Arguably, the key purpose of the NMDAR is to act as a physiological coincidence detector. That is, to sense the simultaneous presence of glutamate and a range of other chemical, metabolic, and physical cues, and by conducting a Ca^{2+}-rich cation current as a response to this information (Burnashev et al. 1992; Schneggenburger 1996). For example, voltage-dependent Mg^{2+} block allows conditional opening of the NMDAR channel when the postsynaptic cell is depolarised coincidently with agonist and co-agonist binding. By this mechanism, NMDARs are key mediators of neuronal development and plasticity: coincidence detection allows the induction of long-term plasticity such as long term potentiation (LTP) or depression (LTD) in a manner consistent with Hebb's predictions (Hebb 1949), often expressed as changes in AMPAR-mediated transmission. Changes in NMDAR function or expression can therefore modify the induction threshold for AMPAR-mediated plasticity; a phenomenon called metaplasticity (Abraham 2008; Hunt and Castillo 2012).

Ca^{2+} influx through NMDARs can activate many downstream signal transduction networks. Initially, changes in intracellular Ca^{2+} concentration are detected by calcium/calmodulin-dependent protein kinases (CaM-kinases; e.g. CAMKI and II) and calcium/calmodulin-dependent protein phosphatases such as calcineurin (Foster et al. 2001; Flavell and Greenberg 2008). Excessive Ca^{2+} influx through NMDARs can also lead to excitotoxicity, and promote cell death signaling pathways: this may be a factor in ongoing neuronal degeneration in diseases such as Parkinson's disease (PD), which is mainly characterised by the loss of

dopaminergic (DA) neurons of the substantia nigra pars compacta (SNc), a region essential to the regulation of voluntary movement control (Koutsilieri and Riederer 2007; Blandini 2010).

A key component controlling the physiological properties of NMDARs is their subunit composition: all NMDARs are composed of four subunits, and depending on which are present within the receptor there can be large differences in regulation, open probability, conductance, and the rate and length of Ca^{2+} influx as a result of receptor activation (Wyllie et al. 2013). The aim of this thesis was to explore expression and subunit composition within functional NMDARs on SNc-DA neurons, as well as their role in responding to potentially pathological conditions. Therefore the relevant properties of NMDARs will be discussed in this chapter, including structure, biophysical properties, and relevance to excitotoxicity and disease. Lastly, the role of SNc-DA neurons will be discussed.

1.1 The NMDA receptor

1.1.1 The biophysical properties of the NMDAR

Whilst NMDARs have a key role in classical NMDAR-dependent LTP/LTD of AMPAR-mediated transmission, they can also play a much larger general role in synaptic transmission, particularly under certain physiological conditions, for example during burst firing activity (Herron et al. 1986), as well as contribute to neural integration (Larkum and Nevian 2008). Neural integration describes how neurons 'add together' all of the inputs to the cell, such as excitatory or inhibitory currents caused by neurotransmission. The noteworthy role of NMDARs in integrative function is enabled by their inherent nonlinear amplification properties: Mg^{2+} block of the channel at resting potentials, high Ca^{2+} permeability, and slow gating kinetics allowing for temporal current summation (Wollmuth et al. 1998a, 1998b; Hunt and Castillo 2012).

Most excitatory synapses have a mix of AMPARs and NMDARs, which affects the shape of the excitatory postsynaptic current (EPSC) arising as a consequence of concurrent activation of these receptor populations: AMPAR currents rise and subside quickly, determining the speed of onset and maximal amplitude of the EPSC. NMDAR-mediated currents rise and decline much more slowly and therefore strongly influence the decay timecourse, and the total

charge transfer over the course of the EPSC (Takumi et al. 1999; Iacobucci and Popescu 2017).

NMDARs are composed of four subunits, typically in a diheteromeric configuration of two GluN1 subunits and two GluN2 or GluN3 subunits. Crystallography has shown that the dimer of the GluNl and GluN2/3 subunit is assembled with the agonist binding domains in a back-to-back configuration (Furukawa et al. 2005; Paoletti et al. 2013), with identical subunits positioned diagonally from one another within the tetrameric complex (Salussolia et al. 2011). In total, there are seven genetically encoded subunits: GluN1, of which there are eight distinct splice variants, four GluN2 (GluN2A–D) and two GluN3 (GluN3A-B; Sugihara et al. 1992).

NMDARs require two GluN1 subunits, each of which contains a glycine binding site, and usually two GluN2 subunits, which contain the glutamate binding site as well as conferring many of the functional properties of the receptor, such as agonist sensitivity, channel open time, and open probability (Chen and Roche 2007; Suárez et al. 2010; Paoletti et al. 2013; Wyllie et al. 2013). GluN3 subunits, like GluN1, bind co-agonist glycine rather than glutamate and therefore the role of the diheteromeric GluN1/GluN3 NMDAR remains unclear (Traynelis et al. 2010), but it may serve to antagonise classical NMDAR functions and act as a gatekeeper for the synaptic refinements which occur during postnatal development (Pérez-Otaño et al. 2016).

Because the subunits confer the functional properties of the receptor, altering the subunit composition of the NMDAR therefore allows control over cellular activity that arises as a consequence of local conditions and agonist availability. Kinases such as cAMP-dependent protein kinase A (PKA), protein kinase C (PKC), protein kinase B (PKB), CaMKII, cyclin-dependent kinase-5 (Cdk5), and casein kinase II (CKII) are able to interact with the NMDAR subunits, and may alter synaptic plasticity by way of regulating NMDAR trafficking or channel properties (Lee 2006; Chen and Roche 2007).

NMDAR function is enabled by the presence of external epitopes which recognise ligands such as glutamate and glycine, as well as H^+ (pH), Mg^{2+}, and Zn^{2+}. Each subunit of the NMDAR has a large ectodomain composed of an amino-terminal domain (ATD) and a ligand-binding domain (LBD; formed by regions S1 and S2) as well as a short transmembrane domain (TMD) which contains the ion channel, and a cytoplasmic carboxyl-terminal domain (CTD; Furukawa and Gouaux 2003; Wyllie et al. 2013). The CTD is where the majority of

structural differences between the GluN2 subunits are found: this region allows interaction with intracellular proteins involved in NMDAR trafficking, regulation, and coupling to other intracellular signalling cascades (see section 1.2). The LBD binds glycine or D-serine in GluN1 and GluN3, and glutamate in GluN2 (Paoletti et al. 2013). The TMD is composed of three transmembrane helices (M1, M3, M4) and a pore loop (M2) that is essential for ion selectivity (Paoletti et al. 2013; Lee et al. 2014): this is explored in more detail below. A schematic of a GluN1/GluN2 dimer is presented in **Figure 1.1**.

In contrast to AMPA or kainate receptors, the ATD of the NMDAR has a unique 'twisted clamshell' conformation, resulting in looser ATD dimer assemblies than the tightly-packed AMPA and kainate ATD dimers (Paoletti et al. 2013). The ATD is essential for allosteric regulation: in GluN2A subunits this region binds Zn^{2+}, which directly and specifically inhibits NMDAR activity (Yuan et al. 2009; Amico-Ruvio et al. 2011). Additionally, the ATD has a substantial influence on deactivation time course: diheteromeric GluN2A-containing NMDARs have a relatively fast deactivation (30-50 ms), therefore allowing more temporally precise encoding with a lower probability of current summation in comparison to GluN2B and GluN2C (300-400 ms), and particularly GluN2D (2000-4000 ms; Monyer et al. 1994; Yuan et al. 2009; Wyllie et al. 2013). Removal of the ATD from GluN2A has been shown to slow the rate of deactivation of the receptor, whilst removal from GluN2B accelerates it (Yuan et al. 2009).

NMDAR channel behaviour is not strictly binary. The channel does not always open or close fully and instead visits an intermediate conductance level. GluN2A and GluN2B-containing NMDARs visit short lived subconductance levels of 80% of the main open state (~50 pS fully open with 40 pS sublevel). In contrast, GluN2C and GluN2D-containing receptors are as equally likely to settle on the full conductance level (~36 pS) as the subconductance level, which in this case is lower at just 50 % (18 pS; Wyllie et al. 1996; Blanke and VanDongen 2009). This property of single channel behaviour can therefore be useful in identifying the subunit composition of native NMDARs (Jones and Gibb 2005).

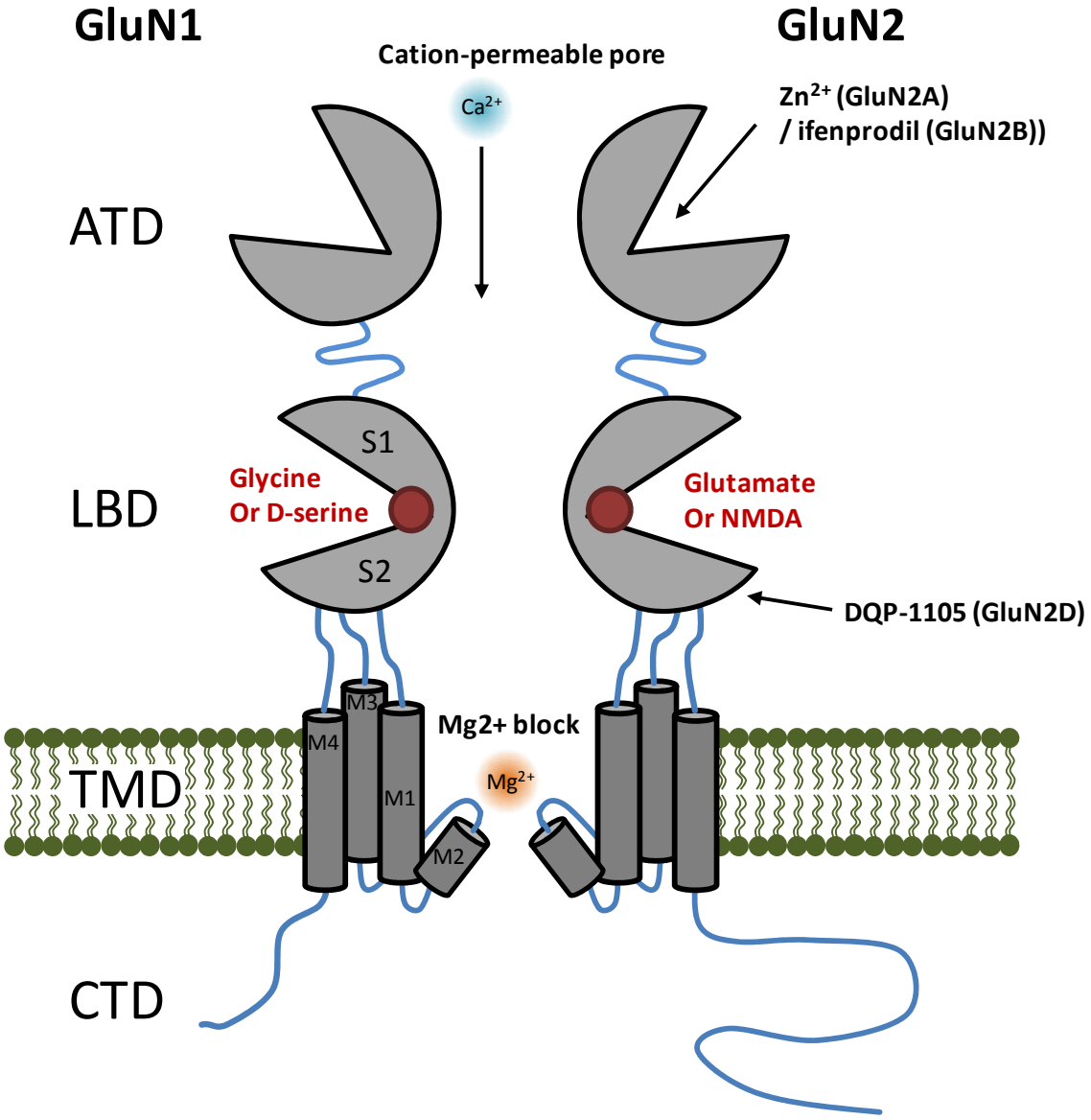

Figure 1.1 – Transmembrane architecture of the NMDAR

A schematic diagram of an example NMDAR subunit dimer, including the structures of the obligatory GluN1 subunit and the GluN2 subunit. The extracellular region includes the amino terminal domain (ATD) which contains modulatory sites which bind Zn^{2+} in GluN2A, or ifenprodil in GluN2B. The S1 and S2 domains together form the ligand binding domain (LBD) for glycine or D-serine in GluN1, and glutamate or NMDA in GluN2. The transmembrane domain (TMD) is formed of the three M1, M3, and M4 alpha helices, along with a re-entrant loop (M2) which forms part of the channel pore. The channel is permeable to Na^{+}, K^{+}, and Ca^{2+}. Extracellular Mg^{2+} is able to bind deep within the channel, allowing voltage-sensitive block. The C-terminal domain (CTD) is able to bind to many intracellular proteins involved in NMDAR trafficking, regulation, and other intracellular signalling cascades. Adapted from Cull-Candy and Leszkiewicz 2004; Blanke and VanDongen 2009; Paoletti et al. 2013.

Interestingly, whilst NMDARs are highly permeable to Ca^{2+}, typically allowing 3-4 times more Ca^{2+} influx than AMPARs (Iino et al. 1990), single channel conductance decreases as extracellular Ca^{2+} increases (Ascher and Nowak 1988; Wyllie et al. 1996). This effect is concentration-dependent but voltage-independent: as well as sites deep within the channel, Ca^{2+} binds to the GluN1 subunit near the entrance to the channel pore, potentially reducing cation conductance by electrostatic interaction (Schneggenburger 1998; Maki and Popescu 2014). The TMD is essential for the ion selectivity of the receptor (Paoletti et al. 2013; Lee et al. 2014): as above, this is composed of three transmembrane helices, and a pore loop composed of the M2 helix and an extended region. The extended region forms the narrowest part of the ion channel, called the selectivity filter: this structure plays a central role in ion permeation, ion selectivity, and channel block. Six M2 region asparagine residues line the pore at the tip of the selectivity filter with their side chains extended into the central cavity of the pore, and it is these side chains which distinguish the larger Ca^{2+} ion from Mg^{2+}, allowing only Ca^{2+} to pass through (Burnashev et al. 1992; Mesbahi-Vasey et al. 2017). Intracellular Ca^{2+} concentration is tightly controlled, with a low amount of free Ca^{2+} within neurons at rest, whereas the extracellular concentration is around 10,000-fold greater. Neurons control intracellular [Ca^{2+}] using binding proteins and organelles that compartmentalize Ca^{2+} (Clapham 2007). Ca^{2+} permeability varies between the subunits, with diheteromeric GluN2A- or GluN2B-containing NMDARs possessing a Ca^{2+} / Cs^{+} permeability ratio (pCa/pCs) of ~7.5. By contrast, diheteromeric GluN2C- or GluN2D-containing receptors have a lower pCa/pCs of 4.5 (Paoletti et al. 2013).

The key feature of the NMDAR is its Mg^{2+} block capability: the binding of Mg^{2+} deep within the channel pore directly blocks currents in a voltage-dependent manner (Mayer et al. 1984; Nowak et al. 1984; Wollmuth et al. 1998b), allowing the receptor to act as a Hebbian coincidence detector (Lüscher and Malenka 2012). Mg^{2+} block sensitivity also varies between GluN2 subunits, and is controlled by a single residue in the M3 segment (Siegler Retchless et al. 2012): diheteromeric GluN2A or GluN2B-containing NMDARs have a high sensitivity to Mg^{2+} blockade, with an Mg^{2+} IC50 (the concentration at which the response is reduced by half) of ~15 μM at −70 mV. By contrast, diheteromeric GluN2C or GluN2D-containing NMDARs have a lower Mg^{2+} IC50 of ~80 μM (Paoletti et al. 2013; Huang and Gibb 2014). This, along with the variation in conductance between the subunits, significantly affects the relative contribution of NMDAR subtypes to synaptic integration and plasticity (Paoletti et al.

2013). The distinct biophysical properties conferred by the GluN2D subunit mean that it may also have unique regulatory roles, such as detection of low levels of glutamate, potentially from synaptic spillover (Dubois et al. 2016): this extra sensitivity and often extrasynaptic location may also mean that it is a mediator of currents which could activate cell death signalling pathways (see section 1.3). Additionally, the slow gating kinetics of GluN2D-containing NMDARs could increase the time window for coincidence detection during induction of synaptic plasticity (von Engelhardt et al. 2015), but at the cost of temporal fidelity in excitatory synaptic transmission. Where GluN2D is involved in either detecting spillover or mediating plasticity, only a small amount of postsynaptic depolarisation may be required, if any, for them to initiate cation influx, due to their relative insensitivity to Mg^{2+} (Hrabetova et al. 2000). For these reasons it is important to ascertain the distribution of GluN2D subunits, both across neuronal populations and indeed on a subcellular level: both of these factors may provide evidence for the function of GluN2D in each individual context.

1.1.2 NMDAR desensitisation

Desensitisation of iGluRs is a conformational change in the receptor resulting from agonist exposure (Sornarajah et al. 2008), which reduces current flow through the channel and may constitute a negative feedback mechanism to prevent against excitotoxicity (Zorumski et al. 1990). Entry of iGluRs into a desensitised state may also be important in determining the overall time course of synaptic responses (Jones and Westbrook 1996). Channel opening is quickly followed by receptor desensitisation, with both of these conformational changes taking around 2-3 ms (Colquhoun et al. 1992; Meyerson et al. 2014).

The mechanism of desensitisation in AMPA and kainate receptors involves disruption of the arrangement of the LBD, which allows glutamate to remain bound but with a closed pore similar to that in the resting state (Plested 2016). NMDAR desensitisation is not as well understood, and in contrast to AMPARs, appears to be determined by elements in the ATD as well as the TMD (Krupp et al. 1998; Villarroel et al. 1998; Alsaloum et al. 2016). In NMDARs, interaction between the ATD and LBD is much more extensive, and so these domains may function less autonomously (Lee et al. 2014). Therefore, desensitisation is not as extensive, as the LBD cannot freely change conformation as it does in AMPA and kainate

receptors (Plested 2016). For this reason, AMPARs are able to desensitise almost fully, whereas NMDAR desensitisation is incomplete (Iacobucci and Popescu 2017).

There are two principal Ca^{2+}-independent mechanisms by which NMDARs can desensitise. Glycine-dependent desensitisation describes a reduction in NMDAR current which occurs in the continued presence of glutamate and when glycine concentration is not oversaturated, occurring due to a negative allosteric interaction between the glutamate binding and glycine binding sites (Zheng et al. 2001). This form of desensitisation manifests as a decrease in glycine affinity and can be overcome by increasing the glycine concentration (Benveniste et al. 1990; Villarroel et al. 1998; Dingledine et al. 1999a). GluN1/GluN2A diheteromers have been shown to deactivate in this manner with a time constant of around 650 ms (Wyllie et al. 1998). Diheteromeric GluN1/GluN2C and GluN1/GluN2D NMDARs, however, do not display any significant glycine-dependent desensitisation (Wyllie et al. 1998; Vance et al. 2011; Alsaloum et al. 2016).

Glycine-*independent* desensitisation is defined as a Ca^{2+}-independent desensitisation of NMDA receptors which cannot be overcome by increasing the concentration of glycine (Sather et al. 1992; Dingledine et al. 1999a; Hu and Zheng 2005). Glycine-independent desensitisation is reportedly observed in GluN1/GluN2A and GluN1/GluN2D diheteromers, is less pronounced in those containing GluN2B, and absent in GluN2C (Krupp et al. 1996; Hu and Zheng 2005).

The elevation of intracellular Ca^{2+} by the activation of NMDARs can also lead to a reduction in NMDAR channel activity (Zilberter et al. 1991): this may be mediated by a direct interaction between calmodulin and the receptor (Ehlers et al. 1996; Villarroel et al. 1998). This phenomenon has previously been known as Ca^{2+}-dependent inactivation, but is not considered a genuine desensitisation because it can be evoked by a rise in intracellular levels of Ca^{2+} triggered independently of NMDA receptor activation (Villarroel et al. 1998; Zheng et al. 2001).

1.1.3 NMDAR pharmacology

Many compounds are available which are able to modulate the activity of NMDARs, with some relevant examples discussed below.

(i) Competitive compounds

NMDAR mediated current can be specifically and competitively inhibited by antagonists such as D-α-aminoadipate and D-(−)-2-Amino-5-phosphonopentanoic acid (D-AP5; Evans et al. 1982), and therefore the discovery of these compounds played an essential role in confirming the presence of NMDARs in neurons (Jespersen et al. 2014). Regarding subunit selectivity, a phenanthrene-based competitive antagonist, piperazine-2,3-dicarboxylic acid (PPDA) was identified more than a decade after D-AP5 which has a moderate selectivity for GluN2C/D over GluN2A/B (Feng et al. 2004), but as the glutamate binding pocket is highly conserved across the GluN2 subunits, competitive antagonists do not in general display high degree of subunit specificity (Jespersen et al. 2014). There is some variation in the outer edge of the binding pocket between GluN2 subunits, and therefore only larger antagonists which block the glutamate binding site whilst also binding at sites outside of this pocket are able to show subunit selectivity, such as PPDA, R-AP7, or R-CPP (Monaghan et al. 2012). However, selectivity for GluN2D was further improved by discovery of UBP141, a competitive compound at the glutamate binding site with a 7- to 10- fold selectivity for GluN2D over GluN2A/GluN2B (Morley et al. 2005; Costa et al. 2009).

(ii) Uncompetitive compounds

These compounds are use-dependent, and can only bind to a site within the NMDAR channel pore when it is opened by the binding of glutamate and glycine. Mg^{2+} ions behave in this way, as described above. Apart from Mg^{2+}, materials which block the NMDAR pore usually discriminate poorly between NMDAR subtypes; this being true of phencyclidine (PCP), thienylcyclohexylpiperidine (TCP), and ketamine. Whilst the selective and irreversible NMDAR channel blocker dizolcipine (MK-801) is more selective for GluN2A and GluN2B in comparison to GluN2C and GluN2D, the difference in affinity is relatively small (Paoletti and Neyton 2007).

As described in section 1.3, excessive NMDAR activation can lead to excitotoxicity under some circumstances, though putatively neuroprotective agents that block most NMDAR activity will inevitably have unacceptable clinical side effects. The adamantane derivative memantine, however, appears to preferentially block excessive NMDAR activity without disruption of normal synaptic activity (Wild et al. 2013). Memantine is a low affinity open-channel blocker with a fast off-rate, and does not substantially accumulate in the NMDAR channel (Lipton 2004). Memantine is therefore well-tolerated and used clinically to help prevent potential excitotoxic damage to neurons in Alzheimer's and Parkinson's diseases (van Marum 2009; Emre et al. 2010; Wild et al. 2013). At resting membrane potentials and physiological [Mg^{2+}], memantine shows a moderate selectivity for GluN2C and GluN2D-containing NMDARs (Kotermanski and Johnson 2009).

(iii) Noncompetitive compounds

There have been several discoveries of noncompetitive allosteric compounds with high subunit selectivity, which are useful experimentally for elucidating the subunit composition of functional NMDARs within the cell membrane: these include ifenprodil (GluN2B; (Gallagher et al. 1996; Hess et al. 1998), TCN 201 (GluN2A; Bettini et al. 2010), QNZ46 (GluN2D; Mosley et al. 2010), and potentiator CIQ (GluN2C/D; Mullasseril et al. 2010). Ifenprodil has a 140-fold preference for GluN2B over GluN2A (Gallagher et al. 1996), and it and its analogues have been used extensively in neuroscience research due to the ubiquity of GluN2B.

Ifenprodil binds to residues located deep within the dimer interface between the extracellular ATD regions of the GluN1 and GluN2B subunits, increasing the energy barrier for activation and resulting in an increased mean closed time of the channel (Amico-Ruvio et al. 2011; Karakas et al. 2011; Tomitori et al. 2012). Inhibition is incomplete, and noncompetitive with other known NMDA receptor agonists or modulators (Amico-Ruvio et al. 2011; Tajima et al. 2016).

DQP-1105, a compound identified by the Traynelis group in 2011, is a noncompetitive antagonist which binds the S2 region of the GluN2D subunit, and blocks a conformational change necessary for channel opening. DQP-1105 is also around 50 times more selective for

GluN2C/D-containing NMDARs over those containing GluN2A or B (Acker et al. 2011), which makes it a good candidate for potential inhibition of GluN2D-containing NMDARs on SNc-DA neurons.

Overall, the pharmacological tools for identifying the subunit composition of native NMDARs are limited. While some insight is obtained by applying a spectrum of compounds at carefully considered concentrations that offer some subunit preference, the outcome is not definitive. Therefore, other approaches would ideally be used in combination with pharmacological intervention. One aim of this PhD was to explore the pharmacological properties of NMDARs in SNc-DA neurons in mice where the GluN2D subunit has been genetically removed.

Compound	GluN2A	GluN2B	GluN2C	GluN2D	Reference
Competitive	*Ki (μM)*	*Ki (μM)*	*Ki (μM)*	*Ki (μM)*	
Racemic AP5	0.28	0.46	1.6	3.7	Feng et al. 2005
PPDA	0.55	0.31	0.096	0.125	Feng et al. 2005
UBP-141	14	19	4.2	2.8	Morley et al. 2005
Uncompetitive	IC50 (μM)	IC50 (μM)	IC50 (μM)	IC50 (μM)	
MK-801	0.015	0.009	0.024	0.038	Dravid et al. 2007
Ketamine	5.4	5.1	1.2	2.9	Kotermanski and Johnson 2009
PCP	0.82	0.16	0.16	0.22	Dravid et al. 2007
Memantine	13	10	1.6	1.8	Kotermanski and Johnson 2009
Noncompetitive	*IC50 (μM)*	*IC50 (μM)*	*IC50 (μM)*	*IC50 (μM)*	
Ifenprodil	39	0.15	29	76	Hess et al. 1998
DQP-1105	206	121	9	3	Acker et al. 2011
TCN 201	0.109	>30	*no data*	>30	Bettini et al. 2010
QNZ46	229	>300	6	3	Mosley et al. 2010
Noncompetitive potentiators	*EC50 (μM)*	*EC50 (μM)*	*EC50 (μM)*	*EC50 (μM)*	
CIQ	NE	NE	2.8	3	Mullasseril et al. 2010

Table 1.1 – Compounds acting on NMDARs, and their subunit specificity

PCP = phencyclidine; TCP = thienylcyclohexylpiperidine; NE = no measurable effect. Ki is the inhibitory constant, with a smaller value reflective of greater binding affinity. IC50 is the half maximal inhibitory concentration, and EC50 is concentration of potentiator giving a half-maximal response. Table partially adapted from Ogden and Traynelis 2011.

1.1.4 Grin2D-null mice

Mice lacking expression of the GluN2D subunit have been previously generated by a gene-targeting recombination technique: the exon encoding the GluN2D transmembrane M4 region was disrupted by the insertion of a neomycin phosphotransferase gene (Ikeda et al. 1995). These mice grow and mate normally and exhibit no major structural brain abnormalities, though show a slight reduction in spontaneous behavioural activity in novel environments and a reduction in sucrose preference (Ikeda et al. 1995), as well as a lower sensitivity to stress induced by elevated maze, light/dark box, and forced swimming tests (Miyamoto et al. 2002). The only morphological anomaly observed is a reduction of dendritic branching in mitral cells in the accessory olfactory bulb (AOB; Yamamoto et al. 2017): GluN2D mRNA has previously been reported in the periglomerular (PG) cells of the mouse AOB (Watanabe et al. 1993), and it is hypothesized that functionally altered PG cell synapses at mitral cell dendrites may inhibit their normal development (Yamamoto et al. 2017).

1.1.5 Development and distribution of NMDARs

The distribution of NMDAR subunits throughout the brain alters with development (Monyer et al. 1994). Whilst the essential GluN1 subunit (and therefore the NMDAR as a whole) is ubiquitously expressed in all brain regions throughout development, expression of GluN2 is much more variable: notably, GluN2B expression is high at birth, particularly in the cortex and hippocampus, and gradually declines to a lower level in the same brain regions in adulthood. Conversely, GluN2A expression is very low at birth and increases throughout development: it was initially thought to replace GluN2B in the cortex and hippocampus, but both GluN2A and GluN2B-containing NMDARs are considered to remain present. GluN2A also increases its expression in the olfactory bulb and striatum (Wenzel et al. 1995, 1997). GluN2C is expressed later in development, and in adult mice and rats is mostly confined to the cerebellum and olfactory bulb (Watanabe et al. 1992; Monyer et al. 1994; Wenzel et al. 1997). GluN2D subunit expression is prominent in the brainstem and diencephalon in neonates but decreases throughout development, with much lower levels in the adult. It is, however, reportedly expressed in the adult rat brain in some cerebellar nuclei, the striatum, the olfactory bulb, and in dopaminergic neurons of the substantia nigra (Watanabe et al. 1993,

1994; Monyer et al. 1994; Standaert et al. 1994; Wenzel et al. 1995, 1997; Jones and Gibb 2005; Brothwell et al. 2008; Mullasseril et al. 2010). More recently, the presence of GluN2D has been observed at the synapse in adult mouse hippocampal interneurons (but not pyramidal cells) along with GluN2A and GluN2B (von Engelhardt et al. 2015; Perszyk et al. 2016); as well as synapses on adult rat subthalamic nucleus (STN) neurons, along with GluN2B (Swanger et al. 2015). However, these studies have at least in part relied on pharmacological tools, the limitations of which are outlined above. NMDARs in SNc-DA neurons at around P7 are thought to be arranged in two populations of diheteromeric receptor: those composed of GluN1/GluN2B and those composed of GluN1/GluN2D. By P17, SNc-DA neurons are thought to possess NMDARs in a triheteromeric GluN1/GluN2B/GluN2D configuration (Jones and Gibb 2005; Brothwell et al. 2008; Suárez et al. 2010).

NMDARs are also distributed in a specific way on the cell surface (**Figure 1.2**). Synaptic receptors in general are defined by their ability to be activated by neurotransmitter released from presynaptic terminals in response to a single action potential under normal physiological conditions. The synaptic receptor pool is involved in signal transduction mechanisms which may be specific to the synapse. The population of receptors termed ‘perisynaptic’ can also be activated by synaptically released neurotransmitter, but only under conditions of increased release in response to strong or high frequency synaptic stimuli. Perisynaptic NMDARs are generally located 100–300 nm from the edge of the PSD, and may be anchored at these locations by submembrane receptor scaffolding proteins (Zhang and Diamond 2006): these may be NMDARs which are ready to be internalised (Pérez-Otaño et al. 2006), or which have been recently exocytosed (Petralia et al. 2009). Finally, extrasynaptic receptors are those not included in the previous two definitions, and are located elsewhere within the cell surface membrane, away from synapses, and are not bound to PSD-95. However, some activation of extrasynaptic NMDARs by presynaptic glutamate release may occur during abnormally high levels of synaptic activity, especially when glutamate reuptake is compromised (Angulo et al. 2004; Pál 2015; Wild et al. 2015). In the rat hippocampus, extrasynaptic NMDARs account for two thirds of all surface NMDARs during early postnatal development, and around a third in adults (Tovar and Westbrook 1999; Groc et al. 2006; Petralia et al. 2010a). In the cerebellum, hippocampus, and spinal cord, GluN2D subunits have been found to comprise a greater proportion of the extrasynaptic NMDAR population than the synaptic population

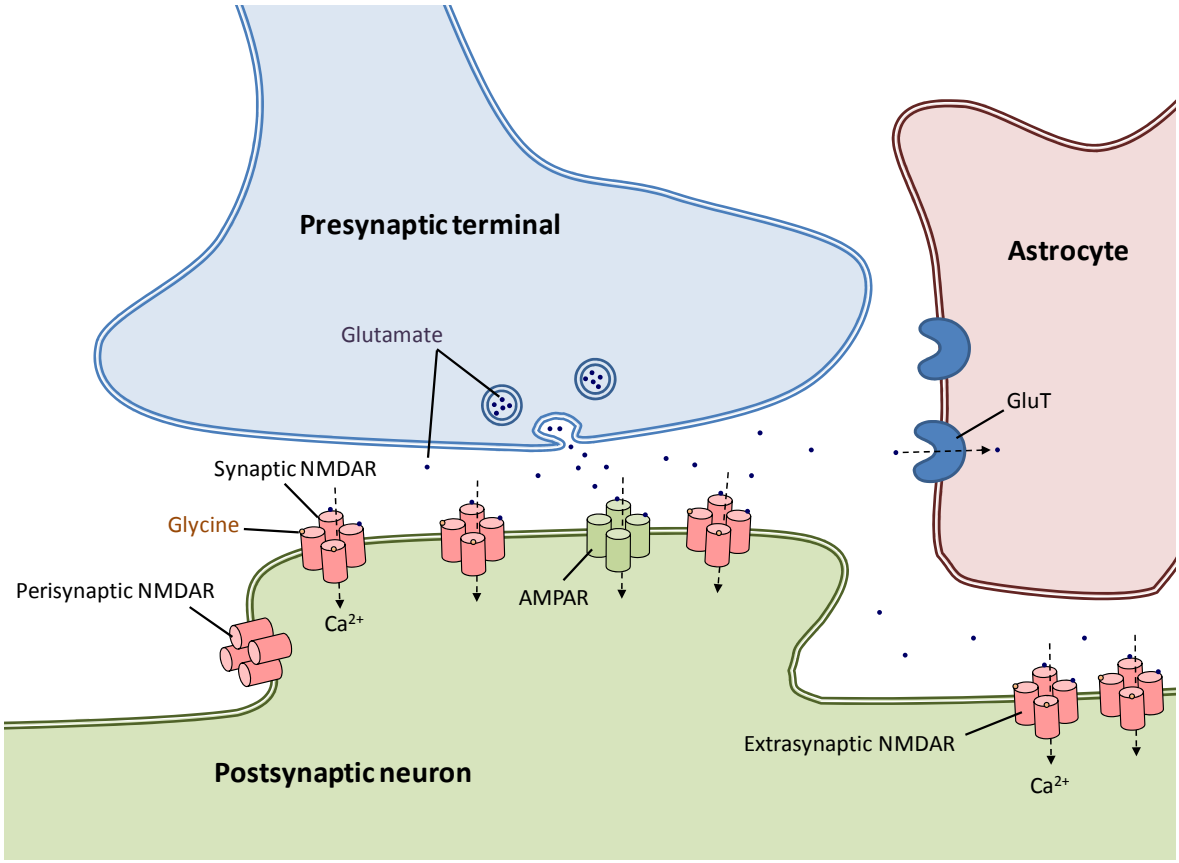

Figure 1.2 – The glutamatergic synapse

A simple schematic showing vesicular glutamate release, as well as the various putative populations of synaptic, perisynaptic, and extrasynaptic NMDAR, as well as AMPARs. Glutamate transporters (GluTs) on nearby astrocytes take up glutamate, and may help to prevent 'spillover' of glutamate from the synapse.

(Momiyama et al. 1996; Misra et al. 2000; Momiyama 2000; Brickley et al. 2003; Lozovaya et al. 2004), although the presence of GluN2D at the synapse is also supported by several studies (Harney et al. 2006, 2008; Logan et al. 2007; Brothwell et al. 2008; von Engelhardt et al. 2015).

While extrasynaptic receptors are able to diffuse laterally through the membrane, they have also been found to accumulate at points in close contact with adjacent cell processes, including axons, axon terminals, and glial cells (Kharazia and Weinberg 1999; Petralia et al. 2010a), where they may associate with scaffolding proteins such as GAIP-interacting protein C-terminus (GIPC), which is primarily excluded from the synapse (Groc et al. 2006; Yi et al. 2007).

There is evidence of a more well defined role for these extrasynaptic populations of NMDAR, in that they can be activated by ambient extracellular glutamate, something which has previously been demonstrated in the hippocampus (Sah et al. 1989; Angulo et al. 2004; Fellin et al. 2004). As the level of desensitisation in NMDARs is much lower than AMPARs, they are likely to mediate the majority of excitation in response to this ambient glutamate, away from the synapse (Iacobucci and Popescu 2017). Blockade of voltage-gated sodium channels or vesicular release has been shown to have no effect on levels of ambient glutamate in the hippocampus (Herman and Jahr 2007; Le Meur et al. 2007), indicating that it is not released by neurons in an action potential dependent manner, but may originate from glial cells (Parpura et al. 1994; Bezzi et al. 1998; Angulo et al. 2004; Fellin et al. 2004). As extrasynaptic NMDARs in the hippocampus are arranged in high density regions opposing astrocytic processes (Jourdain et al. 2007; Petralia 2012), glutamate released from these processes may activate them and therefore influence network synchrony (Angulo et al. 2004; Fellin et al. 2004).

1.2 NMDAR regulation and trafficking

Overall NMDAR activity can be regulated by alteration of membrane NMDAR numbers, by trafficking to different sites within the membrane (for example between synaptic and perisynaptic or extrasynaptic sites), and by alteration of the physiological properties of the receptor (Dingledine et al. 1999b; Groc et al. 2009). Many of these effects occur when

NMDARs bind via the heterogenic C-terminal domains of their subunits to various signal transduction complexes, which can vary depending on their subcellular location (Petralia et al. 2010b; Baucum 2017). Proteomic analysis using diheteromeric GluN1/GluN2B NMDARs has shown that these receptors are associated with around 190 different proteins via the CTD (Collins et al. 2006) including kinases, phosphatases, Ca^{2+}-dependent proteins, scaffolding proteins, and proteins which couple the receptor to the cytoskeleton (reviewed in Kennedy 2000), all of which may play some role in regulation of the activity of the receptor.

Regarding GluN2D, The E3 ligase Nedd4, which allows binding of regulatory protein ubiquitin, has been found to directly bind the CTD of the GluN2D subunit (Gautam et al. 2013). This provides a mechanism which may allow specific targeting of GluN2D-containing NMDARs for intracellular trafficking and degradation (Clague and Urbé 2010), and may be responsible for the developmental downregulation of GluN2D due to the subsequent reduction in Nedd4 expression (Gautam et al. 2013).

Constitutive changes in functional NMDAR expression between synaptic and peri/extrasynaptic locations have been demonstrated to occur by lateral movement of NMDARs within the membrane (Dupuis et al. 2014): GluN2B-containing NMDARs have been shown to be more laterally mobile than those containing GluN2A (Groc et al. 2006), though neither GluN2C or GluN2D were investigated in this way. It is possible that this increased mobility due to the presence of GluN2B may also apply to diheteromeric and/or triheteromeric GluN2B/GluN2D-containing NMDARs, such as those proposed to be present in SNc-DA neurons (Jones and Gibb 2005; Brothwell et al. 2008; Suárez et al. 2010).

The Ca^{2+}-dependence of NMDAR-regulation via the subunit CTD has previously been demonstrated: deletion of the GluN1 subunit CTD removes the Ca^{2+}-dependent element of NMDAR inactivation (Ehlers et al. 1996). Additionally, Ca^{2+}-dependent serine/threonine kinases such as protein kinase A (PKA) and protein kinase C (PKC) can upregulate NMDAR activity (Tingley et al. 1997): upon activation, PKC integrates itself from the cytoplasm into the membrane, binding to anchoring proteins where it is able to then interact with neighbouring NMDARs, promoting increased expression of NMDARs and also increasing the channel opening rate (Lin et al. 2006; Salter et al. 2009). Conversely, serine/threonine phosphatases such as PP1, PP2A, and PP2B (calcineurin) can effect a decrease in NMDAR activity by decreasing the open probability of the channel (Salter et al. 2009). Additionally,

internalisation of NMDARs has been demonstrated by inhibiting the action of dynamin, a GTPase essential for the reformation of clathrin-coated synaptic vesicles for endocytosis (Carroll et al. 1999; Montgomery et al. 2005; Lau and Zukin 2007).

1.2.1 Regulation of 'extrasynaptic' NMDARs

It has previously been shown in SNc-DA neurons that 'whole-cell' NMDARs activated by bath application of NMDA, which putatively includes a large population of extrasynaptic NMDARs, are regulated in a use-dependent manner whereby repeated application of the agonist leads to a persistent reduction in NMDAR-mediated current (Wild et al. 2014). This form of downregulation, termed NMDAR 'rundown' was also found to be largely Ca^{2+}-dependent: intracellular Ca^{2+} chelation, replacement of extracellular Ca^{2+} with Ba^{2+}, and holding the cell at +40 mV to reduce the driving force on Ca^{2+} influx all reduced the effect. Rundown was also measured after incubation with the GluN2B-preferring antagonist ifenprodil. Significant rundown of the ifenprodil-insensitive NMDAR component was observed, but this remaining current showed no sensitivity to intracellular Ca^{2+} chelation, which suggested that the ifenprodil-insensitive component may have been GluN2D-mediated due to the lack of evidence for GluN2A or GluN2C expression in SNc-DA neurons (Wild et al. 2014). In the same study, synaptic NMDAR current rundown was also observed in response to repeated low-frequency presynaptic stimulation (0.1 Hz). This rundown was insensitive to intracellular Ca^{2+} buffering using BAPTA; however rundown was significantly reduced by clamping at +40 mV, which reduces the driving force on Ca^{2+} influx. This insensitivity to Ca^{2+} chelation may be due to the mode of NMDAR activation (brief versus prolonged), or due to a closer coupling of the synaptic NMDARs to the Ca^{2+}-dependent mechanism of run-down, such that even the fast chelator BAPTA is not able to bind Ca^{2+} before it initiates this mechanism (Wild et al. 2014).

1.2.2 Activity-dependent regulation of synaptic NMDARs

NMDARs are key mediators of neuronal development and plasticity in the forms of classical Hebbian long-term potentiation (LTP) and long-term depression (LTD), which comprise

mostly the addition and removal of AMPARs from the synapse. To effect these forms of plasticity, iGluRs interact with many proteins within the PSD; some of which regulate receptor function and some of which govern insertion or removal from the membrane, or trafficking within it. An important protein for classical NMDAR-mediated plasticity of AMPARs is stargazin, a regulatory protein (TARP) that affects the conductance, kinetics, and rectification of AMPARs. Another regulatory protein, PICK1, interacts primarily with GluA2 to effect insertion and removal from the membrane (Lüscher and Malenka 2012).

While it has been long recognised that the NMDAR is essential for classical long term plasticity with regards to AMPAR regulation, previous work suggested that the NMDAR itself is immune to activity induced synaptic plasticity (Lissin et al. 1998; Montgomery et al. 2005). However, many studies have subsequently shown that both LTP and LTD of NMDAR-mediated currents (NMDAR-LTD and NMDAR-LTD) can be induced by alterations in presynaptic activity (Montgomery et al. 2005; Harnett et al. 2009; Hunt and Castillo 2012). Because NMDARs contribute significantly to information transfer at the synapse, plasticity involving regulation of NMDARs themselves will therefore significantly alter the characteristics of postsynaptic currents (Hunt and Castillo 2012).

In the hippocampus (CA1, CA3, and the dentate gyrus), high-frequency stimulation (HFS) can rapidly induce NMDAR-LTP (Lozovaya et al. 2004; Harney et al. 2006, 2008; Lau and Zukin 2007). Induction of NMDAR-LTP involves several stages and requires activation of three types of postsynaptic receptor: NMDARs, metabotropic glutamate receptors (mGluRs; in this case mGluR5), and adenosine A_{2A} receptors. Intracellularly, NMDAR-LTP also requires activation of a G-protein (via A_{2A} receptor activation) and a rise in intracellular Ca^{2+} leading to activation of the intracellular kinases PKC and Src (Kotecha et al. 2003; Harney et al. 2006, 2008; Kwon and Castillo 2008; Rebola et al. 2008).

Plasticity of NMDAR-mediated currents effected by the same activity paradigm can vary greatly: for example, it has been shown in the hippocampus that bidirectional plasticity of NMDAR-EPSCs is possible in dentate gyrus granule cells using the same high frequency stimulation protocol, whereas only NMDAR-LTD occurs in dentate gyrus interneurons (Harney and Anwyl 2012). The bidirectionality of HFS-induced NMDAR plasticity in granule cells is Ca^{2+}-dependent: NMDAR-LTD is induced in the presence of a high intracellular concentration of Ca^{2+} buffer EGTA (Ethylene-bis(oxyethylenenitrilo)tetraacetic acid ; 10

mM) and NMDAR-LTP with a lower concentration (0.2 mM). Interestingly, dentate gyrus interneurons that express only NMDAR-LTD appeared to express GluN2B- and GluN2D-containing NMDARs at the synapse (Harney and Anwyl 2012), whereas granule cells only express synaptic GluN2A and GluN2B- containing NMDARs: however, induction of LTP in granule cells may recruit extrasynaptic GluN2D-containging NMDARs to the synapse (Harney et al. 2008).

At the calyx of Held–principal neuron synapse in the medial nucleus of the trapezoid body (MNTB), a subset of fast synapses in the auditory system, spike timing is critical for sound localisation. The ability of postsynaptic neurons to phase-lock spikes to presynaptic inputs is compromised in immature synapses by the presence of NMDARs, due to their slow gating kinetics. NMDARs are therefore present only transiently within the first two postnatal weeks (Joshi et al. 2007). To preserve timing fidelity during high-frequency neurotransmission at mature synapses, NMDARs are downregulated: auditory activity begins in mice when the ear canal opens at P10–P12 resulting in high frequency firing of the presynaptic calyx of held neurons, and it is this excitatory activity which may begin to cause downregulation of postsynaptic NMDARs in MNTB neurons (Futai et al. 2001). Recordings made from these neurons in acute mouse brain slices at P10-13 along with presynaptic burst stimulation (100 Hz bursts every 1 s for 60 s and paired with postsynaptic depolarisation), showed that summated NMDAR-EPSCs 18 minutes following this activity were significantly decreased, whilst single NMDAR-EPSCs remained stable (Joshi et al. 2007): this suggested that perisynaptic or extrasynaptic NMDARs were being preferentially downregulated. However, differences in morphological structure between the giant calyx synapse and typical small central nervous system (CNS) synapses may lead to different transmitter release and spillover profiles and, therefore, a different profile of NMDAR regulation in these neurons. The downregulation observed at these synapses was found to be prevented by BAPTA-mediated Ca^{2+} chelation, as well as by inhibiting the activity of dynamin, suggesting internalisation of NMDARs in this process (Takei et al. 1996; Joshi et al. 2007). The potential for activity dependent synaptic regulation of NMDRs has not yet been explored in SNc-DA neurons, and was one of the aims of this thesis.

1.3 NMDARs and Excitotoxicity

Excessive Ca^{2+} influx through NMDARs is implicated in excitotoxicity through activation of cell death signalling pathways (Choi 1987; Hardingham and Bading 2010; Surmeier et al. 2010, 2011). This increased NMDAR activity can promote cell death under pathological conditions, for example during ischemia, or as part of the pathophysiology of neurodegenerative illnesses such as Parkinson's disease (PD) and Alzheimer's disease (AD) (Dong et al. 2009). The role of NMDARs under potentially excitotoxic conditions is discussed in this section, beginning with hypoxia.

1.3.1 NMDARs and hypoxia-ischemia

Hypoxic conditions, such as may be caused by ischemia, can lead to metabolic stress and excitotoxicity in neurons (Lai et al. 2014). Low oxygen availability causes cellular ATP levels to deplete, which disrupts the ionic gradients maintained by ATP-powered Na^+/K^+ pumps, therefore leading to depolarisation. Depolarisation causes increased glutamate release from excitatory neurons, and this, along with potential impairment of glutamate reuptake (see section 1.3.2), leads to increased extracellular glutamate and therefore an increase in NMDAR-mediated Ca^{2+} influx, and consequent neuronal cell death (Dugan and Choi 1999; Lai et al. 2014).

The effects of hypoxia have been extensively studied in the mammalian hippocampus (Bickler and Hansen 1998; Larson and Park 2009; Peterson et al. 2012). In rat hippocampal CA1 neurons, the concentration of intracellular Ca^{2+} is increased by around 20 % during periods of hypoxia, which is frequently associated with a decrease in NMDAR responses. Ca^{2+} increase in this case can downregulate NMDARs via the cytoskeleton, as application of the actin stabiliser phalloidin has been shown to prevent the hypoxic treatment from decreasing receptor function (Bickler et al. 2003).

The effects of hypoxia have also previously been studied in mammalian/rodent SNc-DA neurons, but less extensively (Häusser et al. 1991; Röper and Ashcroft 1995; Singh et al. 2007). At glutamatergic synapses onto rat SNc-DA neurons, oxygen and glucose depravation (OGD) treatment for 5 minutes was found to cause a potentially neuroprotective presynaptic depression of glutamate release (Singh et al. 2007). Postsynaptic AMPAR and NMDAR-

mediated currents were depressed to a similar extent, and presynaptic inhibition was mediated by activation of G protein-coupled presynaptic adenosine A_1 receptors (A_1Rs), as the effect was blocked by application of A_1R-selective antagonist 8-cyclopentyl-1,3-dipropylxanthine (DPCPX; Singh et al. 2007). This inhibitory effect did not recover following the withdrawal of OGD. SNc-DA neurons have also been shown to exhibit a postsynaptic hyperpolarisation in response to low ATP levels, which is mediated via ATP-sensitive K^+ (K_{ATP}) channels (Häusser et al. 1991; Röper and Ashcroft 1995). These receptors open in response to an increase in the ADP/ATP ratio, thereby coupling neuronal excitability to metabolic status, a mechanism which is neuroprotective during acute metabolic stress (Roeper et al. 1990; Singh et al. 2007; Sun and Feng 2013).

Young animals have greater resistance to hypoxic conditions than adults. Survival of CA1 neurons in slices from rats at around postnatal day (P)5 following hypoxic stress is greater than in ~P20 animals, with young neurons also displaying smaller increases in and enhanced recovery of intracellular Ca^{2+}, less accumulation of glutamate, and less NMDAR-mediated Ca^{2+} influx (Bickler and Hansen 1998). This effect may be partially due to the actions of GluN2D-containing NMDARs, which are much more widely expressed in neonates. Recordings made from *xenopus laevis* oocytes expressing different configurations of NMDAR show that diheteromeric GluN1/GluN2D NMDAR currents are significantly decreased under low oxygen conditions, and that GluN1/GluN2C NMDAR currents are increased, due to alterations in the channel open probability (P_{open}). GluN2A and GluN2B subunits were not found to alter their properties in response to low to O_2 (Bickler et al. 2003). A reduction in P_{open} reduces the amount of Ca^{2+} entering the cell, thereby reducing depolarisation and potentially cell death signalling. High GluN2D expression is therefore thought to be an important mechanism for hypoxia resistance in neonatal mammals (Bickler et al. 2003; Peterson et al. 2012)

Neurons from turtles are able to survive long periods of anoxia: under these conditions, Ca^{2+}-dependent protein phosphatases have been found to play a critical role in regulating the open probability of NMDARs (Bickler and Buck 1998; Bickler et al. 2000). Another animal which has adapted to surviving under conditions of low oxygen is the naked mole-rat: these notably long-living, eusocial, and poikilothermic mammals live in low O_2, high CO_2 conditions due to sharing underground colonies with up to 300 other animals (Larson and Park 2009;

Schuhmacher et al. 2015). Much of the adaptation to survive in low oxygen conditions comes from their haemoglobin, which has a higher O_2 affinity than mice; from their low basal metabolic rate, which is further reduced during more intense periods of hypoxia (Schuhmacher et al. 2015); and the ability to switch to anaerobic metabolism pathway powered by fructose-driven glycolysis (Park et al. 2017). In addition, their NMDAR composition may also play a major role in this tolerance. In most mammals a developmental reduction in GluN1 expression (which reflects a reduction in NMDARs) occurs; an effect which is blunted in naked mole rats. However, whilst adult naked mole rats therefore have higher overall expression of NMDARs, they also retain far higher expression of GluN2D, which as outlined above is associated with hypoxia tolerance in neonatal mammals. As with other species, GluN2A expression is increased and GluN2B is decreased with development (Peterson et al. 2012). Interestingly, because GluN2D-containing NMDARs have different biophysical properties even under normoxic conditions in comparison with those containing other GluN2 subunits, a high expression of GluN2D in the naked mole rat might be expected to affect behaviour or cognition: however, naked mole-rats are able to learn operant conditioning tasks as well as rats (LaVinka et al. 2009). A similar profile of high adult GluN2D expression has also been measured in the subterranean mole rat, *spalax*, which also is highly adapted to similar low-oxygen conditions (Band et al. 2012).

During a 10 minute period of hypoxia, hippocampal neurons from naked mole-rats display an attenuated increase in internal Ca^{2+} concentration comparable to that observed in neonatal neurons from many mammalian species (Peterson et al. 2012). Hippocampal neurons from naked mole-rats are even able to recover fully from periods of anoxia exceeding 30 minutes. Low oxygen treatment (15 %) can cause unrecoverable disruption of synaptic activity after 40 minutes in 60 % of mouse neurons, whereas no disruption of synaptic activity is observed in the naked mole rat under the same conditions (Larson and Park 2009). Therefore the presence of GluN2D in neurons may confer a practical resistance to hypoxia-related excitotoxicity, something which may also apply to dopaminergic neurons within the SNc. One aim of this thesis was to explore the potential role of GluN2D in conferring resistance to hypoxia-mediated excitotoxicity using *Grin2D*-null mice.

1.3.2 Glutamate transporters: regulation of extracellular glutamate & NMDAR activity

Glutamate concentration at the synapse normally exceeds 1 mM for a period of less than 10 ms, before quickly returning to 20 nM or less due to glutamate reuptake by glutamate/aspartate (excitatory amino acid) transporters (GluTs; Clements 1996; Diamond and Jahr 1997; Shimamoto et al. 1998; Dzubay and Jahr 1999). The most accepted estimates of the concentration of glutamate in the extracellular space, away from the synapse, are in the range of 1-5 μM (Moussawi et al. 2011), and GluTs have a role in controlling diffusion of glutamate away from the synapse (McCullumsmith and Sanacora 2015), thereby preventing a loss of synaptic specificity and potential excitotoxicity. GluT activity may be important in human patients with PD, in which glutamatergic fibres from the STN fire at a much higher frequency (Magnin et al. 2000; Piallat et al. 2011; see section 1.3.3). GluT activity can be compromised in PD, and in several other neurodegenerative disorders including amyotrophic lateral sclerosis, Huntington's disease, and Alzheimer's disease. It is not clear whether glutamate dysfunction contributes to pathogenesis, or results from the disease pathology (Sheldon and Robinson 2007), but in either case GluTs are therefore considered to be potential therapeutic targets (Jensen et al. 2015).

In vivo pharmacological GluT inhibition in rat substantia nigra using DL-*threo*-β-Benzyloxyaspartate (TBOA) has been shown to generate a neurodegenerative process mimicking several PD symptoms, caused by excitotoxic cell death of dopamine neurons: this was mediated by NMDARs, as application of NMDAR antagonists ifenprodil and memantine provided significant neuroprotection (Assous et al. 2014). Other work in the SNc has shown that rat dopamine neurons are preferentially affected by GluT dysfunction when compared with non-dopamine neurons using the selective GluT inhibitor L-*trans*-Pyrrolidine-2,4-dicarboxylate (Nafia et al. 2008). SNc-DA neurons may be highly dependent on maintaining adequate levels of the essential brain antioxidant glutathione (GSH), and preferential toxicity for DA neurons by GluT inhibition may occur by decreasing the availability of GSH precursors such as cysteine, which are also directly transported by GluTs (Hayes et al. 2005; Nafia et al. 2008). Therefore susceptibility to oxidative stress caused by low GSH may be an additional factor in SNc-DA degeneration, in addition to the increased likelihood of glutamate-mediated excitotoxicity caused by GluT dysfunction.

In SNc-DA neurons, application of TBOA alone been shown to have no effect on the amplitude of elicited summated EPSCs (Wild et al. 2015). Whilst TBOA likely does bind to glutamate transporters, evidenced by a slower NMDAR response decay (which may indicate diffusion of glutamate further from the synapse), it was found that additional inhibition of presynaptic group II metabotropic glutamate receptors (mGluR2) by antagonist LY 341495 was necessary to allow a TBOA-induced increase in amplitude. Application of LY 341495 alone had no effect (Wild et al. 2015). Presynaptic feedback mechanisms therefore exist at excitatory synapses onto SNc-DA neurons which limit glutamate release in situations where spillover is likely, or where extracellular concentration of glutamate is likely to reach excitotoxic levels. One aim of this thesis was to explore the role of TBOA in regulating NMDAR activity, and whether this was altered in mice lacking the GluN2D subunit.

1.3.3 Pathophysiology of Parkinson's disease

Parkinson's disease (PD) is a neurodegenerative disease characterised by inhibited motor control, including bradykinesia, muscle rigidity, and tremor (Bolam et al. 2000; Shulman et al. 2011; Surmeier et al. 2017). Many of the motor manifestations of PD are attributed to the progressive loss of SNc-DA neurons (Hammond et al. 2007), which form part of the basal ganglia system, discussed in section 1.4. Lewy pathology is also a commonly observed characteristic of PD: this comprises abnormal, proteinaceous aggregates in the neuronal cytoplasm that are rich in α-synuclein. However, LP also occurs in other age-related neurodegenerative diseases, with its precise relationship to disease progression remaining unclear (Surmeier et al. 2017). Previous studies have observed morphological changes to SNc-DA neurons in human Parkinson's patients, including reductions in dendritic branching and partial loss of dendritic spines (Patt et al. 1991), which may be in response to abnormal neuronal function.

In PD, one neurophysiological change is that glutamatergic afferents originating from the subthalamic nucleus (STN) to dopaminergic neurons of the SNc reportedly display a higher frequency firing, as well as increased burst firing. This was originally observed in primates after treatment with MPTP (a compound with preferential toxicity for nigrostriatal dopaminergic neurons; Bergman et al. 1994), and electrophysiological recordings have

subsequently been gathered from human patients undergoing surgery for deep brain stimulation (DBS; Magnin et al. 2000). Whilst this kind of data is not obtainable from healthy human subjects, control recordings have been possible from patients with other neurological disorders: one study showed that patients with severe obsessive-compulsive disorder (OCD) had a mean STN neuron firing rate of 20.5 Hz, with a mean discharge frequency during bursting phases of 50.9 Hz. In comparison, PD patients had an overall mean of 30.8 Hz, with a much higher mean during burst frequency of 83.4 Hz (Piallat et al. 2011). Other studies showed that late stage PD patients had a higher mean firing frequency than early stage PD patients (28.7 vs 36.3 Hz; Remple et al. 2011), and that PD patients had a higher mean firing (40.5 Hz) frequency in comparison to those with essential tremor (ET; 19.3 Hz) (Steigerwald et al. 2008).

A consequence of this increased bursting activity is likely to be increased NMDAR activity due to increased glutamate release and NMDAR-EPSC summation, as well as increasing the likelihood of spillover of glutamate from the synapses and activating perisynaptic or extrasynaptic NMDARs: this pathological STN activity may therefore promote excitotoxicity in SNc-DA neurons (Bergman et al. 1994; Wild et al. 2013). Activity-dependent rundown or downregulation of NMDARs in response to repeated agonist application may be a response to such activity, and consequently one of the aims of this thesis was to explore this idea.

As stated above, PD is characterised by the progressive loss of SNc-DA neurons, and proper NMDAR regulation may be important for neuronal function and survival under these conditions. The sensitivity of a neuron to excitotoxicity is determined by several factors relating to NMDARs, such as the surface localisation of the receptor (Hardingham and Bading 2010), the subunit profile (Liu et al. 2007; Martel et al. 2012), and the ability of NMDARs to be regulated in an activity-dependent manner (Wild et al. 2014). Firstly, with regards to surface localisation, several studies have reported that sole activation of synaptic NMDARs is able to promote downstream cell survival pathways, such as activation of cAMP-responsive element binding protein (CREB); and that additional activation of the functionally separate population of extrasynaptic NMDARs is able to activate cell death pathways, for example by activation of protease enzyme caspase-3 (Liu et al. 2007; Zhou et al. 2013). In the hippocampus, around 36% of NMDARs are extrasynaptic, and in the SNc a minimum of around 10 % are extrasynaptic, though this figure likely to be higher (Wild et al. 2015). High

frequency or burst firing may enable released glutamate to 'spill over' from the synapse (Rosenmund et al. 1995; Asztely et al. 1997; Clark and Cull-Candy 2002; Harris and Pettit 2007, 2008) and additionally bind to extrasynaptic NMDARs, promoting cell death (Hardingham and Bading 2010; Zhou et al. 2013; Parsons and Raymond 2014). Whilst the processes underlying the death of SNc-DA neurons in PD are not fully understood, the increased excitatory input to these neurons, discussed above, may lead to NMDAR-mediated excitotoxicity: this is therefore implicated as a contributing factor to the ongoing degeneration in occurring in PD (Koutsilieri and Riederer 2007; Blandini 2010). With regards to subunit profile, there is evidence that the GluN2D subunit may be a mediator of excitotoxicity: its low Mg^{2+} sensitivity may allow it to pass more current in response to glutamate spillover (Paoletti et al. 2013), and GluN2D-containing NMDARs have been implicated as extrasynaptic mediators of cell death signalling, which are therefore a good target for inhibition (Kotermanski and Johnson 2009; Hardingham and Bading 2010). SNc-DA neurons are thought to possess NMDARs in a triheteromeric GluN1/GluN2B/GluN2D configuration (Jones and Gibb 2005; Brothwell et al. 2008; Suárez et al. 2010). With regards to activity-depended regulation, due to the clear role for NMDARs in mediating potentially excitotoxic influxes in Ca^{2+} under conditions of overstimulation, it follows that a responsive regulation of NMDARs could be an essential mechanism for maintaining equilibrium in postsynaptic excitability: this is relevant both as a response to natural alterations in excitatory input, and potentially in responding to more pathological changes in glutamatergic input. NMDARs may therefore be regulated in response to these changes in order to maintain Ca^{2+} homeostasis and prevent excitotoxicity, or simply overexcitability (Sandoval et al. 2011; Semerdjieva et al. 2013; Wild et al. 2014). It is possible that this is a mechanism which may be tested to its limit in neurodegenerative illness.

1.4 The role of the substantia nigra pars compacta and basal ganglia

The SNc, located in the midbrain, contains both γ-aminobutyric acid (GABA)-ergic and dopaminergic neurons. It is a part of the basal ganglia, which are a group of functionally and anatomically interconnected subcortical nuclei consisting of the striatum (caudate and putamen in primates), the globus pallidus (internal and external segments), the subthalamic

nucleus, and the substantia nigra (pars reticulata and pars compacta); which together have a major role in the control of voluntary movement (Nelson and Kreitzer 2014). The basic anatomy and connectivity of the basal ganglia are preserved across most vertebrates, and all mammals (Reiner et al. 1998; Stephenson-Jones et al. 2012), making rodent data obtained from this system highly relevant to humans. The basal ganglia system in mammals is more advanced than that observed in birds and reptiles, with considerably more highly developed output to the cortex, which contributes to the capacity for more sophisticated behaviours (Reiner et al. 1998).

The primary inputs to the basal ganglia come from the striatum and STN. The striatum, composed primarily of GABAergic medium sized spiny projection neurons, receives input from almost all areas of the cortex, which can mediate sensorimotor, cognitive, and affective (emotional) functions (Redgrave et al. 2010; Nelson and Kreitzer 2014). The striatum also receives excitatory input from the thalamus, and from dopaminergic SNc and ventral tegmental area (VTA) neurons. Striatal medium spiny neurons can be divided into two groups based on their projections: around half project directly to basal ganglia output nuclei (SNr or globus pallidus pars interna; GPi) forming the direct pathway, and half project to the globus pallidus pars externa (GPe) which then projects to the output nuclei, forming the indirect pathway (Nelson and Kreitzer 2014). The other input nucleus to the basal ganglia, the STN, receives cortical input from the primary motor, supplementary motor, and premotor cortices (Nambu et al. 1996; Nelson and Kreitzer 2014), and sends glutamatergic efferents to the basal ganglia output nuclei, and the SNc (Parent and Hazrati 1995; Watabe-Uchida et al. 2012). An overview of connections within the basal ganglia is presented in **Figure 1.3**.

Inputs from the cortex are processed by the basal ganglia, and then relayed back to the cortex via the motor thalamus (Albin et al. 1989; Blandini et al. 2000; Kopell et al. 2006). Uniquely, the basal ganglia are dominated by tiers of inhibitory GABAergic neurons. However, the output of the basal ganglia is tonically active and exhibits phasic pauses in association with movement (Surmeier et al. 2005): the balance between direct and indirect pathways is regulated by the opposing actions of dopamine released from SNc-DA afferents onto striatal neurons. DA release in the striatum increases activity along the direct pathway (acting on D1 receptors) and reduces activity along the indirect pathway (acting on D2 receptors). Together

increased activity in SNc-DA neurons will result in a net reduction in activity within the GPi and SNr (DeLong and Wichmann 2007).

According to the pathophysiological 'rate' model of PD, direct pathway neurons reduce their firing frequency, whereas those in the indirect pathway increase their activity in response to a reduction in dopamine transmission. As a result, firing in GPe neurons is reduced leading to further disinhibition of STN neurons, and promoting excitation of STN targets (SNc, SNr, and GPi). The outcome of these changes is that the basal ganglia exert increased inhibition on their thalamic and brainstem targets (Galvan et al. 2015).

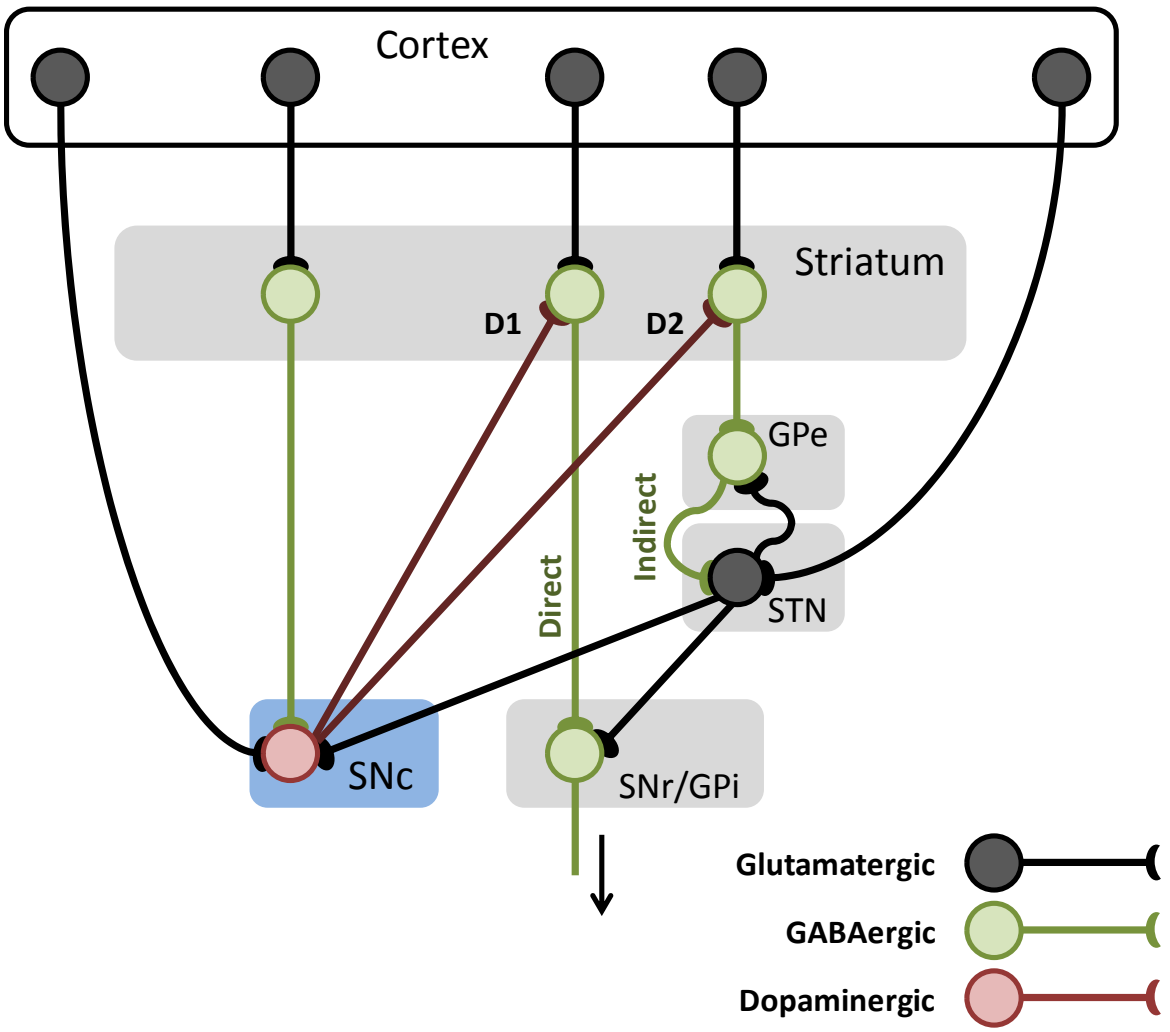

Figure 1.3 – The SNc and basal ganglia

A simplified diagram of the basal ganglia (BG) system. The substantia nigra pars compacta (SNc) receives excitatory input from the cerebral cortex and subthalamic nucleus (STN), and releases dopamine in the stratum, which has opposing actions on the direct and indirect pathways to the output nuclei. DA release in the striatum increases activity along the direct pathway (acting on D1 receptors) and reduces activity along the indirect pathway (acting on D2 receptors). Increased activity in SNc-DA neurons results in a net reduction in activity within the globus pallidus pars interna (GPi; entopeduncular nucleus in rodents) and substantia nigra pars reticulata (SNr; DeLong and Wichmann 2007). Thalamic connections not pictured. Diagram adapted from Watabe-Uchida et al. 2012.

1.4.1 Dopaminergic neurons of the substantia nigra pars compacta

As part of their role in the regulation of voluntary motor control, SNc-DA neurons display tonic or pacemaker firing activity in the range of 4-10 Hz, but when excited will modulate into periods of high frequency burst firing (Wilson et al. 1977; Blythe et al. 2009). Tonic activity in SNc-DA neurons maintains a low level of DA in the striatum, while the phasic increases in firing promote nigrostriatal DA release activating low affinity D1 receptors, which are essential to the initiation of movement (Surmeier et al. 2005). In addition, this tonic release of DA is essential for glutamatergic corticostriatal induction of Hebbian bidirectional long term plasticity in the striatum: pauses in the activity of giant cholinergic interneurons elicited by phasic burst firing events in afferent fibres from SNc-DA neurons are thought to generate a learning signal in the striatum (Graybiel et al. 1994; Blythe et al. 2009). In models of PD, decreased tonic striatal DA levels throw this system out of balance, leading to unidirectional changes in plasticity which could cause PD-associated symptoms (Centonze et al. 2001; Shen et al. 2008).

SNc-DA neurons are characterised by a particular combination of features: broad action potentials spikes, slow rhythmic (2–10 Hz) autonomous pacemaker activity accompanied by large oscillations in intracellular Ca^{2+}, driven by the opening of voltage-dependent L-type Ca^{2+} channels; and low levels of Ca^{2+}-buffering proteins such as calbindin. These features together distinguish SNc-DA neurons from others less vulnerable in PD. DA neurons within the VTA, for example, show much less PD-related cell death: these neurons are autonomous pacemakers with broad spikes, but have smaller L-type Ca^{2+} channel currents and strong intrinsic Ca^{2+} buffering by calbindin (Surmeier et al. 2017). Glutamatergic inputs to the SNc originate mainly from the subthalamic nucleus (STN) and pedunculopontine nucleus (PPN), but also from the laterodorsal tegmentum and prefrontal cortex (Kita and Kitai 1987; Charara et al. 1996; Tong et al. 1996; Watabe-Uchida et al. 2012; Pearlstein et al. 2015).

Previously, there was a lack of clear evidence for functioning dendritic spines in SNc-DA neurons, and so they have been classically regarded as aspiny. However, recent studies have explored the morphology and functionality of spines on SNc-DA neurons in detail using two-photon confocal microscopy and glutamate uncaging in mouse brain slices (Jang et al. 2015;

Hage et al. 2016). Both spine synapses and shaft synapses are present, but only one third of the total number of synapses are spiny. In comparison to the shaft synapses, spine synapses on SNc-DA neurons have lower EPSC amplitudes and longer decay times, as well as lower AMPAR/NMDAR-EPSC amplitude ratios, which together indicate a greater number of NMDARs at spiny synapses (Jang et al. 2015). Interestingly, when the authors stimulated with 5 consecutive burst pulses, the decay time at spiny synapses was significantly increased in comparison to the increase in amplitude, which may be due to receptor saturation and glutamate spillover, or potentially a difference in NMDAR subunit composition. Therefore, it is possible that these two synapse types may function differently if they receive bursting input from glutamatergic afferents.

1.5 Aims of this thesis

NMDARs present in the membrane of SNc-DA neurons are involved in the maintenance of tonic excitability, thereby contributing to normal basal ganglia output; and are essential in effecting long term plasticity at the synapse in many cells across the brain. Previous work suggests the presence of the GluN2D subunit in adult SNc-DA neurons: however, this is largely based on pharmacological compounds with limited selectivity. Therefore, a mouse genetically engineered to lack expression of GluN2D (*Grin2D*-null) was used to investigate GluN2D expression profiles along with additional pharmacological intervention using GluN2B and GluN2D subunit-preferring antagonists, ifenprodil and DQP-1105. The importance of GluN2D in the sensitivity of SNc-DA neurons to ambient extracellular glutamate was explored in the *Grin2D*-null mouse under normal conditions, and under conditions where glutamate transport was compromised, such as may occur in neurodegenerative disease.

NMDARs on SNc-DA neurons have been shown to respond to repeated application of agonist (NMDA) with downregulation. Glutamatergic neurons originating in the STN and terminating on SNc-DA neurons increase their mean firing frequency and peak burst firing frequency in PD. Therefore, activity-dependent downregulation was explored at the synapse in response to electrically evoked burst firing of excitatory fibres along with postsynaptic depolarisation.

The same paradigm was applied in *Grin2D*-null animals in order to elucidate whether any changes were dependent on the presence of the GluN2D subunit.

Because GluN2D-containing NMDARs decrease their P_{open} in response to low O_2, it was also of interest to explore whether the presence of GluN2D in SNc-DA neurons conferred any resistance to hypoxia-related excitotoxicity: a previously tested hypoxic treatment protocol was applied along with immunofluorescent staining and a cellular viability assay in both wild type and *Grin2D*-null animals.

Together, the work in this thesis aimed to build a picture of the functional NMDAR expression profile in SNc-DA neurons, along with how they and the GluN2D subunit allow these neurons to react to various potentially excitotoxic conditions such as inhibited glutamate reuptake, increased excitatory burst input, and hypoxia-ischemia.

CHAPTER 2

MATERIALS AND METHODS

2 Materials and Methods

2.1 Animals

C57BL/6 ('C57') mice were obtained from Charles River UK. *Grin2D*-null and *Grin2D* wild type (WT) mice were bred in house from *Grin2D* +/- mice obtained from the Masayoshi Mishina c/o the Riken BRC, Japan, and crossed with each other or with C57 mice to generate both *Grin2D* -/- ('*Grin2D*-null') and WT mice ('*Grin2D*-WT') on the same background. The mutant line was originally generated by disruption of the exon encoding the GluN2D transmembrane M4 region by insertion of a neomycin phosphotransferase gene (Ikeda et al. 1995).

All experiments were performed using these animals at P5-48 as indicated in the text, and were carried out in accordance with the United Kingdom Animal (Scientific Procedures) Act 1986 Amendment Regulations 2012, and local ethical approval. Up to 8 mouse pups were housed with the dam in each cage. All animals were provided with *ad libitum* access to food and water, and kept on a 12 hour alternating light/dark cycle. The mice were genotyped from crude tail tissue sample lysates using the following primer set: GluR4 WT F 5'-GTGCTCCTAATAAGTGACTCTGA-3' and GluR4 WT R 5'-CCTCCTCGCTCCCTTTCTT-3' produce a 289 bp product for the WT locus; NeoF 5'-CGGTGCCCTGAATGAACT-3' and NeoR 5'-CACGGGTAGCCAACGCTATG-3' produce a 618 bp product for the mutant locus; see **Figure 2.1**. Samples were outsourced for genotyping to the Andrew Huxley Genotyping Facility, University College London.

2.2 Brain slice preparation

Animals were anaesthetised using isoflurane until the loss of the withdrawal reflex in response to a foot pinch, before decapitation. The brain was then extracted into ice-cold slicing solution composed of (mM) NaCl 52.5, $NaHCO_3$ 25, KCl 2.5, NaH_2PO_4 1.25, kynurenic acid 0.1, glucose 25, sucrose 100, $CaCl_2$ 1, and $MgCl_2$ 5, saturated with 95 % O_2 /

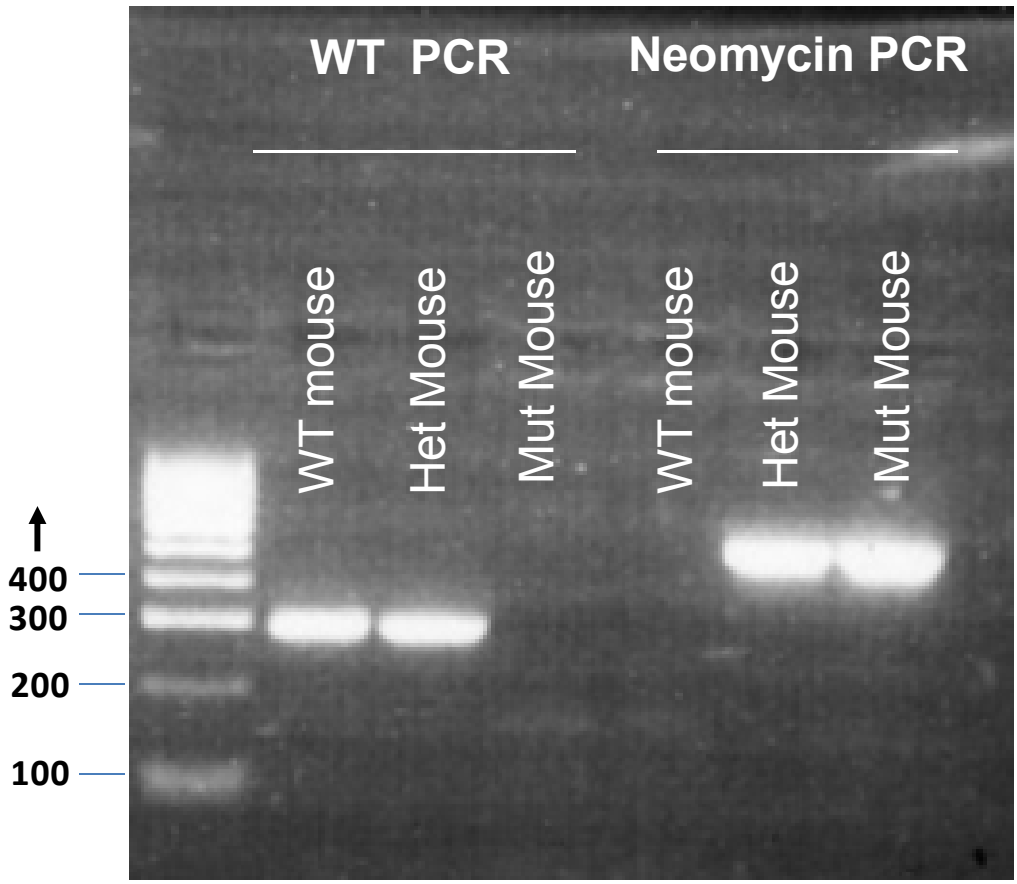

Figure 2.1 – Genotyping of *Grin2D*-wild type and *Grin2D*-null mice

An example electrophoresis gel showing PCR products from genotyping of homozygous *Grin2D*-wild type (WT), heterozygous, and homozygous *Grin2D*-null (Mut) mice, alongside HyperLadder™ 100 bp molecular weight markers from Bioline (London, UK).

PCR reactions were performed using crude tail tissue sample lysates using the following primer set: GluR4 WT F 5'-GTGCTCCTAATAAGTGACTCTGA-3' and GluR4 WT R 5'-CCTCCTCGCTCCCTTTCTT-3' produce a 289 bp product for the WT locus; NeoF 5'-CGGTGCCCTGAATGAACT-3' and NeoR 5'-CACGGGTAGCCAACGCTATG-3' produce a 618 bp product for the mutant locus.

5 % CO_2 at pH 7.4. The brain was trimmed and glued to the stage of a 7000smz-2 vibrating microslicer (Campden Instruments, Loughborough, UK). Horizontal slices including the substantia nigra region (**Figure 2.2A**) were prepared at a thickness of 230 µm (unless specified), and immediately transferred into a Gibb submersion chamber containing (mM): NaCl 119, $NaHCO_3$ 26, KCl 2.5, NaH_2PO_4 1.25, glucose 25, $CaCl_2$ 2, and $MgCl_2$ 6, saturated with 95 % O_2 / 5 % CO_2 at 30 °C, for 1-6 hours prior to use.

2.3 Electrophysiology

Slices were transferred to a chamber, held in place with a platinum and nylon net and perfused with (mM) NaCl 119, $NaHCO_3$ 26, KCl 2.5, NaH_2PO_4 1.25, glucose 10, $CaCl_2$ 2, and $MgCl_2$ (1 or 0.1) saturated with 95 % O_2 / 5 % CO_2 at 30±2 °C (TC-344B temperature controller, Warner Instruments, Hamden, CT, USA), before being visualised using an Olympus BX51W microscope with differential interface contrast optics.

Whole-cell patch-clamp recordings were made using borosilicate glass micropipettes (Harvard Apparatus, Holliston, MA, USA) prepared using a Sutter P-87 micropipette puller to a resistance of 2-3 MΩ when filled with intracellular solution composed of [mM]: $CsMeSO_3$ 120, CsCl 5, NaCl 2.8, $MgCl_2$ 3, HEPES 20, ATP [Adenosine 5′-triphosphate magnesium salt] 2, GTP [Guanosine 5′-triphosphate sodium salt hydrate] 0.3, EGTA 5, and $CaCl_2$ 0.5, giving a final osmolality of 275-285 mOsmoles/kg. The final pH was adjusted to 7.2-7.3 using CsOH, and the solution passed through a 0.2 µm filter.

Signals were low-pass filtered at 2-3 kHz, and digitised at 20 kHz using a Micro1401 interface (Cambridge Electronic Design, Cambridge, UK). Cells were voltage clamped potentials of -60, -50, -20, or +40 mV as indicated in the text, using HEKA Pulse v8.53 software along with a EPC9 amplifier (HEKA, Hamden, CT, USA). Signals were stored and measured using Spike2 version 4 (Cambridge Electronic Design, Cambridge, UK). Series resistance (R_{series}) was estimated using the HEKA Pulse software, and was typically within the range 3.5-10 MΩ: however, the experiment was abandoned if a change of more than 3 MΩ was observed.

The SNc region was identified under low magnification (**Figure 2.2A**), and SNc dopamine neurons by somatic morphology (large ovoid or polygonal soma; Tepper et al. 1994; **Figure 2.2B**) and anatomical location relative to the medial terminal nucleus of the accessory optic tract (MT), which is identifiable by its expression of melanin and therefore dark appearance. Dopaminergic status was confirmed by the presence of a non-specific cation current (Ih) measured as a sag component of at least 40 pA (**Figure 2.2C**), in response to a voltage step from -60 to -110 mV. This current is a key electrophysiological marker of dopamine neurons within the SNc, and is mediated via hyperpolarization-activated cyclic nucleotide–gated (HCN) channels (Neuhoff et al. 2002).

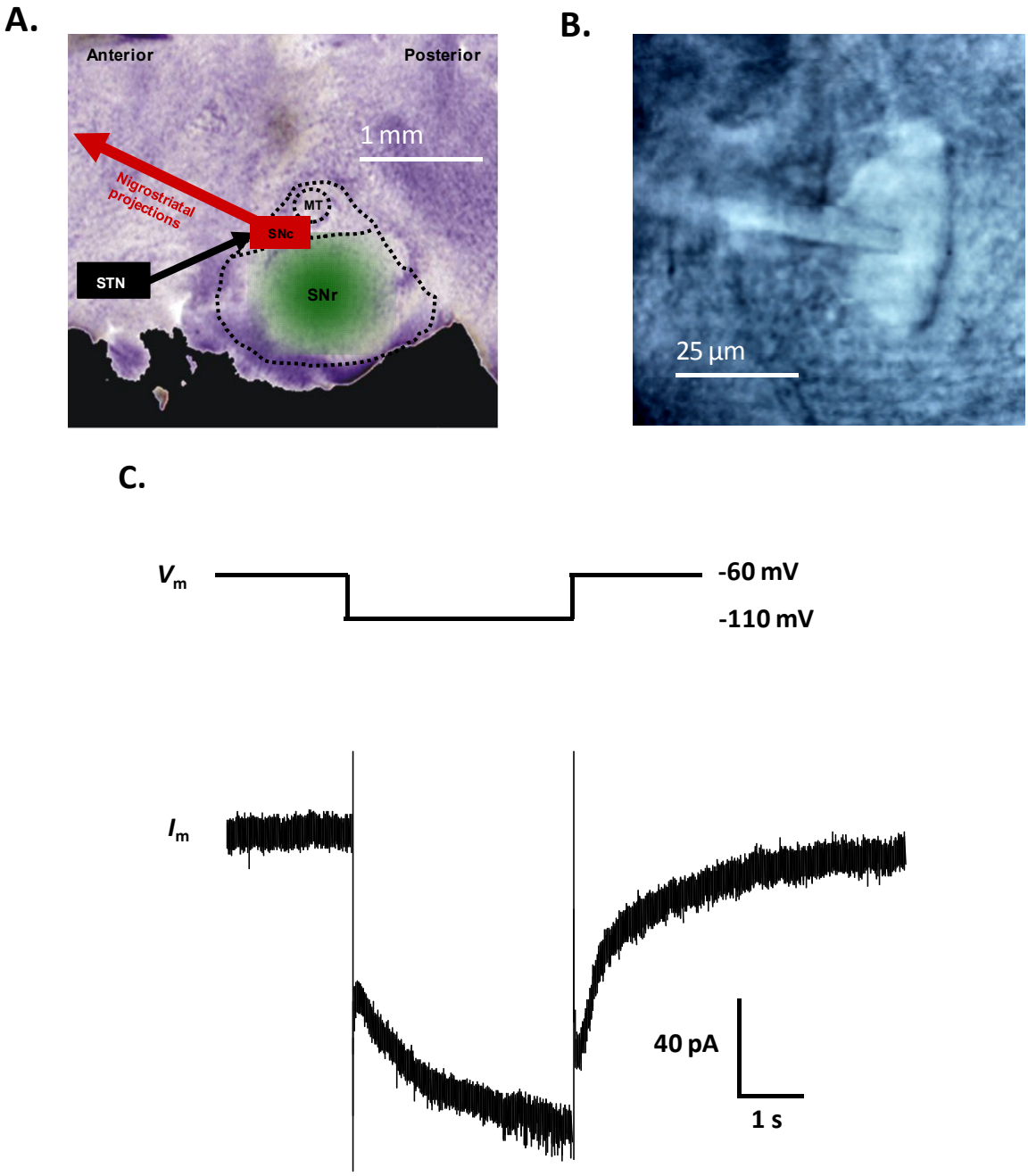

Figure 2.2 – Identification of SNc-DA neurons

(A) Horizontal brain slices containing the substantia nigra were freshly prepared from C57Bl6 (wild type) or *Grin2D*-null mice at the age specified. (B) Whole cell patch clamp electrophysiology was used to record NMDAR responses from dopaminergic neurons of the substantia nigra pars compacta. (C) Current response to holding potential change from -60 to -110 mV in a dopaminergic neuron within the substantia nigra pars compacta region. Trace taken from a wild type mouse at P18; amplitude of the 'sag' component during the -110 mV holding period is 56 pA.

2.4 Experimental design

2.4.1 NMDAR-mediated current

Peak currents generated by NMDARs across the whole cell were elicited by bath applications of NMDA at the concentration specified in the text, in the presence of picrotoxin (50 μM), glycine (10 μM), and TTX (100 nM). Currents elicited by ambient extracellular glutamate via NMDARs were measured (with or without TTX at 100 nM) by obtaining a stable baseline current in picrotoxin (50 μM) and glycine (10 μM), before applying NMDAR blocker D-(-)-2-Amino-5-phosphonopentanoic acid (D-AP5; 50 μM) and measuring the amplitude of the resulting deflection. Changes in current amplitude resulting from inhibition of glutamate reuptake were explored by applying the competitive glutamate transporter blocker TBOA (30 μM) along with group II metabotropic glutamate receptor antagonist LY 341495 (200 nM), and the NMDAR-mediated potion of this isolated by then applying D-AP5 as above.

When applying electrical stimulation, stainless steel electrodes (Frederick Haer and Co., USA) were placed rostral to the cell to optimize the possibility of stimulating afferent glutamatergic fibres, and the intensity varied in order to ensure a graded excitatory postsynaptic current (EPSC), before being fixed at a submaximal intensity (pulse duration 100 μs; amplitude 30-250 μA) for the duration of the experiment.

To determine the ratio of AMPAR/NMDAR (A/N) EPSC amplitude, picrotoxin (50 μM) and glycine (10 μM) were added to the perfusion. Cells were held at +40 mV to bypass voltage-dependent Mg^{2+} blockade ($MgCl_2$ 1 mM) of NMDARs, and EPSCs of a stable amplitude elicited at 0.1 Hz for at least 200 s before addition of D-AP5 (50 μM) to the perfusion, leaving the AMPAR-EPSC. At least 10 traces immediately before, and 10 traces in the presence of D-AP5 were averaged using Spike2. The +D-AP5 trace ('AMPAR-EPSC') was subtracted from the pre-D-AP5 trace ('total-EPSC') using Microsoft Excel to give the NMDAR-EPSC (**Figure 2.5)** Peak amplitudes of each component were measured within the period 8-15 ms following the stimulus artifact (**Figure 2.3**).

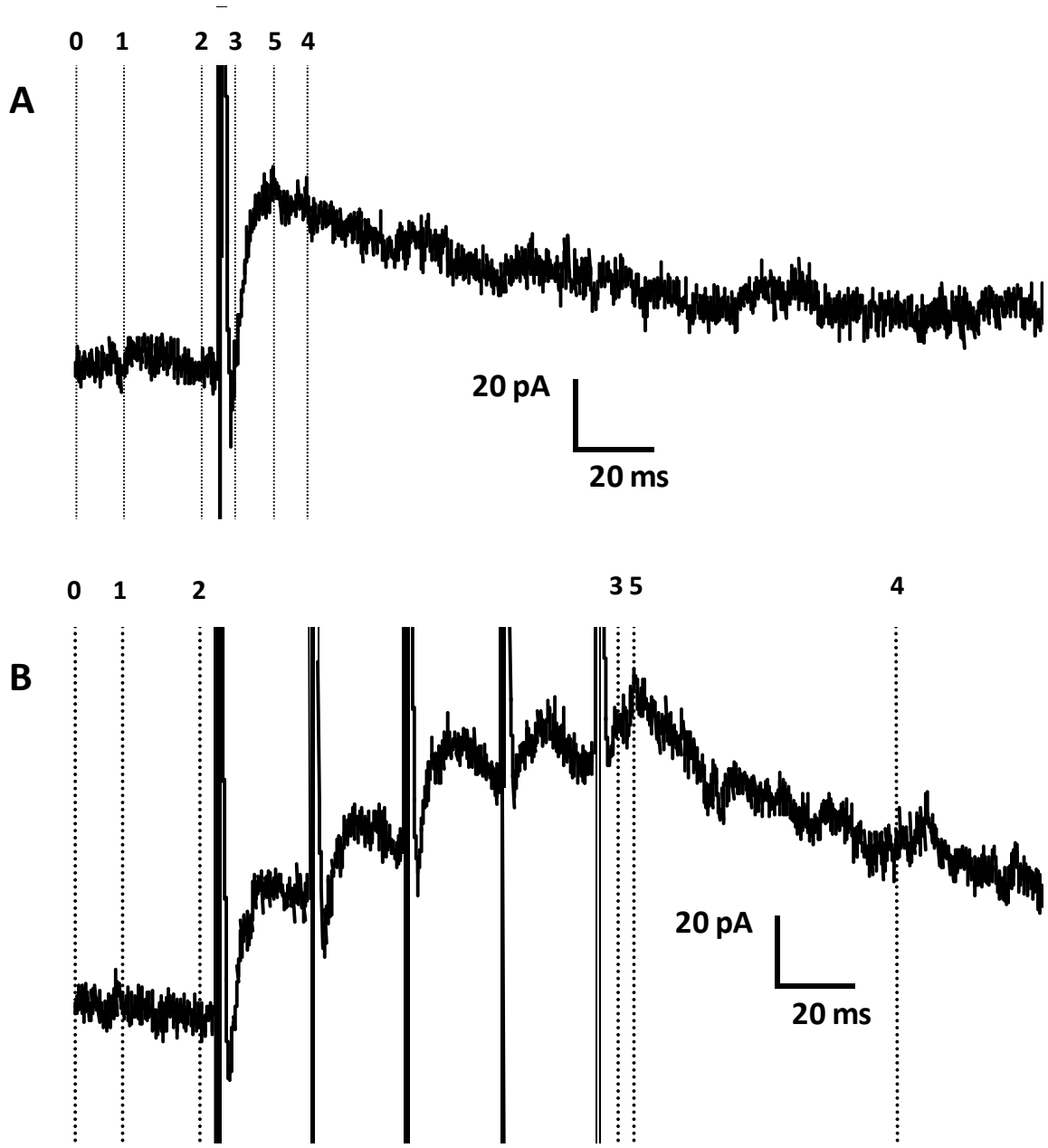

Figure 2.3 – Measurement of single and summated EPSCs

(A) Example single NMDAR-EPSC at a holding potential of +40 mV, elicited by a single pulse stimulation of afferent glutamatergic fibres. Amplitudes are extracted using Spike2 v4 software, with the pre-EPSC baseline value taken as the mean of all values recorded between cursor 1 and 2, and the peak EPSC amplitude as the mean of the 1 ms period around the highest value between cursors 3 and 4, as indicated by cursor 5. (B) Example summated NMDAR-EPSC at a holding potential of +40 mV, elicited by a train of five stimulations of afferent glutamatergic fibres at 50 Hz. Amplitudes are calculated as in A, but with different time values specified for cursors 3 and 4.

For experiments evaluating pharmacological inhibition of synaptic NMDAR currents, the patched cell was held at +40 mV to avoid Mg^{2+} block, and EPSCs elicited at 0.1 Hz with picrotoxin (50 μM), glycine (10 μM), and AMPA and kainate receptor selective antagonist 6,7-dinitroquinoxaline-2,3-dione (DNQX; 10 μM) applied via bath perfusion. Once a stable NMDAR-EPSC amplitude was obtained, either GluN2B-selective inhibitor ifenprodil (10 μM) or GluN2D-selective inhibitor DQP-1105 ('DQP'; 10 μM) was applied via the bath perfusion, and stimulation continued for a further 15-20 minutes. NMDAR-EPSC amplitude within the period between 13-20 minutes following ifenprodil/DQP application was compared to the pre-drug amplitude to determine the percent inhibition.

For measurement and comparison of EPSC decays, 6-10 EPSCs at 0.1 Hz in the presence of picrotoxin (50 μM), glycine (10 μM), and DNQX (10 μM) were averaged, and a two-component exponential decay function fitted to the EPSC decay using WinWCP version 5.3.2 as below:

$$y(t) = A1 \cdot e(-t/\tau 1) + A2 \cdot e(-t/\tau 2)$$

Where, respectively, A1 and A2 are the fast and slow component amplitudes, and τ1 and τ2 are the fast and slow time constants (Stocca and Vicini 1998; Brothwell et al. 2008; Wild et al. 2015).

To determine activity-dependent regulation of electrically evoked NMDAR responses, picrotoxin (50 μM), glycine (10 μM), and DNQX (10 μM) were added to the perfusion. Membrane holding potential was set to +40 mV to avoid Mg^{2+} block and in order to reduce the driving force for Ca^{2+} influx, and EPSCs were elicited by application of single stimuli (to activate synaptic NMDARs) or short high frequency (50 Hz) trains of stimuli (to activate synaptic and also potentially extrasynaptic NMDARs; **Figure 2.4**). After a stable baseline of at least 300 s, the holding potential was changed to -20 mV, increasing the driving force for Ca^{2+} influx whilst still alleviating Mg^{2+} block, and a protocol of patterned activity (trains of 3 pulses at 100 Hz, each followed by a 1 s break) initiated. This induction paradigm (IP) was adapted from Joshi et al. 2007, where it was shown to induce a downregulation in synaptic NMDARs. On completion, holding potential was returned to +40 mV and single and 50 Hz pulses continued. For analysis of EPSC amplitudes, mean amplitudes of ten single EPSCs and four summated EPSCs (taken here to refer to the EPSCs generate in response to trains of

stimuli at 50 Hz, **Figure 2.3**) were taken immediately preceding the onset of the patterned activity, and then for 25 minutes (1500 seconds) following.

Paired pulse data was also extracted from the summated NMDAR-EPSC data: the first two EPSCs (p1 and p2) generated from the train of five electrical stimuli at 50 Hz were collected and the paired pulse ratio (PPR; p2/p1) calculated. Four pairs of EPSCs generated 20 ms apart were therefore collected from immediately before the onset of the patterned activity protocol and used to generate an average waveform and PPR: The pairs of EPSCs generated between 1200-1500 s following the end of the protocol were also averaged and the PPR compared to that from before the patterned activity.

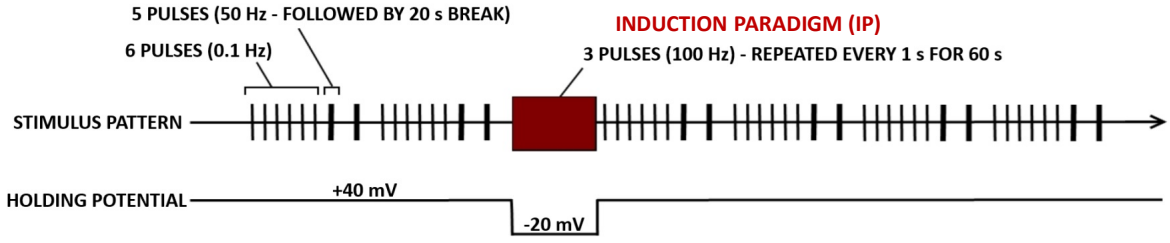

Figure 2.4 – Paradigm for determining activity dependent regulation of NMDARs

"Induction paradigm" (IP; red) applied to glutamatergic afferent fibres in order to evoke activity-dependent changes in synaptic (single stimulus; indicated by thin vertical line) and synaptic + extrasynaptic NMDAR responses (5 stimulus pulses at 50 Hz; thick vertical line).

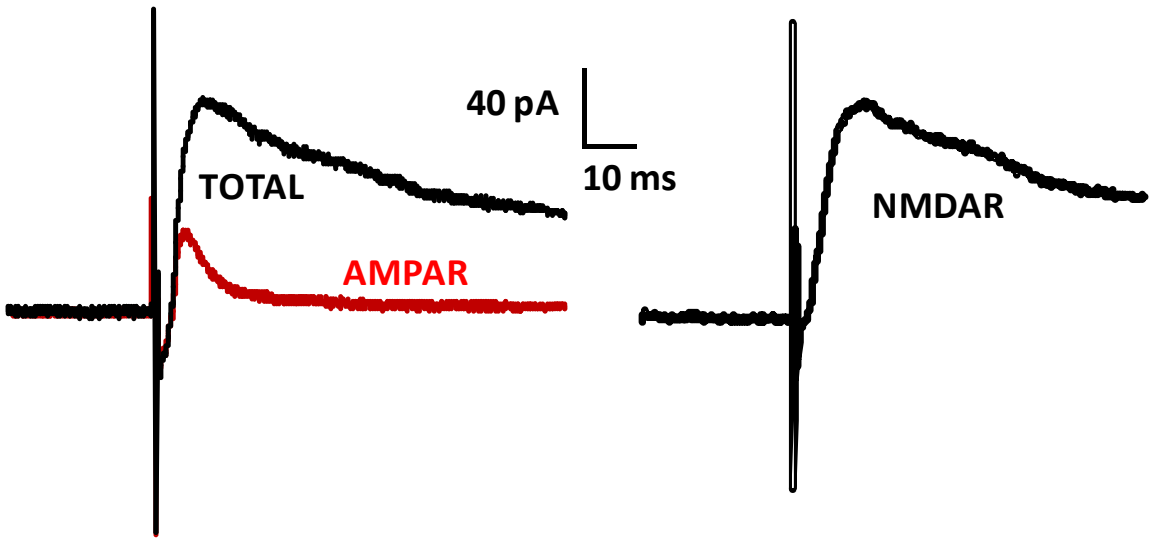

Figure 2.5 – AMPAR/NMDAR EPSC amplitude ratio methodology

On the left is an example trace from a wild type SNc-DA neuron, showing excitatory postsynaptic current (EPSC) in response to electrical stimulation before (black - TOTAL) and after (red - AMPAR) the application of D-AP5 (50 μM). On the right is the resultant NMDAR EPSC calculated by subtracting the AMPAR EPSC from the TOTAL EPSC.

2.4.2 Hypoxic treatment protocol and immunofluorescence

The hypoxia treatment protocol was adapted from Larson and Park 2009 and Tasca et al. 2015. Horizontal slices through the substantia nigra region were carefully made as described above ('*Brain slice preparation*') at a thickness of 100 µm. For each slice produced, a cut was made along the midline and one hemisphere randomly assigned to a high oxygen (normoxic) treatment group, and one to a hypoxic treatment group (below). Previous studies have shown that in mice, treatment with 15% O_2 / 80% N_2 / 5% CO_2 as a hypoxic condition for 20-40 minutes causes a submaximal effect whereby only 60% of cells show functional recovery after 95% O_2 / 5% CO_2 is restored (Larson and Park 2009). Therefore this concentration was chosen as a submaximal effect is desirable for comparison between genotypes.

Following a 40 minute recovery in normoxic conditions (gassed with 95% O_2 / 5% CO_2) slices in both groups were transferred to new Gibb submersion chambers for a 40 minute treatment period: the normoxic group to a new chamber gassed again with 95% O_2 / 5% CO_2, and the hypoxic group to a chamber gassed with 15% O_2 / 80% N_2 / 5% CO_2. The slices in both groups were then carefully transferred back to their original, separate normoxic chambers, and 20 mM fluorescent propidium iodide (PI) was added to the chamber (0.5 mL of 4 mM stock per 100 mL chamber; Lossi 2009). After 20 minutes, all slices were briefly and gently washed twice in Krebs buffer composed of NaCl 126 mM; KCl 2.5 mM; $MgCl_2$ 1.2 mM; $CaCl_2$ 2.4 mM; $NaHCO_3$ 25 mM; NaH_2PO_4 1.2 mM; and glucose 11 mM (Pisani et al. 2006), before being stored in darkness in a vial containing 4% paraformaldehyde (PFA) in phosphate-buffered saline (PBS; Sato et al. 2011). After four hours, slices were PBS containing 0.1 M glycine for 5 minutes to bind free aldehyde groups (Jamur and Oliver 2010), before three more 5 minute washes in PBS. These and all subsequent washes and incubations were performed on a rotating shaker. Slices were then transferred into a permeation / blocking solution (1% w/v fish gelatine in TBS-T, containing 0.2% Tween-20 and 0.2% Triton X100) for 30 minutes at room temperature, before three washes each lasting 15 minutes in TBS (Tris 50 mM, NaCl 150 mM).

For immunological staining, slices were incubated in primary antibody (rabbit anti-TH polyclonal Ab, Millipore AB152, 1:500 in TBS) overnight, and washed three times (15

minutes each) in TBS. Slices were then incubated in the secondary antibody, (Alexa-fluorophore 488 nm, donkey anti-rabbit, Thermo Fisher A21206, 1:500 in TBS) for 90 minutes, followed by three 15 minute washes in TBS.

For viewing and quantification, each hemislice was placed in PBS on the stage of an Olympus BX51W microscope with differential interface contrast optics and optional green/red optical emission filters. The SNc was visually identified by proximity to MT and then scanned systematically using an excitation wavelength of 470 nm in order to count all TH+ cells. For each TH+ cell observed, the excitation wavelength was switched to 565 nm in order that the PI status of each cell could be recorded.

2.5 Statistical analysis

Unless otherwise specified, reported n values are each from a different animal.

In comparing samples from two groups of data, the Student's t-test was used: if any groups were found to be non-normally distributed (using the D'agostino-Pearson Omnibus K2 test), then a paired t-test was replaced with the Wilcoxon matched pairs test, and the unpaired t-test replaced with the Mann-Whitney U test. For multiple comparisons, a one-way ANOVA was applied along with Tukey's multiple comparison test, or for multiple characteristics a two-way ANOVA along with the Holm-Sidak or Dunnett tests for post-hoc analysis. If any groups were found to be non-normally distributed, a repeated measures ANOVA was replaced with the Friedman test, and for unpaired data the Kruskal-Wallis test was applied, along with Dunn's multiple comparison test.

Throughout, data are displayed as the mean ± the standard error. Graphs and statistical analyses were generated using Graphpad Prism 7 (ISI Software, San Diego, CA, USA).

Nonlinear regression was used to analyse the bath perfused NMDA dose-response data in both wild type and *Grin2D*-null mice. The least squares (ordinary) fit method was used in Graphpad Prism 7.03 to fit an [agonist] vs response curve, as defined below:

$$Y = Bottom + X \cdot (Top - Bottom)/(EC50 + X)$$

Electrophysiological recordings were excluded if the result was classed as a significant outlier according to the Grubbs' Extreme Studentized Deviate (ESD) method.

$$G = \frac{\max_{i=1,\ldots,N} \left| Y_i - \bar{Y} \right|}{s}$$

Where $\bar{Y}$ is the sample mean, and s is the standard deviation. The difference between the outlier and the mean is divided by s. The G statistic is the largest absolute deviation from the sample mean in units of the standard deviation (Grubbs 1950). The only values removed from any of the results presented in this thesis as outliers were from the activity dependent regulation experiments: one sample was from the wild type induction paradigm treatment group, and one from the *Grin2D*-null induction paradigm treatment group; both of which showed very large increases, in stark contrast to the rest of the dataset.

2.6 Materials

2.6.1 Electrophysiology

For electrophysiological recordings, standard laboratory salts were obtained from BDH Laboratory Supplies (Poole, UK). All drugs were obtained from Sigma-Aldrich (Dorset, UK), apart from tetrodotoxin (TTX) and Group II metabotropic glutamate receptor antagonist LY 341495, which were obtained from Tocris Bioscience (Bristol, UK).

2.6.2 Immunohistochemistry

For Immunohistochemistry, PFA, tris, Triton-X100, and Tween-20 were obtained from BDH Laboratory Supplies (Poole, UK). Fish gelatine and PBS tablets were obtained from Sigma-Aldrich (Dorset, UK). Antibodies were obtained from either Millipore (MA, USA) or Thermo Fisher (MA, USA) as specified.

CHAPTER 3

RESULTS

3 Results

3.1 Characterisation of synaptic NMDARs in SNc DA neurons of *Grin2D* null mice

3.1.1 Constitutive NMDAR expression at Grin2D-null synapses

Experiments were performed in order to investigate whether removal of the *Grin2D* gene caused any change in the overall expression of NMDARs at the synapse, relative to AMPARs at the same age (A/N ratio). To determine the A/N ratio, picrotoxin (50 μM) and glycine (10 μM) were added to the perfusion. Cells were held at +40 mV to bypass Mg^{2+} blockade ($MgCl_2$ 1 mM), and EPSCs of a stable amplitude recorded at 0.1 Hz for at least 200 s before addition of NMDAR blocker D-AP5 (50 μM) to the perfusion, leaving the AMPAR-EPSC (**Figure 3.1**). At least 10 traces immediately before, and 10 traces in the presence of D-AP5 were averaged using the CED Spike2 software. The +D-AP5 trace ('AMPAR-EPSC') was subtracted from the pre-D-AP5 trace ('total-EPSC') using Microsoft Excel to give the NMDAR-EPSC. Peak amplitudes of each component were measured 8-15 ms following the stimulus artifact.

Three age groups were tested: results in P5-7 mice produced an A/N value of 0.840 ± 0.124 in *Grin2D*-WT (n=7), and 0.577 ± 0.113 in *Grin2D*-null mice (n=7; from 6 different animals). P12-15 mice produced an A/N value of 0.389 ± 0.061 in wild type (C57 n=8, and *Grin2D*-WT n=1), and 0.460 ± 0.089 in *Grin2D*-null mice (n=6). Results in P17-21 mice gave an A/N value of 0.721 ± 0.079 in wild type (C57 n=9, and *Grin2D*-WT n=1), and 0.827 ± 0.104 in *Grin2D*-null mice (n=7). An unpaired 2-way ANOVA was performed on all groups, examining the effect of age group and genotype. Age had a significant (p=0.0016**) effect on A/N, whereas genotype was not significant (**Figure 3.2**).

3.1.2 Altered properties of synaptic NMDARs in Grin2D null mice

It has been shown previously that NMDAR-EPSCs in rat SNc-DA neurons are inhibited by the GluN2B preferring antagonist ifenprodil, and by the GluN2D-preferring antagonist UBP-141 up to postnatal week 3; consistent with the expression of GluN2B and GluN2D-containing synaptic NMDARs. These are proposed to form diheteromeric receptors at P7 and have a likely triheteromeric composition by P21 (Brothwell et al. 2008). Therefore the possibility of an altered pharmacological response was investigated in *Grin2D*-null mice, with picrotoxin (50 μM), glycine (10 μM), and DNQX (10 μM) added to the perfusion.

Two age groups were tested. Example recordings and combined data from SNc-DA neurons taken from *Grin2D* WT and null mice are shown in **Figures 3.3** (~P7) and **3.4** (~P21). In animals aged P5-9, application of the GluN2B-preferring antagonist ifenprodil (10 μM) caused a mean inhibition of NMDAR-EPSCs within the 13-20 minute timeframe of 62.9 ± 3.7 % in *Grin2D*-WT (n=7), significantly less than the 78.8 ± 2.4 % observed in *Grin2D*-null mice (n=6) (**Figure 3.5;** p=0.006**; difference of 15.95 ± 4.64 %; two tailed t). In mice aged P18-21, application of ifenprodil caused a mean inhibition at of 48.8 ± 5.5 % in wild type (n=9 [C57 n=7, *Grin2D*-WT n=2]), significantly less than the 65.4 ± 4.1 % in *Grin2D*-null mice (n=7) (**Figure 3.5;** p=0.037*; difference of 16.6 ± 7.2 %; two tailed t-test).

Similar experiments were also performed using GluN2D-preferring antagonist DQP-1105 (10 μM). Example recordings and combined data from SNc DA neurons are shown in **Figures 3.6** (~P7) and **3.7** (~P21). In P5-9 mice, there was a mean inhibition of NMDAR-EPSCs 9-20 minutes following application of DQP of 24.9 ± 7.5 % in *Grin2D*-WT (n=8), significantly greater than the 10.0 ± 4.2 % in *Grin2D*-null mice (n=11) (**Figure 3.8;** p=0.042*; difference of 14.8 ± 8.1 %; one tailed t). In P17-22 mice, there was a mean reduction at 13-20 minutes of 23.10 ± 3.10 % in *Grin2D*-WT (n=7), significantly greater than the 14.5 ± 2.6 % in *Grin2D*-null mice (n=7) (**Figure 3.8;** p=0.036*; difference of 9.4 ± 4.8 %; one tailed t). The one-tailed t test is used here because sensitivity is only required for a *decreased* effect in *Grin2D*-null mice using this GluN2D-specific antagonist. Overall the pharmacological data suggest that GluN2D is replaced with GluN2B at the synapse in *Grin2D*-null animals. The ifenprodil data are also consistent with a general developmental decrease in diheteromeric GluN1/GluN2B NMDARs in SNc-DA neurons (Brothwell et al. 2008).

τ1 decay time constants were also compared between wild type (**Figure 3.8**; n=10; C57 n=6, Grin2D-WT n=4) and Grin2D null mice (n=11) aged P17-21, with a two-trailed t-test reporting no significant difference between the two groups (p=0.117).

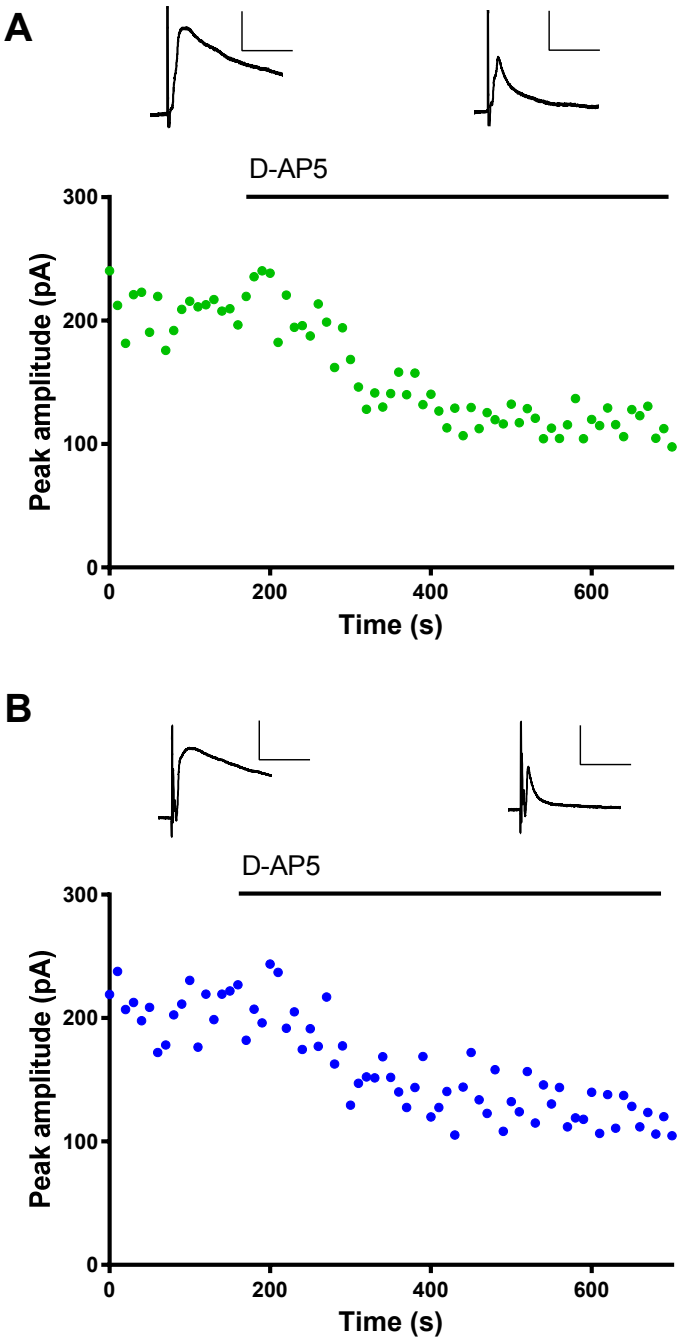

Figure 3.1 – Example EPSC amplitudes before and during application of D-AP5

To generate AMPAR/NMDAR EPSC amplitude ratios 50 µM D-AP5 was applied via the bath perfusion after a stable baseline period. Example experiments including before and after traces are shown from a P21 C57 mouse (**A**), and a P21 *Grin2D*-null mouse (**B**). Scale bar axes: x=40 ms; y=100 pA.

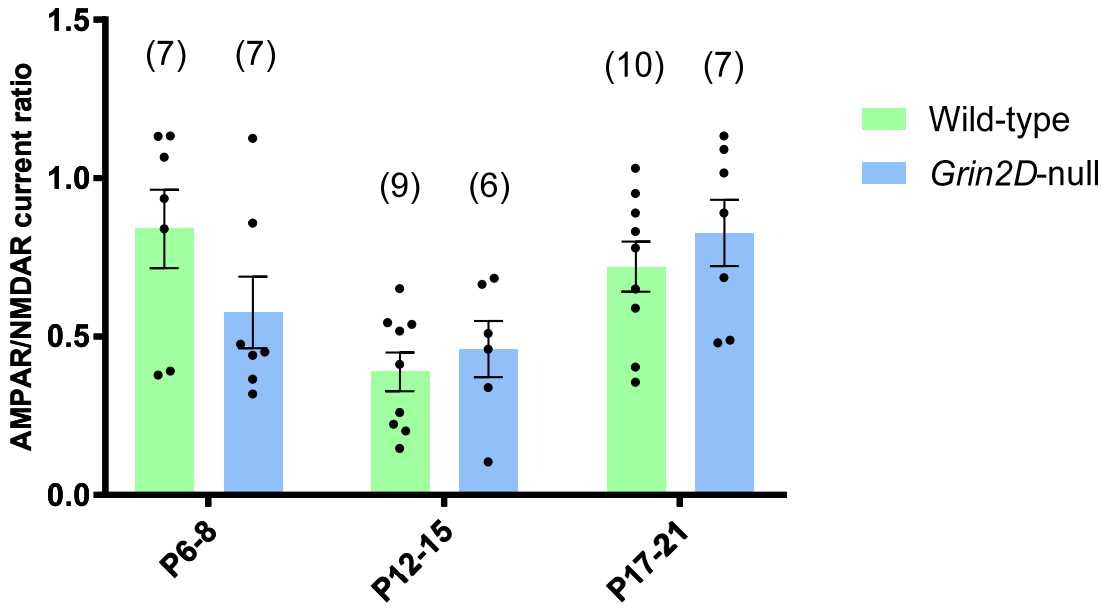

Figure 3.2 – AMPAR/NMDAR EPSC amplitude ratio alters with age but not by genotype.

Scatter plot showing AMPAR/NMDAR EPSC amplitude ratios in wild type (C57 and *Grin2D*-WT) and *Grin2D*-null mice at three age groups, approximately one, two, and three weeks old. No significant difference was observed based on genotype, whereas age was highly significant (p=0.0016, unpaired two factor ANOVA). The P6-8 *Grin2D*-null group has an n=7 from 6 different animals.

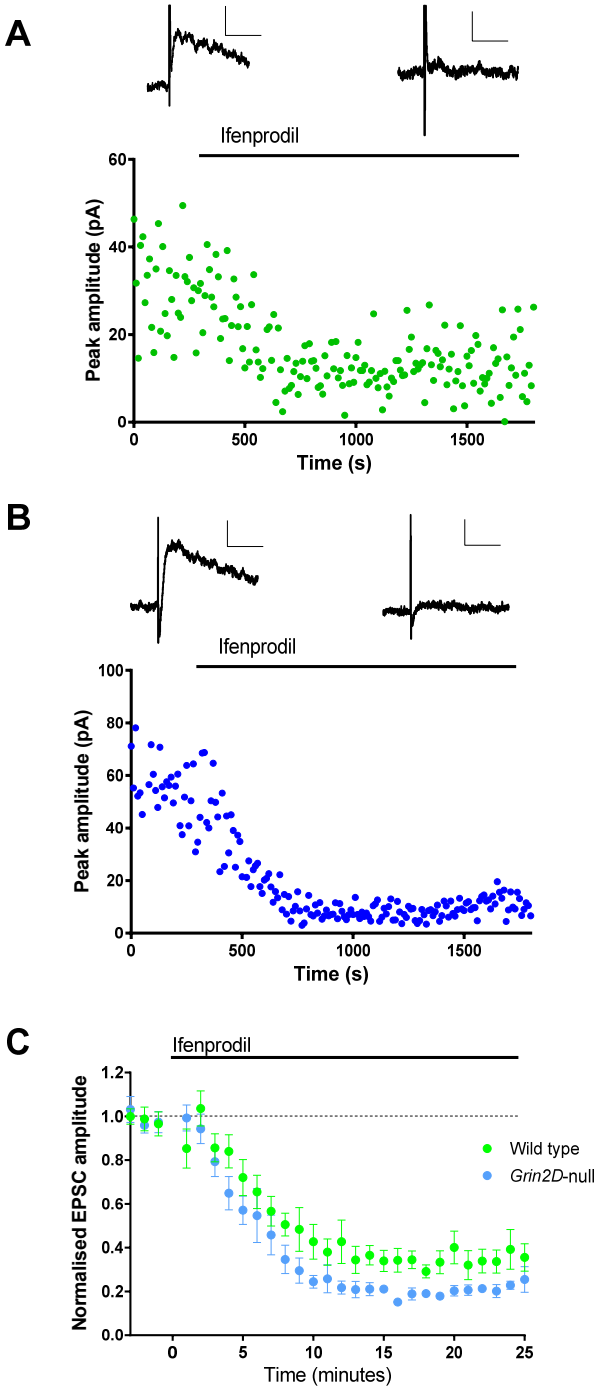

Figure 3.3 – EPSC amplitudes before and during application of ifenprodil in one-week old mice

NMDAR-EPSCs generated in the presence of glycine, picrotoxin, and DNQX were inhibited by application of GluN2B-preferring inhibitor ifenprodil (10 μM) via the bath perfusion following a stable baseline period. Example experiments including before and after traces are shown from a P9 *Grin2D*-WT mouse (**A**), and a P8 *Grin2D*-null mouse (**B**). Scale bar axes: x=40 ms; y=30 pA. Summary data from P5-9 mice are shown in **C**: WT n=7, *Grin2D*-null n=6.

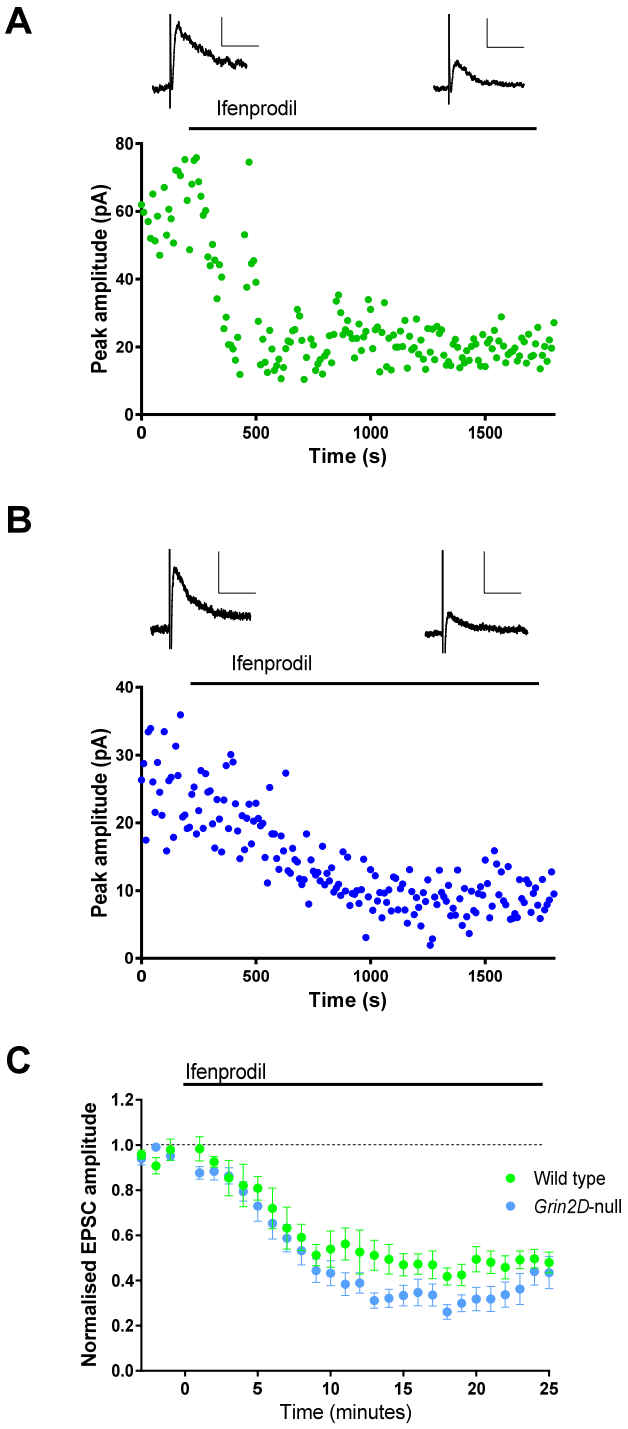

Figure 3.4 – EPSC amplitudes before and during application of ifenprodil in three-week old mice

NMDAR-EPSCs generated in the presence of glycine, picrotoxin, and DNQX were inhibited by application of GluN2B-preferring inhibitor ifenprodil (10 µM) via the bath perfusion following a stable baseline period. Example experiments including before and after traces are shown from a P21 C57 mouse (**A**), and a P20 *Grin2D*-null mouse (**B**). Scale bar axes: x=40 ms; y=30 pA. Summary data from P18-21 mice are shown in **C**: WT n=9, *Grin2D*-null n=7.

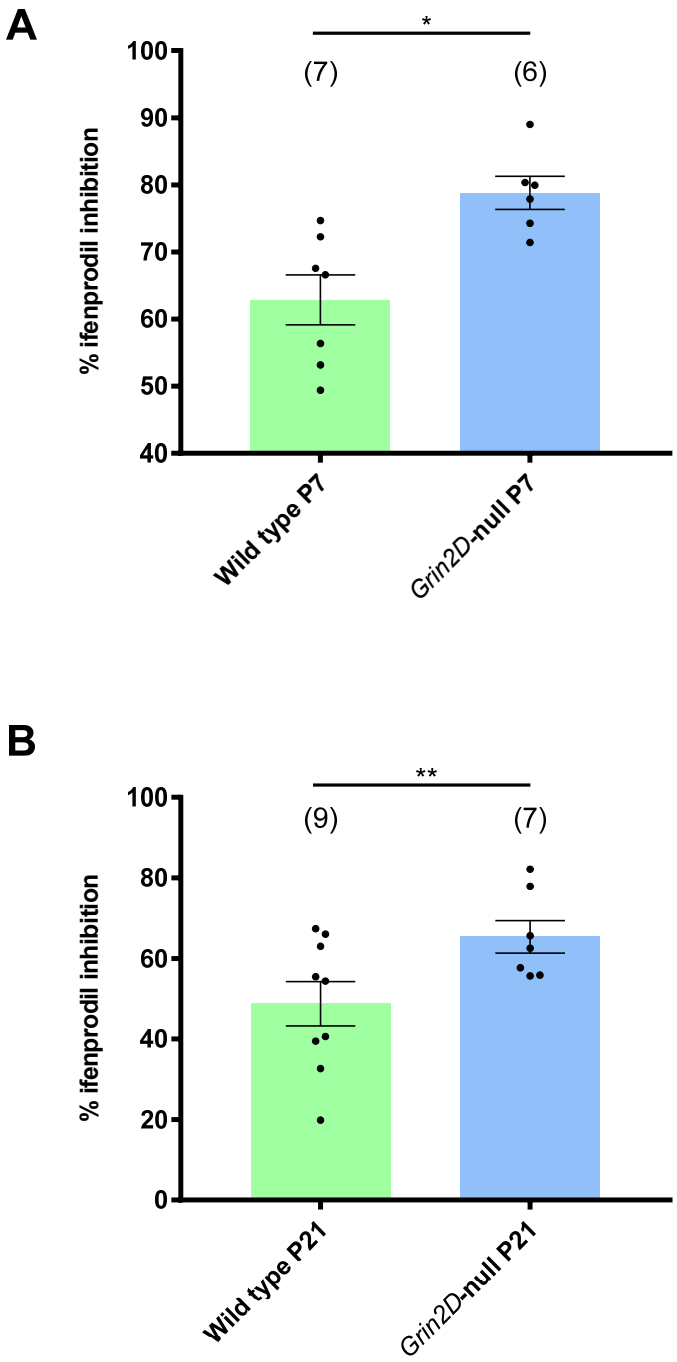

Figure 3.5 – GluN2B inhibition by ifenprodil is greater in mice lacking GluN2D

Mean reduction in amplitude of NMDAR-EPSCs during the period 13-20 minutes following addition of GluN2B-preferring inhibitor ifenprodil (10 μM). (**A**) In one-week old mice, inhibition was significantly greater in *Grin2D*-null (n=6) compared to *Grin2D*-WT (n=7) mice (p=0.006**; two tailed t). (**B**) In three-week old mice, inhibition was again significantly greater in *Grin2D*-null (n=7) compared to wild type (n=9 [C57 n=7, *Grin2D*-WT n=2]) mice (p=0.037*; two tailed t).

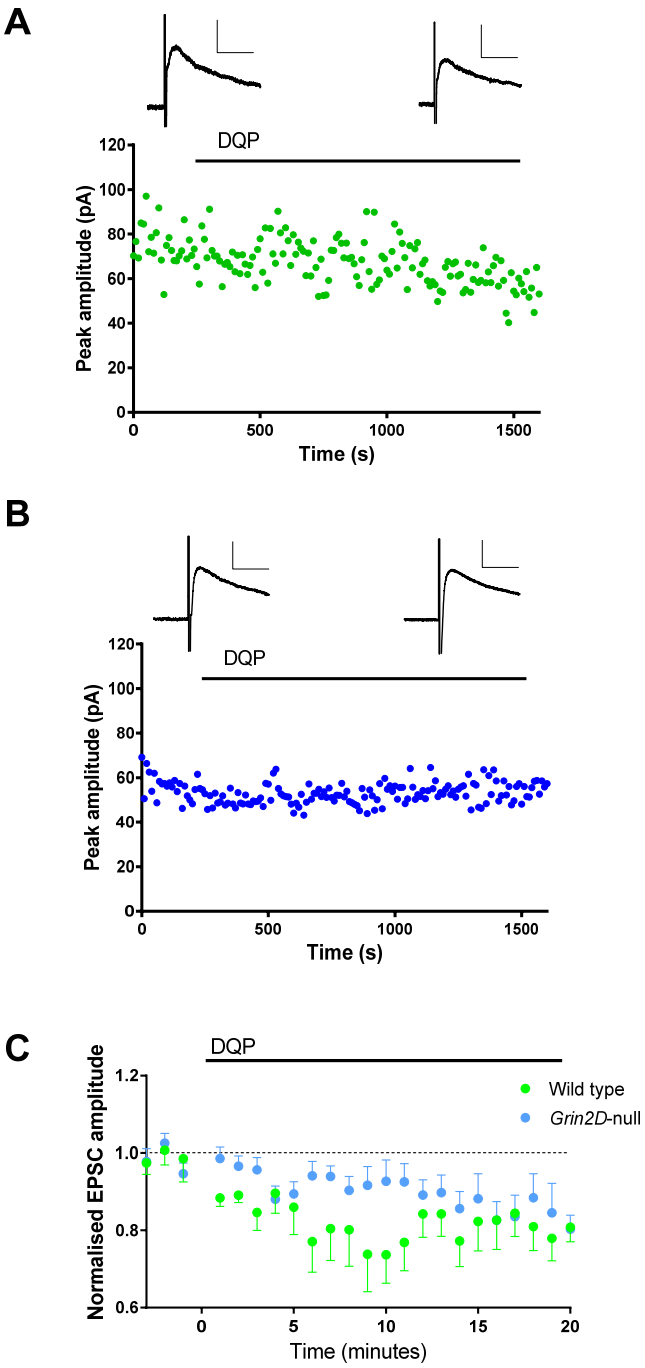

Figure 3.6 – EPSC amplitudes before and during application of DQP-1105 in one-week old mice

NMDAR-EPSCs generated in the presence of glycine, picrotoxin, and DNQX were inhibited by application of GluN2D-preferring inhibitor DQP-1105 (10 µM) via the bath perfusion following a stable baseline period. Example experiments including before and after traces are shown from a P5 *Grin2D*-WT mouse (**A**), and a P8 *Grin2D*-null mouse (**B**). Scale bar axes: x=40 ms; y=30 pA. Summary data from P5-9 mice are shown in **C**: WT n=8, *Grin2D*-null n=11.

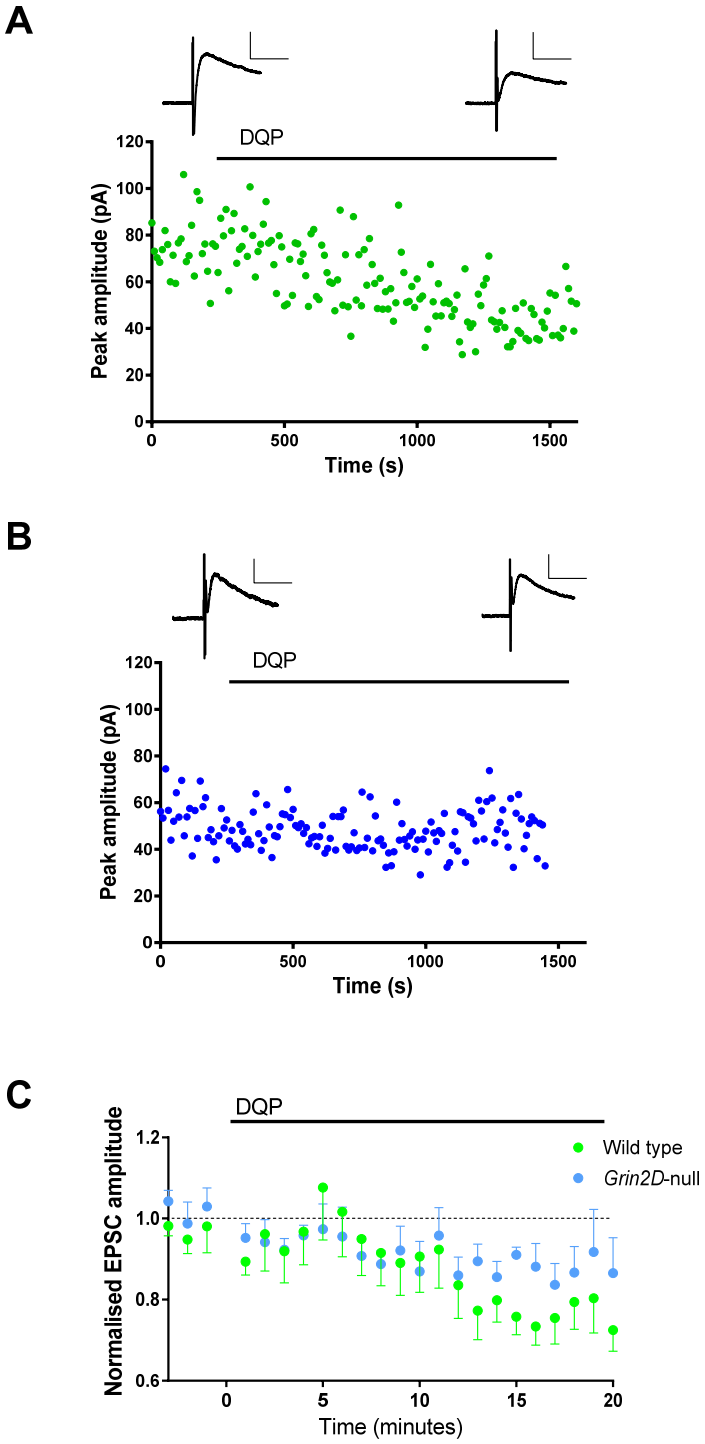

Figure 3.7 – EPSC amplitudes before and during application of DQP-1105 in three-week old mice

NMDAR-EPSCs generated in the presence of glycine, picrotoxin, and DNQX were inhibited by application of GluN2D-preferring inhibitor DQP-1105 (10 µM) via the bath perfusion following a stable baseline period. Example experiments including before and after traces are shown from a P17 C57 mouse (**A**), and a P20 *Grin2D*-null mouse (**B**). Scale bar axes: x=40 ms; y=30 pA. Summary data from P17-22 mice are shown in **C**: WT n=7, *Grin2D*-null n=7.

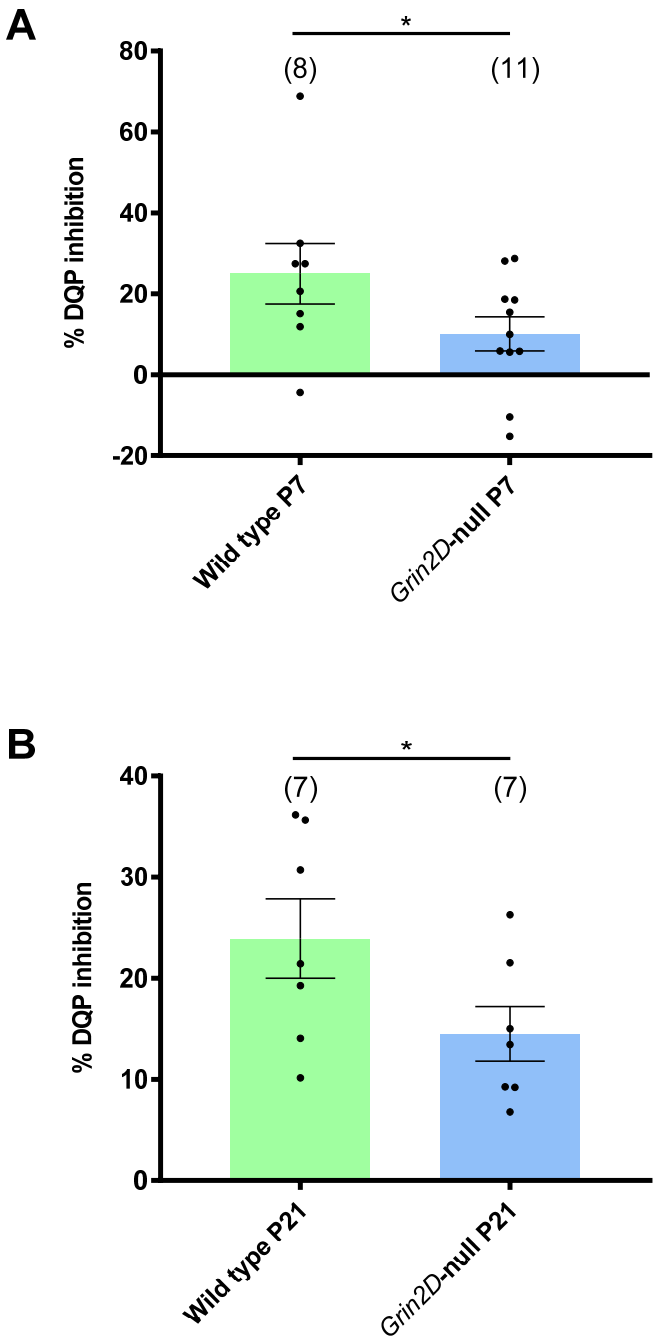

Figure 3.8 – GluN2D inhibition by DQP-1105 is reduced in mice lacking GluN2D

Mean reduction in amplitude of NMDAR-EPSCs during the period 13-20 minutes following addition of GluN2D-preferring inhibitor DQP-1105 (10 µM). (**A**) In one-week old mice, inhibition was significantly greater in *Grin2D*-WT (n=8) compared to *Grin2D*-null mice (n=11) (p=0.042*; one tailed t). (**B**) In three-week old mice, inhibition was again significantly greater in *Grin2D*-WT mice (n=7) compared to *Grin2D*-null mice (n=7) (p=0.036*; one tailed t).

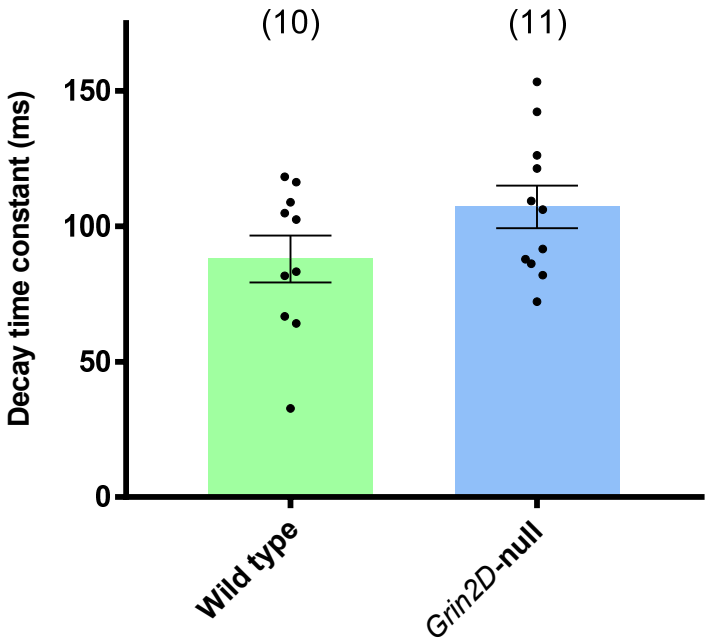

Figure 3.9 – NMDAR-EPSC decay constants do not differ between wild type and Grin2D-null mice

The decay time constant τ1 was compared between wild type (n=10; C57 n=6, *Grin2D*-WT n=4) and Grin2D null mice (n=11) aged P17-21. There was no significant difference between the two groups (two-tailed t; p=0.117).

3.2 Activity-dependent regulation of NMDA receptors

3.2.1 Reduction in NMDA-EPSC amplitude in response to high frequency burst firing of excitatory afferents

To investigate activity-dependent regulation of electrically evoked NMDAR responses, picrotoxin (50 μM), glycine (10 μM), and DNQX (10 μM) were added to the perfusion. Membrane holding potential was set to +40 mV in order to inhibit Ca^{2+} entry, and EPSCs elicited by application of single stimuli (to activate synaptic NMDARs) or short high frequency (50 Hz) trains of stimuli (to activate synaptic and also potentially extrasynaptic NMDARs); an example recording is shown in **Figure 3.10A**). After a stable baseline of at least 300 s, the holding potential was changed to -20 mV in order to allow Ca^{2+} entry whilst still alleviating Mg^{2+} block, and a protocol of burst firing activity (the induction protocol, or IP: trains of 3 pulses at 100 Hz, each followed by a 1 s break, adapted from Joshi et al. 2007) initiated. On completion, holding potential was returned to +40 mV and single and 50 Hz pulses continued. For analysis of EPSC amplitudes, mean amplitudes of ten single EPSCs and four summated EPSCs (taken here to refer to the EPSCs generate in response to trains of stimuli at 50 Hz) were taken immediately preceding the onset of the IP, and then for 25 minutes (1500 seconds) following the cessation of the IP. Comparisons were made between the NMDAR-EPSC amplitudes pre-IP and those within the 1200-1500 s time window: In wild type mice (C57 n=6, *Grin2D*-WT n=4), where the IP was applied at -20 mV, there was a significant reduction in mean NMDAR-EPSC amplitude of 18.05 ± 4.80 pA (**Figure 3.10B**; p=0.0045**; paired two-tailed t-test; n=10).

Two control experiments were performed in wild type mice. In the first, the holding potential was changed to -20 mV but the IP was not applied, there was no change in mean NMDAR-EPSC amplitude (increase of 0.17 ± 4.50 pA; **Figure 3.11A, B**; p=0.9711; paired two-tailed t-test; n=11 [C57 n=4, *Grin2D*-WT n=7]): these data showed significantly less down-regulation of single NMDAR-EPSCs than observed in response to the test IP, as explained in 3.2.3 below and summarized in **Figure 3.12**. As the assaying pulses in this protocol were always taken at +40 mV in order to minimize Ca^{2+} entry, another control was performed in which the IP was applied at +40 mV, to see whether this holding potential still allowed the cell to respond to the IP: in this control there was no change in mean NMDAR-EPSC amplitude

(reduction of 5.25 ± 2.34 pA; **Figure 3.11C, D**; p=0.0552; paired two-tailed t-test; n=9 [C57 n=3, *Grin2D*-WT n=6]).

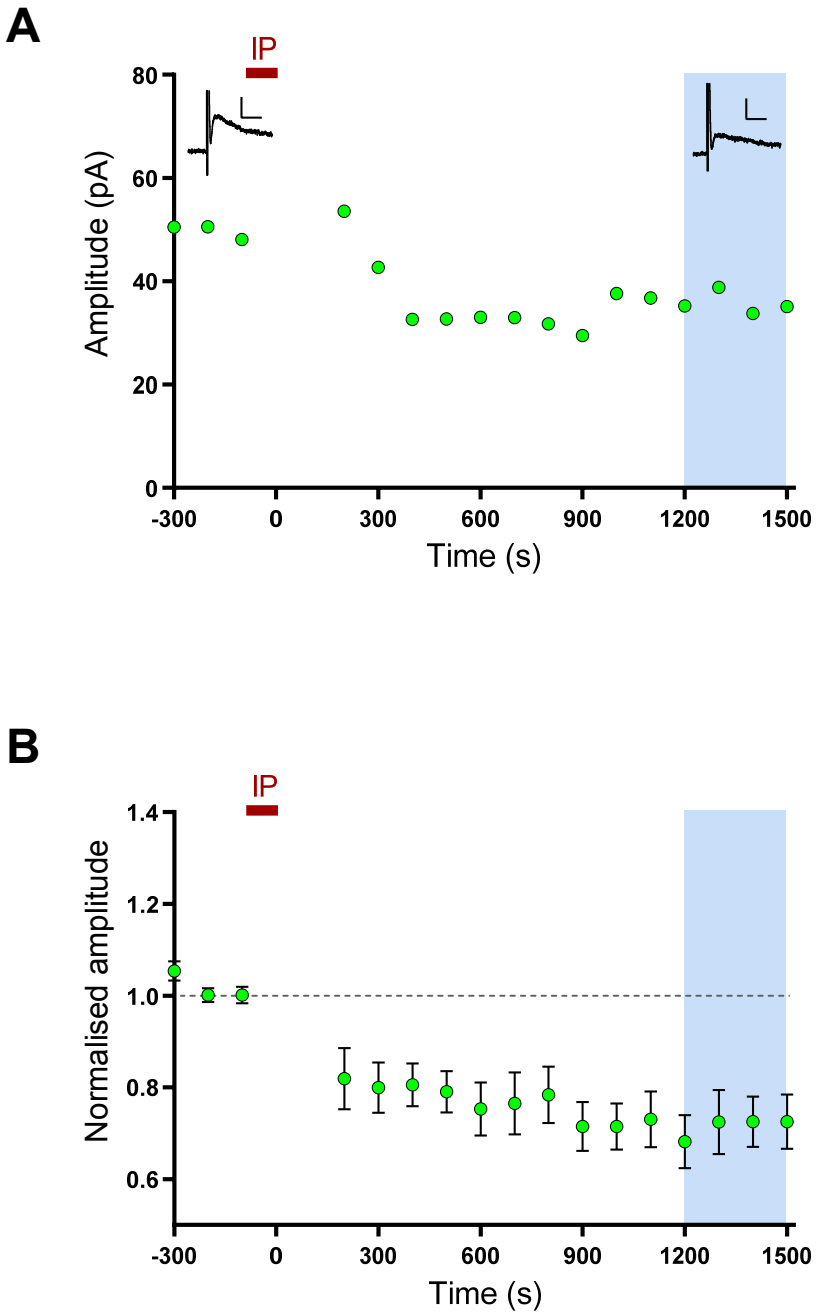

Figure 3.10 – Single NMDAR-EPSC amplitude is reduced following treatment by the IP at -20 mV in wild type mice

Following a stable baseline period of NMDAR-EPSCs elicited at +40 mV, the induction paradigm (IP) was applied at -20 mV. **A**: An example experiment including before and after traces from a P19 *Grin2D*-WT mouse. Scale bar axes: x=20 ms; y=25 pA. Each data point represents mean y values from each 100 s period. **B**: Summary data. In comparison to the pre-IP period, mean single NMDAR-EPSC amplitudes 1200-1500 seconds following the end of the IP were significantly reduced (p=0.0045**; paired two-tailed t-test; n=10).

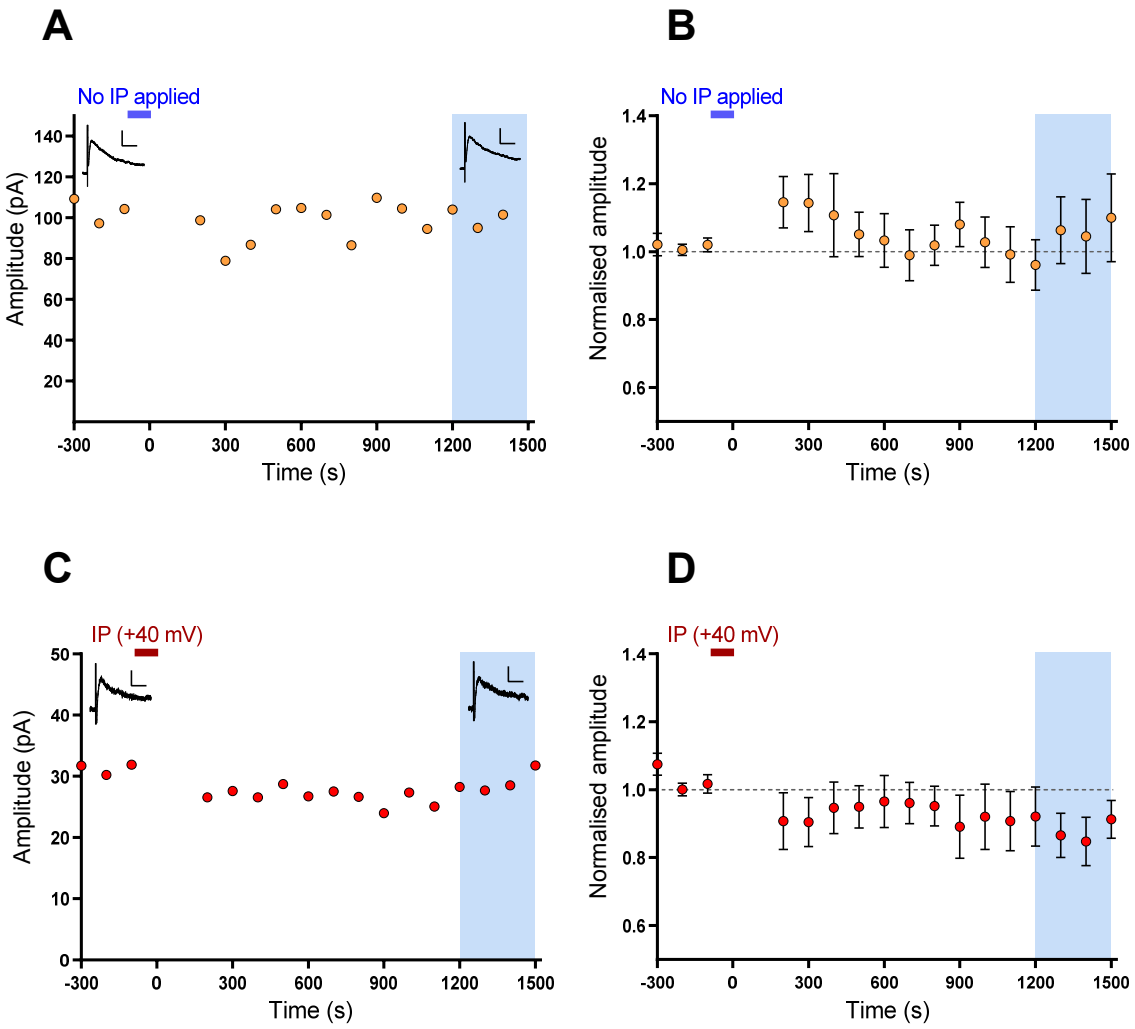

Figure 3.11 – Single NMDAR-EPSC amplitude remains stable where the IP is not applied, and where Ca^{2+} driving force is reduced

A: Example recording from a P19 *Grin2D*-WT mouse: following a stable baseline period of NMDAR-EPSCs elicited at +40 mV, the holding potential was switched to -20 mV as in the treatment group, but no stimulation applied. Scale bar axes: x=20 ms; y=50 pA. Each data point represents mean y values from each 100 s period. **B**: Summary data of these experiments: in comparison to the pre-IP period, mean single NMDAR-EPSC amplitudes 1200-1500 seconds following the end of the pseudo-IP were not reduced; n=11.

C: Example recording from a P20 *Grin2D*-WT mouse: in this case the IP was applied, but the holding potential was not changed from +40 mV. Scale bar axes: x=20 ms; y=15 pA. **D**: Summary data of these experiments: in comparison to the pre-IP period, mean single NMDAR-EPSC amplitudes 1200-1500 seconds following the end of stimulation were not reduced; n=9.

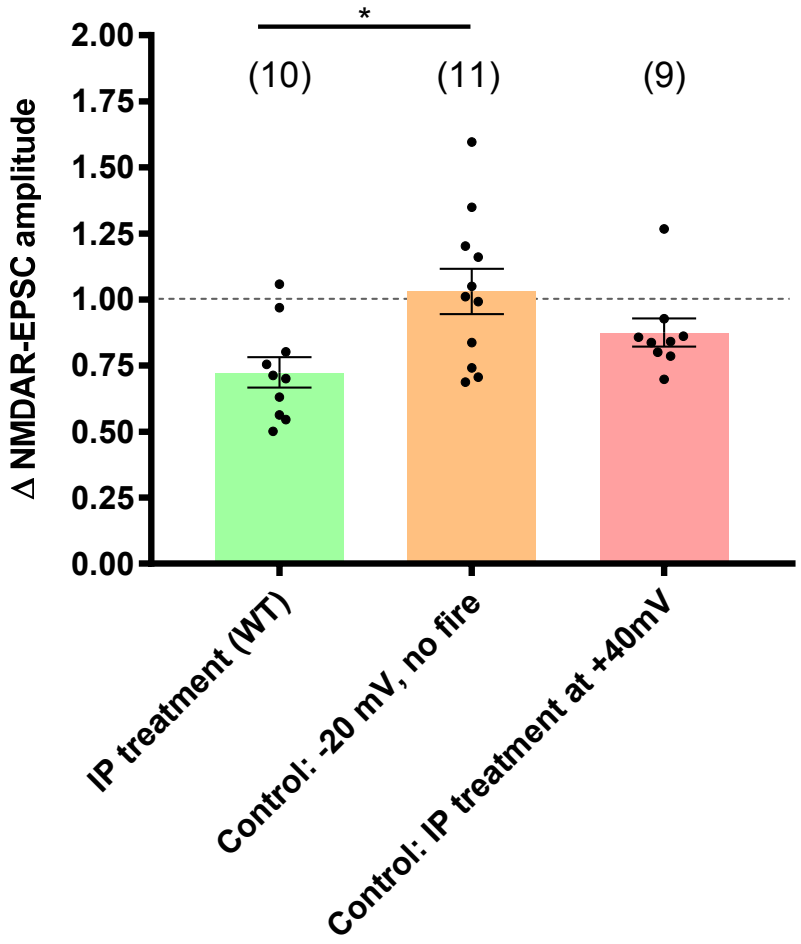

Figure 3.12 – Single NMDAR-EPSC amplitude is reduced by application of the induction paradigm

Scatter plot showing the change in single NMDAR-EPSC amplitude. The treatment group in which the IP was applied at -20 mV had a significantly reduced mean NMDAR-EPSC amplitude after 1200-1500 s in comparison to the same time period from the control group, in which holding potential was changed to -20 mV but no stimulation applied ($p<0.05$*; ANOVA, Sidak post-hoc). The treatment group was also compared to the group in which the IP was applied at +40 mV, but this did not yield a significant result.

3.2.2 Summated NMDA-EPSC amplitudes were also reduced in response to high frequency burst firing of excitatory afferents

In wild type mice (C57 n=6, *Grin2D*-WT n=4), where the IP was applied at -20 mV, there was a significant reduction in mean summated NMDAR-EPSC amplitude of 36.26 ± 12.41 pA (**Figure 3.13A, B**; p=0.0170*; paired two-tailed t-test; n=10). In control experiments performed in wild type mice, where the holding was moved to -20 mV but the IP was not applied, there was no change in mean NMDAR-EPSC amplitude (increase of 13.81 ± 10.87 pA; **Figure 3.14A, B**; p=0.233; paired two-tailed t-test; n=11 [C57 n=4, *Grin2D*-WT n=7]): these data showed significantly less down-regulation of single NMDAR-EPSCs than observed in response to the test IP, as explained in 3.2.3 below and summarized in **Figure 3.15**. In control experiments performed in wild type mice where the IP was applied at +40 mV, there was no change in mean NMDAR-EPSC amplitude (reduction of 6.07 ± 4.52 pA; **Figure 3.14C, D**; p=0.216; paired two-tailed t-test; n=9 [C57 n=3, *Grin2D*-WT n=6]).

3.2.3 A significant effect of the IP in comparison to control, and a difference based on EPSC type

In order to examine effect of the IP at both -20 and +40 mV, and to compare single and summated responses, the data were normalised as a proportion of the pre-IP amplitude. A paired two-factor ANOVA was performed. For each group the paired data for the remaining EPSC proportion of both single and summated EPSCs were entered. The test reported a significant (p=0.0201*) difference between groups (IP applied at -20 mV, IP applied at +40 mV, and no IP applied at -20 mV), and a significant (p=0.0077**) difference based on EPSC type (paired data).

Multiple comparisons were then performed: for the single NMDAR-EPSC data, Sidak post-hoc testing reported a significant difference in the remaining EPSC proportion in the ‘no IP’ control vs that in the wild type treatment group ($p<0.05$*). There was no significant difference between the wild type and +40 mV IP treatment groups, or the no IP control and the +40 mV IP groups.

Within the same round of Sidak multiple comparison testing, similar results were reported for the summated NMDAR-EPSC data: there was a significant difference in the remaining EPSC proportion in the 'no IP' control vs that in the wild type treatment group ($p<0.01$*). There was no significant difference between the wild type and +40 mV IP treatment groups, or the no IP control and the +40 mV IP groups.

Together this testing indicates that the IP reduces NMDAR-EPSC amplitude, and that summated responses do not proportionally decrease as much as single EPSCs.

3.2.4 The fast Ca^{2+} chelator BAPTA does not prevent activity dependent downregulation

The effect of fast Ca^{2+} chelation was examined by the addition of BAPTA (10 mM) into the intracellular patch solution, where the IP was applied at -20 mV. In these experiments there was a significant reduction in mean single NMDAR-EPSC amplitude of 12.06 ± 3.60 pA ($p=0.0203$*; paired two-tailed t-test; n=6 [C57 n=4, *Grin2D*-WT n=2]). A similar reduction in summated NMDAR-EPSCs of 17.15 ± 6.10 pA was also observed ($p=0.0374$*; paired two-tailed t-test). The alterations in single or summated NMDAR-EPSCs at 1200-1500 with BAPTA did not differ from those without (single EPSC $p=0.25$, two-tailed t. Summated EPSC $p=0.68$, two-tailed t.). These data are summarized in **Figure 3.16**.

3.2.5 Reduction in NMDA-EPSC amplitude in response to high frequency burst firing of excitatory afferents is also seen in Grin2D-null mice

Given the change in the pharmacological properties of synaptic NMDARs in mice lacking the GluN2D subunit (**Figures 3.3-3.8**), activity dependent regulation of synaptic NMDARs was next explored. In *Grin2D*-null mice, where the IP was applied at -20 mV, there was a significant reduction in median single NMDAR-EPSC amplitude of 18.45 pA (**Figure 3.17**; $p=0.0244$*; paired two-tailed Wilcoxon; n=11). Additionally, there was significant reduction in median summated NMDAR-EPSC amplitude of 35.49 pA (**Figure 3.18**; $p=0.0420$*; paired two-tailed Wilcoxon; n=11).

There was no difference in the remaining NMDAR-EPSC proportion between the two IP treatment groups in wild type and *Grin2D*-null mice, in either single (**Figure 3.19**; p=0.58; two-tailed t-test) or summated EPSCs (p=0.54; two-tailed t-test)

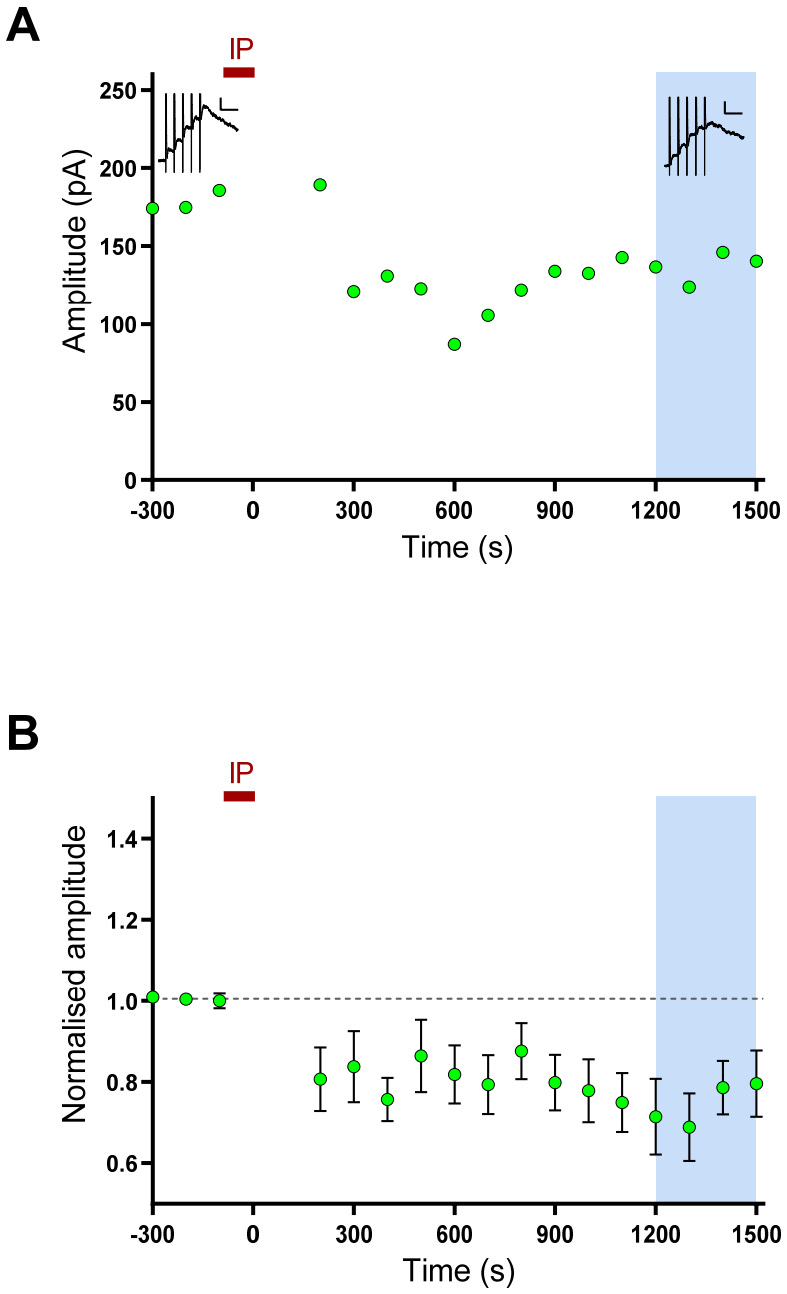

Figure 3.13 – Summated NMDAR-EPSC amplitude is reduced following treatment by the IP at -20 mV in wild type mice

Following a stable baseline period of NMDAR-EPSCs elicited at +40 mV, the induction paradigm (IP) was applied at -20 mV. **A**: An example experiment including before and after traces from a P19 *Grin2D*-WT mouse. Scale bar axes: x=40 ms; y=50 pA. Each data point represents mean y values from each 100 s period. **B**: Summary data. In comparison to the pre-IP period, mean summated NMDAR-EPSC amplitudes 1200-1500 seconds following the end of the IP were significantly reduced (p=0.0170*; paired two-tailed t-test; n=10).

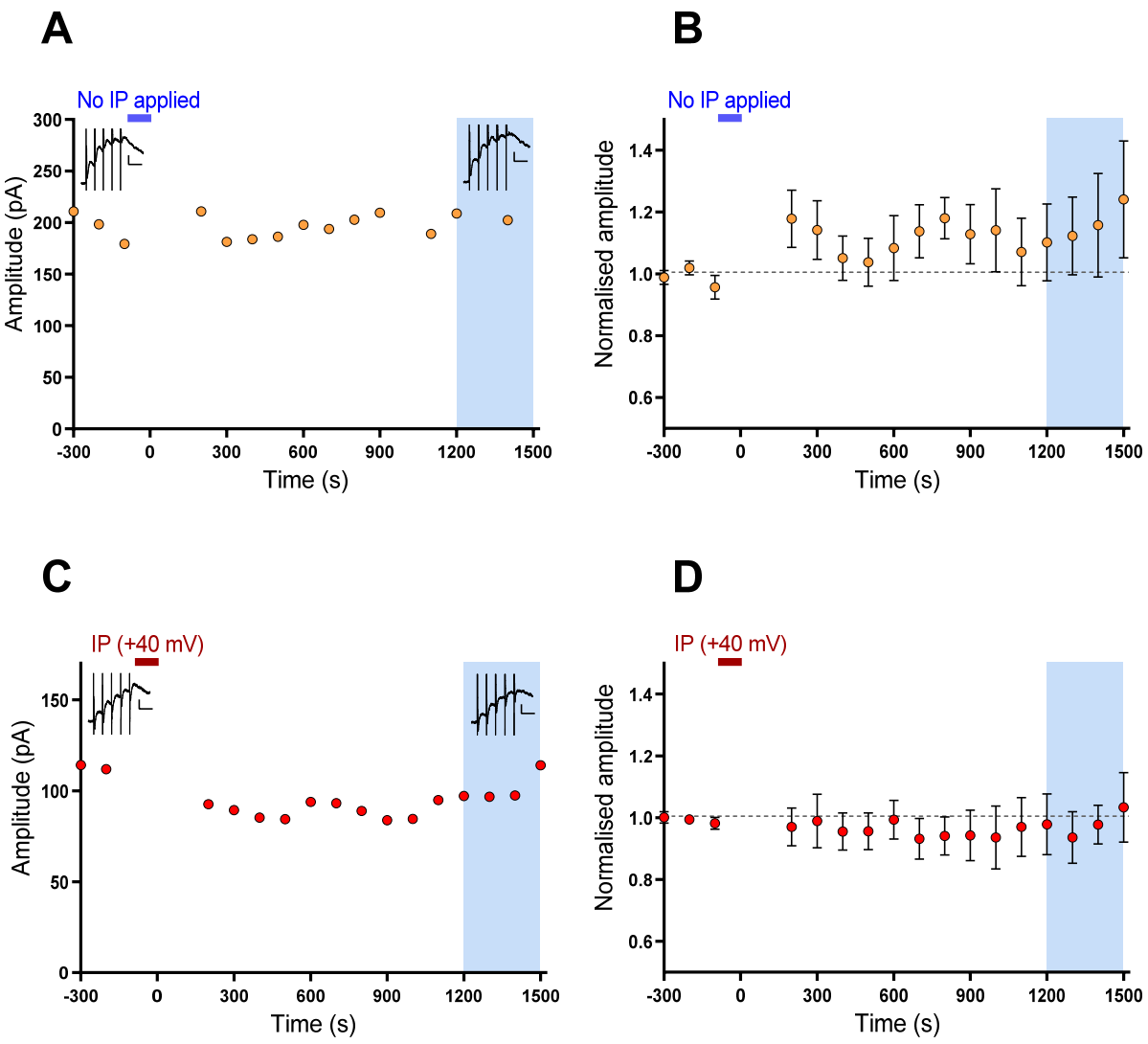

Figure 3.14 – Summated NMDAR-EPSC amplitude remains stable where the IP is not applied, and where Ca^{2+} driving force is reduced

A: Example recording from a P19 *Grin2D*-WT mouse: following a stable baseline period of summated NMDAR-EPSCs elicited at +40 mV, the holding potential was switched to -20 mV as in the treatment group, but no stimulation applied. Scale bar axes: x=40 ms; y=50 pA. Each data point represents mean y values from each 100 s period. **B**: Summary data of these experiments: in comparison to the pre-IP period, mean summated NMDAR-EPSC amplitudes 1200-1500 seconds following the end of the pseudo-IP were not reduced; n=11.

C: Example recording from a P20 *Grin2D*-WT mouse: in this case the IP was applied, but the holding potential was not changed from +40 mV. Scale bar axes: x=40 ms; y=30 pA. **D**: Summary data of these experiments: in comparison to the pre-IP period, mean summated NMDAR-EPSC amplitudes 1200-1500 seconds following the end of stimulation were not reduced; n=9.

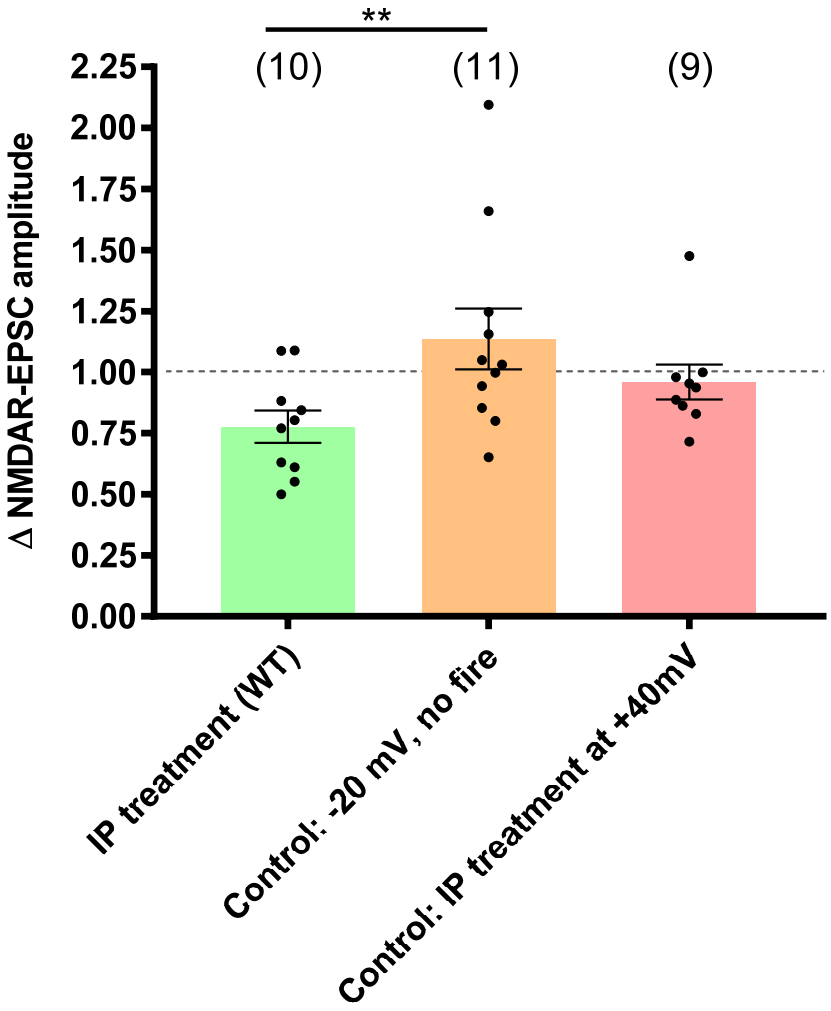

Figure 3.15 – Summated NMDAR-EPSC amplitude is reduced by application of the induction paradigm

Scatter plot showing the change in summated NMDAR-EPSC amplitude. The treatment group in which the IP was applied at -20 mV had a significantly reduced mean summated NMDAR-EPSC amplitude after 1200-1500 s in comparison to the same time period from the control group, in which holding potential was changed to -20 mV but no stimulation applied ($p<0.01$**; ANOVA, Sidak post-hoc). The treatment group was also compared to the group in which the IP was applied at +40 mV, but this did not yield a significant result.

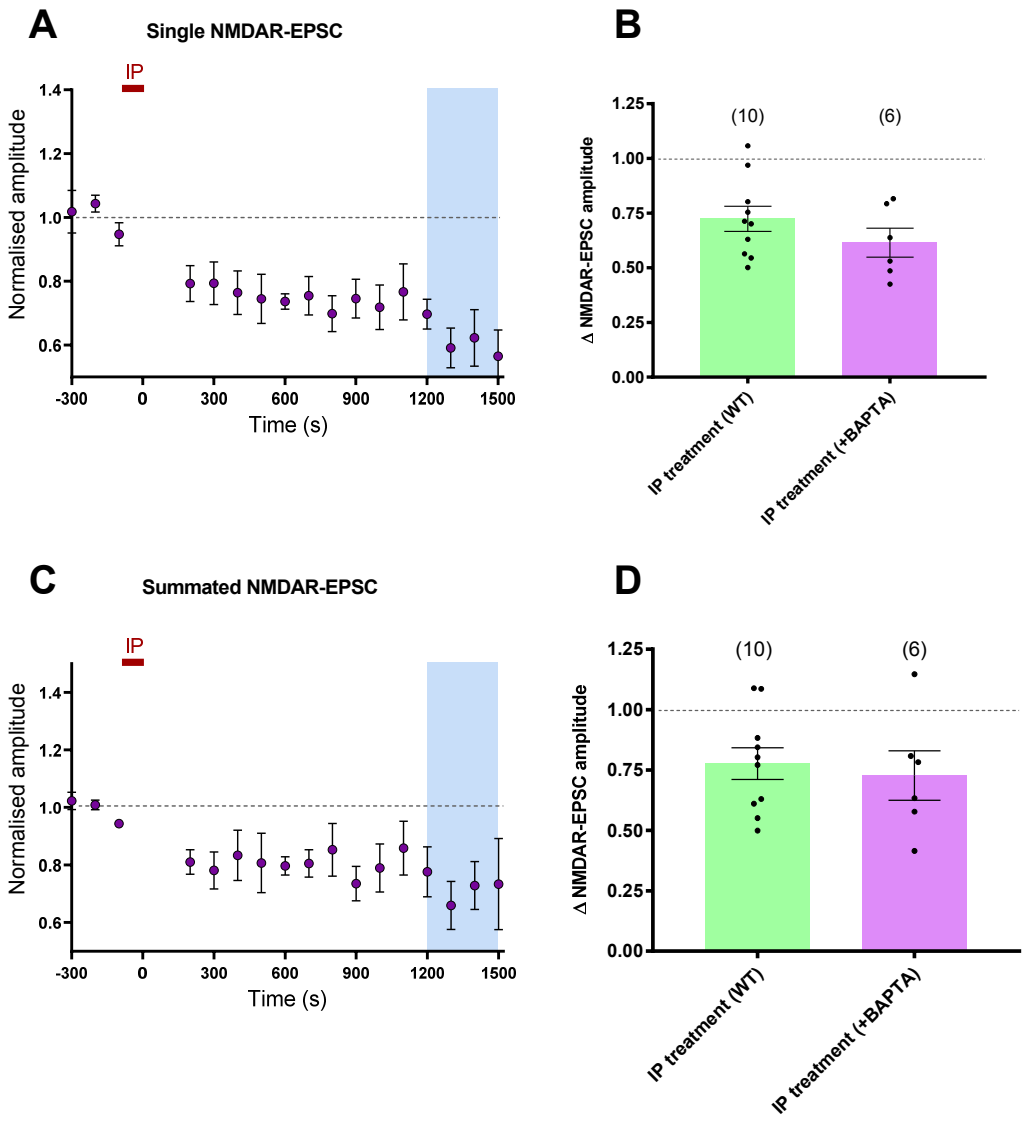

Figure 3.16 – Single and summated NMDAR-EPSC amplitudes are reduced following treatment by the IP at -20 mV along with intracellular Ca^{2+} chelation

Single (A,B) and summated (C,D) NMDAR-EPSC data where the induction paradigm (IP) was applied at -20 mV, along with BAPTA (10 mM) in the patch pipette. **A**: Summary timecourse data. In comparison to the pre-IP period, mean single NMDAR-EPSC amplitudes 1200-1500 seconds following the end of the IP were significantly reduced (p=0.020*; paired two-tailed t-test; n=6). **B**: Scatter plot showing change in single NMDAR-EPSC amplitude in the IP treatment groups with and without BAPTA: there was no significant difference between the two groups. **C**: Summary timecourse data. In comparison to the pre-IP period, mean summated NMDAR-EPSC amplitudes 1200-1500 seconds following the end of the IP were significantly reduced (p=0.037*; paired two-tailed t-test; n=6). **D**: Scatter plot showing change in summated NMDAR-EPSC amplitude in the IP treatment groups with and without BAPTA: there was no significant difference between the two groups.

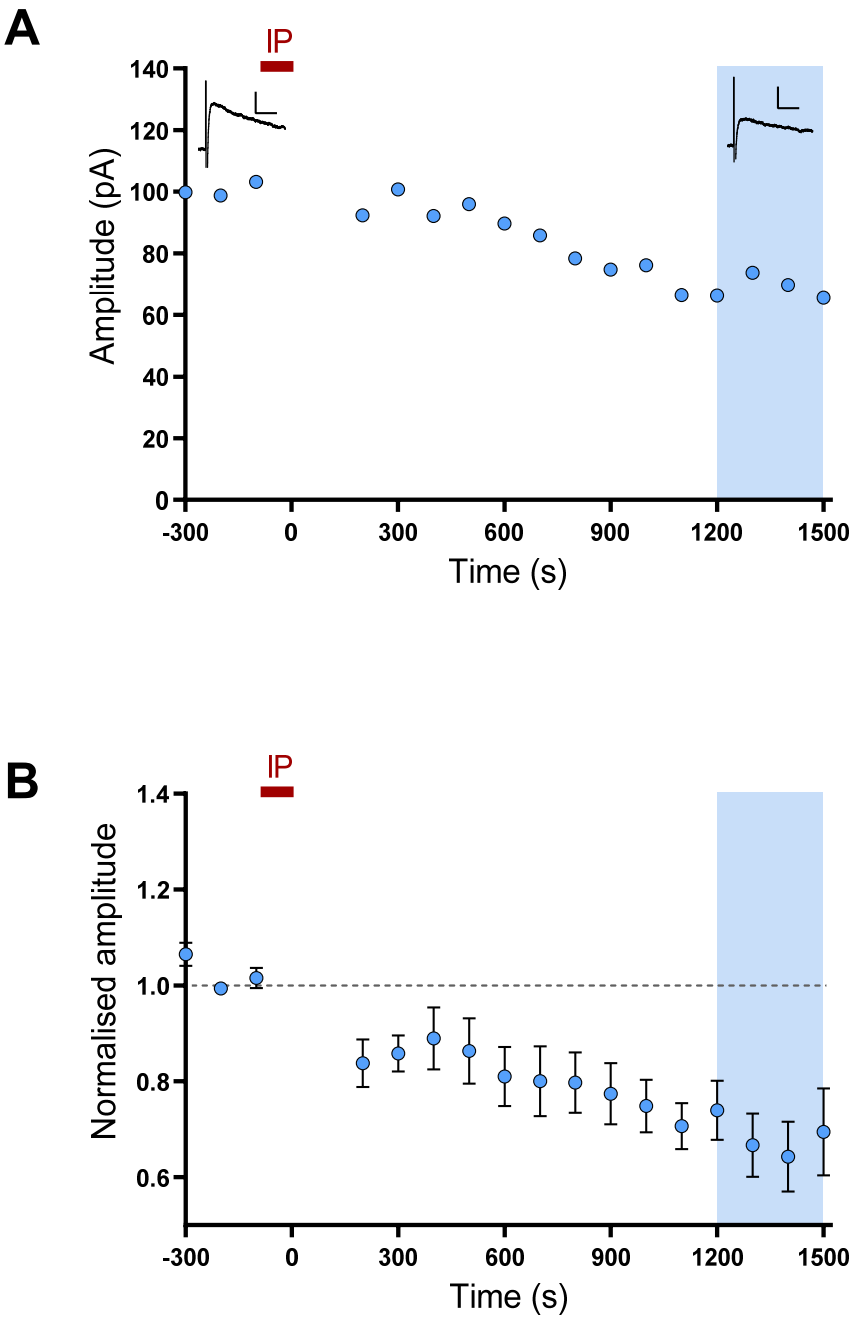

Figure 3.17 – Single NMDAR-EPSC amplitude is reduced following treatment by the IP at -20 mV in *Grin2D*-null mice

Following a stable baseline period of NMDAR-EPSCs elicited at +40 mV, the induction paradigm (IP) was applied at -20 mV. **A**: An example experiment including before and after traces from a P17 *Grin2D*-null mouse. Scale bar axes: x=20 ms; y=50 pA. Each data point represents mean y values from each 100 s period. **B**: Summary data. In comparison to the pre-IP period, mean single NMDAR-EPSC amplitudes 1200-1500 seconds following the end of the IP were significantly reduced (p=0.024*; paired two-tailed Wilcoxon; n=11).

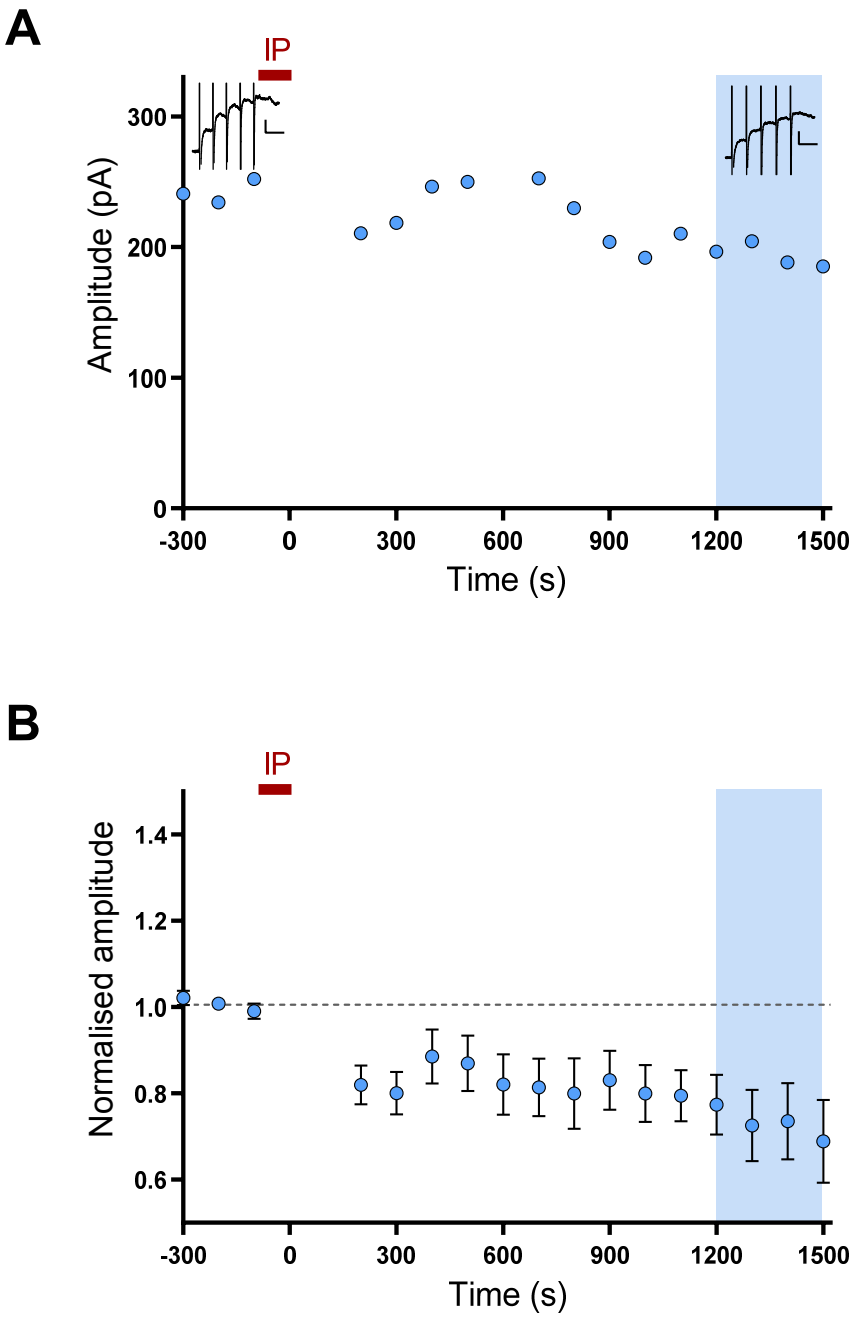

Figure 3.18 – Summated NMDAR-EPSC amplitude is reduced following treatment by the IP at -20 mV in *Grin2D*-null mice

Following a stable baseline period of NMDAR-EPSCs elicited at +40 mV, the induction paradigm (IP) was applied at -20 mV. **A**: An example experiment including before and after traces from a P17 *Grin2D*-null mouse. Scale bar axes: x=40 ms; y=50 pA. Each data point represents mean y values from each 100 s period. **B**: Summary data. In comparison to the pre-IP period, mean summated NMDAR-EPSC amplitudes 1200-1500 seconds following the end of the IP were significantly reduced (p=0.042*; paired two-tailed Wilcoxon; n=11).

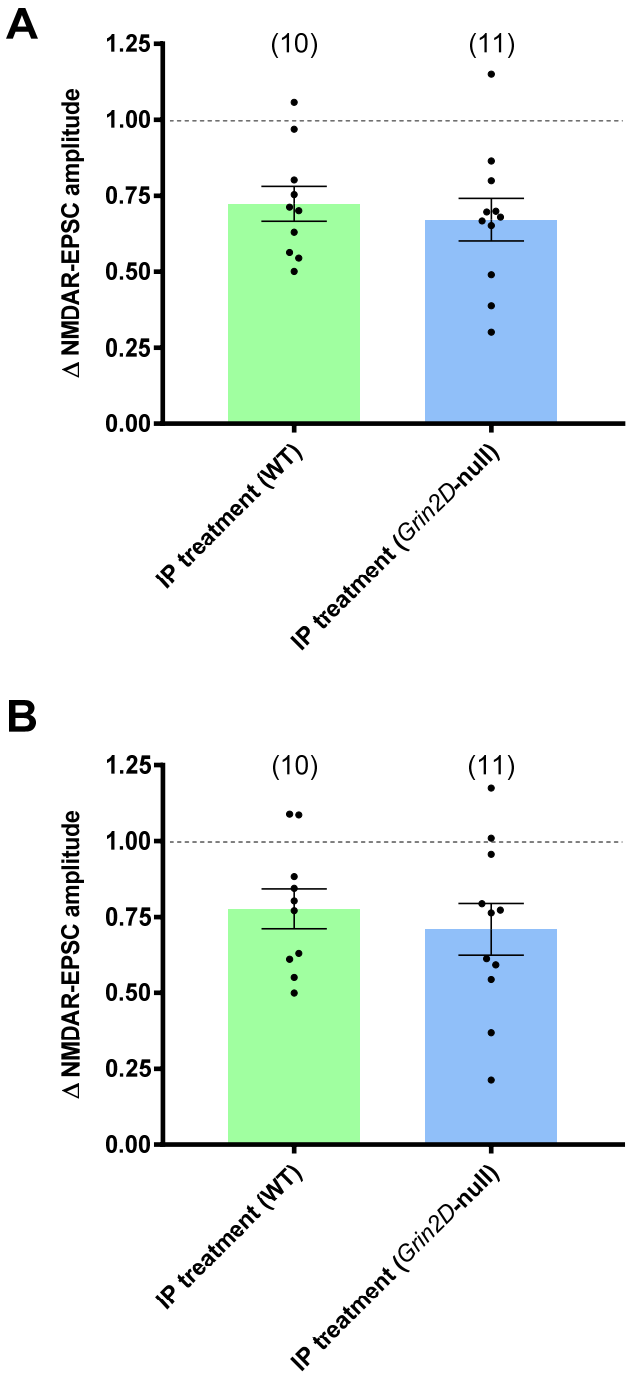

Figure 3.19 – Regulation of both single and summated NMDAR-EPSCs is similar between wild type animals and those lacking GluN2D

Scatter plots showing the change in single (**A**) and summated (**B**) NMDAR-EPSC amplitudes at 1200-1500 s following the IP, which was applied at -20 mV in wild type (n=10) and *Grin2D*-null (n=11) mice: there was no significant difference between the two in either case.

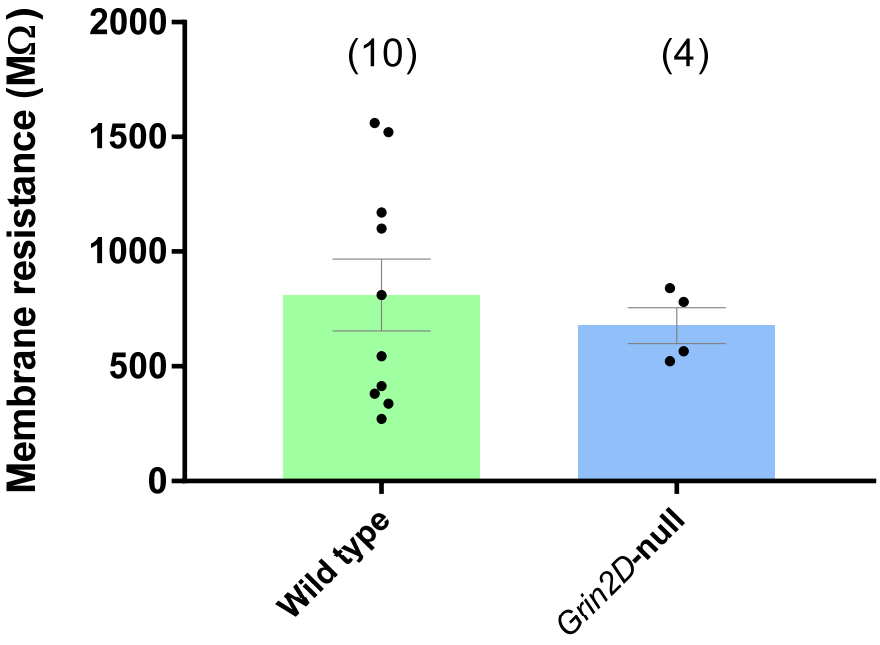

Figure 3.20 – Membrane resistance does not differ between wild type and *Grin2D*-null mice

Scatter plot showing the membrane resistance measured at a holding potential of -60 mV in both wild type (n=10; C57 n=3, *Grin2D*-WT n=7) and *Grin2D*-null (n=4) mice. There was no difference in the means of the two groups.

3.2.6 Membrane resistance is equal in wild-type and Grin2D-null animals

The membrane resistance (R_{memb}) was recorded in a sample of SNc-DA cells at a holding potential of -60 mV using the value estimated by the HEKA Pulse software: the mean value was 810.5 ± 156.6 MΩ in wild-type mice (P17-21; n=10 [C57 n=3, *Grin2D*-WT n=7]), not significantly different from that in *Grin2D*-null mice, 677.3 ± 78.1 MΩ (P17-20; n=4) (**Figure 3.20**; p=0.615; two-tailed t-test). Additionally, within the wild type group the R_{memb} of the C57 and *Grin2D*-WT animals did not significantly differ (p=0.37, two tailed t-test).

3.2.7 NMDAR-paired pulse ratio alters slightly over time

The NMDA paired pulse ratio (PPR) within each experiment was calculated as the amplitude of peak 2 divided by the amplitude of peak 1 (or p2/p1). Four pairs of EPSCs generated 20 s apart were therefore collected immediately before the onset of the patterned activity protocol and used to generate an average waveform and NMDAR-PPR: The pairs of EPSCs generated between 1200-1500 minutes following the cessation of the protocol were also averaged and the PPR compared to that from before the IP. Because NMDAR-EPSCs summate strongly (a postsynaptic effect of NMDAR channel kinetics), p2 amplitude is higher than p1, giving a PPR value greater than 1. A two-way ANOVA was performed on four IP groups, examining the effect of treatment group and time point (paired: pre-IP vs the 1200-1500 s time window). Time point had a significant (p=0.0048**) effect on PPR, with a mean increase from 1.659 ± 0.067 to 1.763 ± 0.060; whereas treatment group was not significant, implying that PPR was likely to increase whether the IP was applied or not. These data are summarized in **Figure 3.21**.

3.2.8 Zero-current potential is increased with the use of BAPTA-containing intracellular solution

The overall zero-current potential (V_{Izero}) for SNc-DA cells was measured in the HEKA Pulse software by initiating current clamp mode at zero pA. In wild type animals, using the regular Cs^+-based intracellular solution, V_{Izero} was -8.25 ± 1.33 mV (age P17-21; n=16 [C57 n=5,

Grin2D-WT n=11]): this was significantly different to the value produced when 10 mM BAPTA was present in the intracellular solution, +11.3 ± 1.9 mV (age P17-20; n=5 [C57 n=3, *Grin2D*-WT n=2]) (**Figure 3.22**; p=0.0003***; two-tailed t). Additionally a comparison was performed in the basic Cs group, and the V_{Izero} did not significantly differ based on the breeding background of the animals (p=0.15, two tailed t-test).

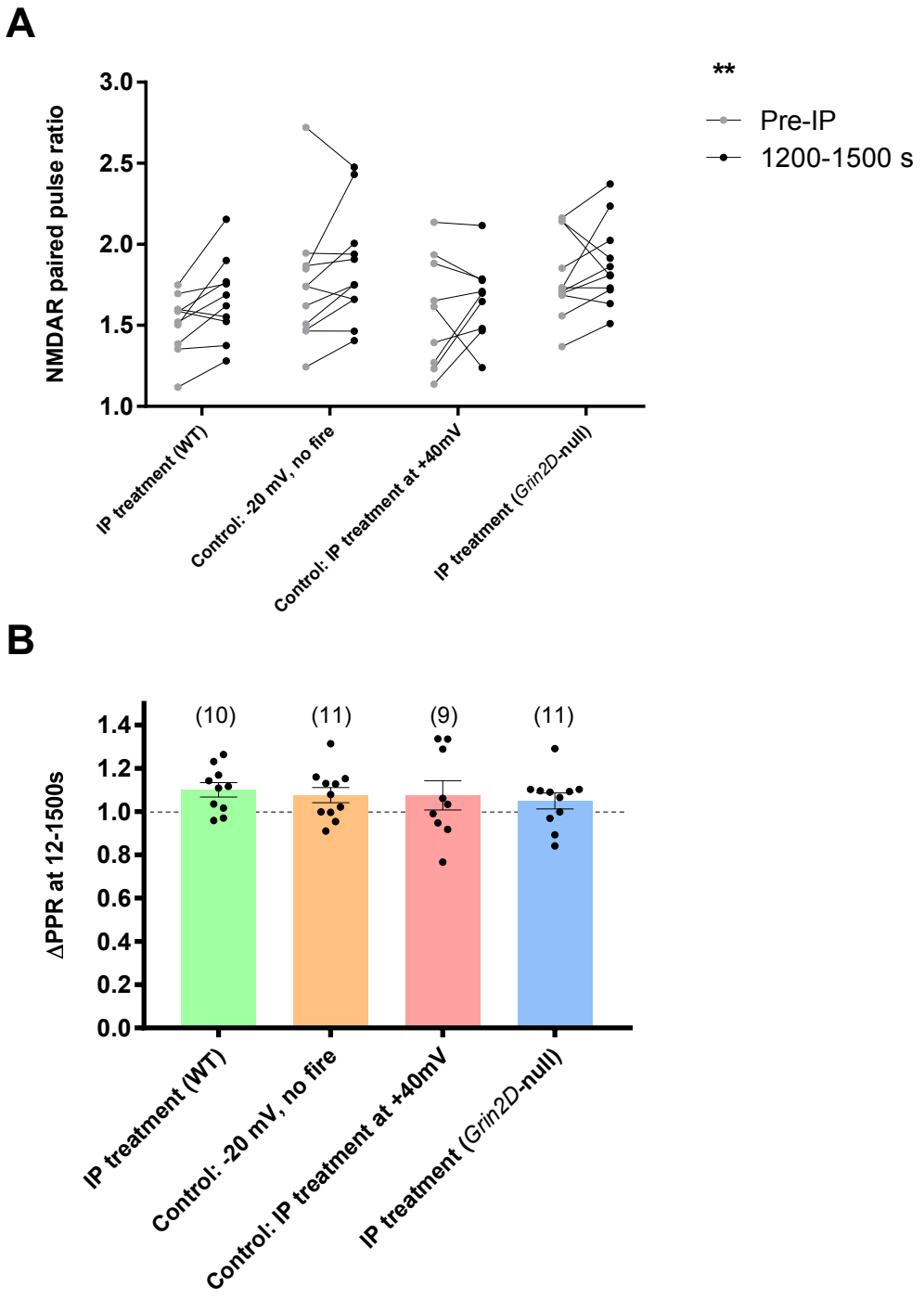

Figure 3.21 – NMDA-PPR alters slightly over time, but not between groups

A: Paired data showing the NMDAR-paired pulse ratio (PPR) before the IP (or control pseudo-treatment) and at 1200-1500 s afterwards. There was no difference found between the groups, but the small increase in NMDAR-PPR at the end of the experiment was highly significant (p=0.0048**; paired two-factor ANOVA). **B**: Scatter plot showing the change in the NMDAR-PPR at 1200-1500s, showing more clearly that the means are above the 1.0, indicating a small change.

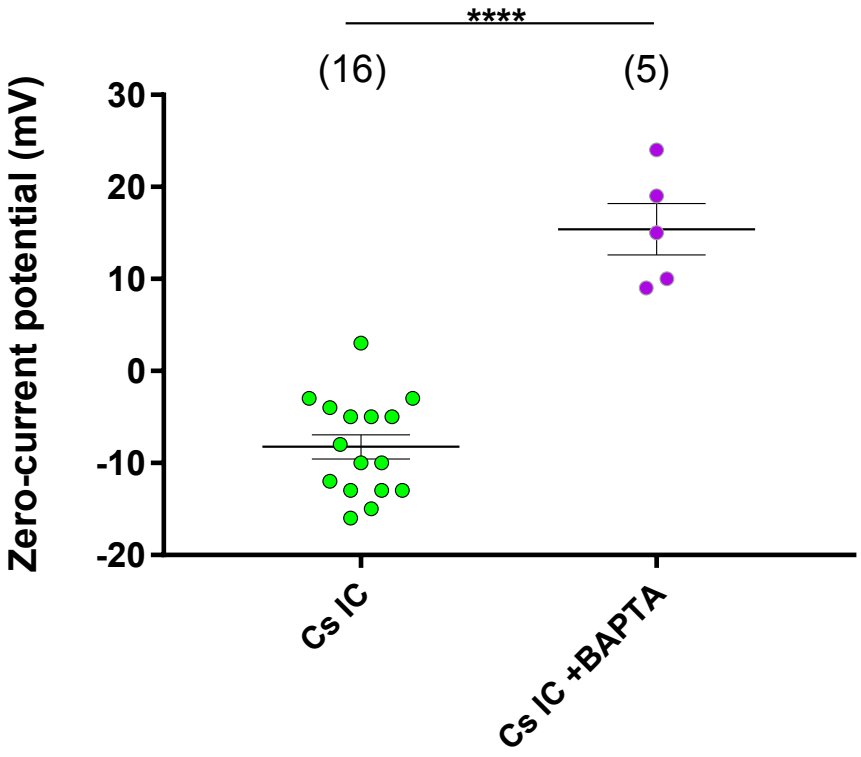

Figure 3.22 – V_{Izero} is altered when BAPTA is added to the patch pipette

The overall zero-current potential (V_{Izero}) for each SNc-DA neuron was recorded in a group of wild type (C57 and *Grin2D*-WT) animals, both with (n=5) and without (n=16) BAPTA (10 mM) present in the Cs^+-based intracellular solution in the patch pipette. The presence of BAPTA significantly altered the mean V_{Izero} value from -8.25 ± 1.33 mV to +11.3 ± 1.9 mV (p=0.0003***; two-tailed t).

3.3 The role of GluN2D and the NMDAR in responding to ambient glutamate

3.3.1 Ambient extracellular glutamate in the SNc elicits NMDAR-mediated currents in dopamine neurons, which are unaffected by pharmacological inhibition of action potential firing

Currents mediated via NMDARs by ambient extracellular glutamate were determined by applying a fast bath perfusion to the slice, obtaining a stable baseline current in picrotoxin (50 μM) and glycine (10 μM), before applying the competitive NMDAR antagonist D-AP5 (50 μM) and measuring the resulting deflection in current: example recordings are shown in **Figure 3.23**. In wild type mice, application of D-AP5 significantly reduced the baseline current from 214.1 ± 15.28 to 197.8 ± 15.07 pA (**Figure 3.24A**; p=0.0001***; n=19 [C57 n=15, *Grin2D*-WT n=4]; paired two-tailed t). Additionally, the D-AP5-sensitive current did not significantly differ based on the breeding background of the animals (C57 vs Grin2D-WT) (p= 0.92; two-tailed t-test).

In C57 mice, in the presence of TTX (100 nM) to block action potential-dependent glutamate release, application of D-AP5 again significantly reduced the baseline current from 165.3 ± 22.2 pA to 149.0 ± 19.3 pA (**Figure 3.24B**; p=0.0180*; n=8; paired two-tailed t-test). There was no difference between the D-AP5 sensitive current without TTX; 16.32 ± 3.32 pA (n=19), vs. that with TTX 16.25 ± 5.29 pA (n=8) (**Figure 3.25**; p=0.9999; ANOVA, Dunnett's Multiple Comparisons test: wild type, wild type +TTX, and *Grin2D*-null groups). In SNc-DA neurons from *Grin2D*-null mice, application of D-AP5 did not alter the amplitude of the current (**Figure 3.24C**; p=0.4057; n=15; paired two-tailed t). The pre-D-AP5 current was 200.5 ± 18.04 pA, and in D-AP5 was 197.7 ± 18.44 pA. There was a significant difference between the D-AP5-blockable current obtained in wild type mice 16.32 ± 3.32 pA (n=19) and that in *Grin2D*-null mice (**Figure 3.25**; 2.80 ± 3.26 pA; n=15; p=0.0148*; ANOVA, Dunnett's Multiple Comparisons test).

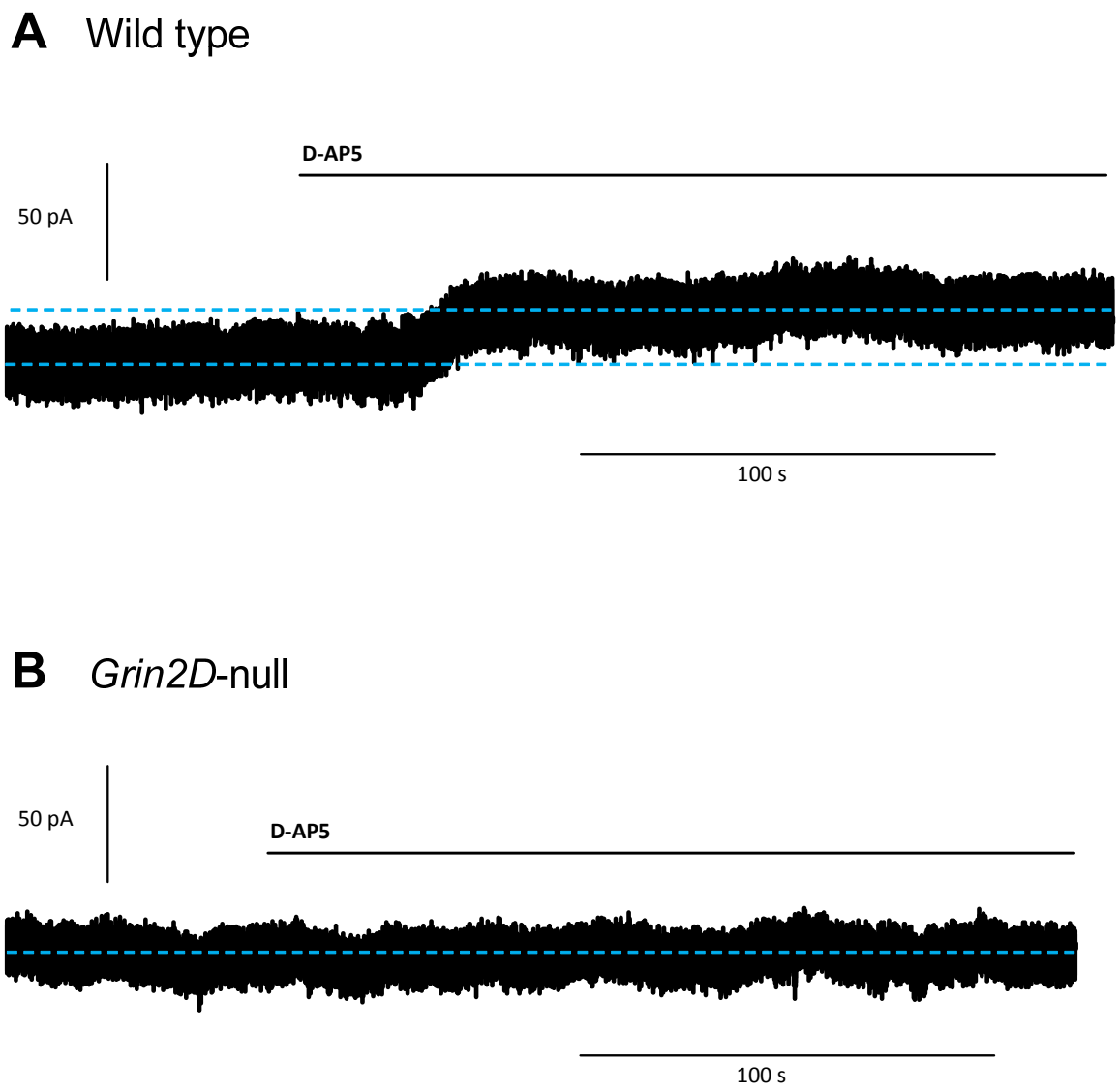

Figure 3.23 – Example traces showing the D-AP5-sensitive current in wild type and *Grin2D*-null mice

Example traces from SNc-DA neurons held at -50 mV, showing a typical alteration in baseline current resulting from the addition of 50 µM D-AP5 in a P20 C57 mouse (**A**), and a P19 *Grin2D*-null mouse (**B**).

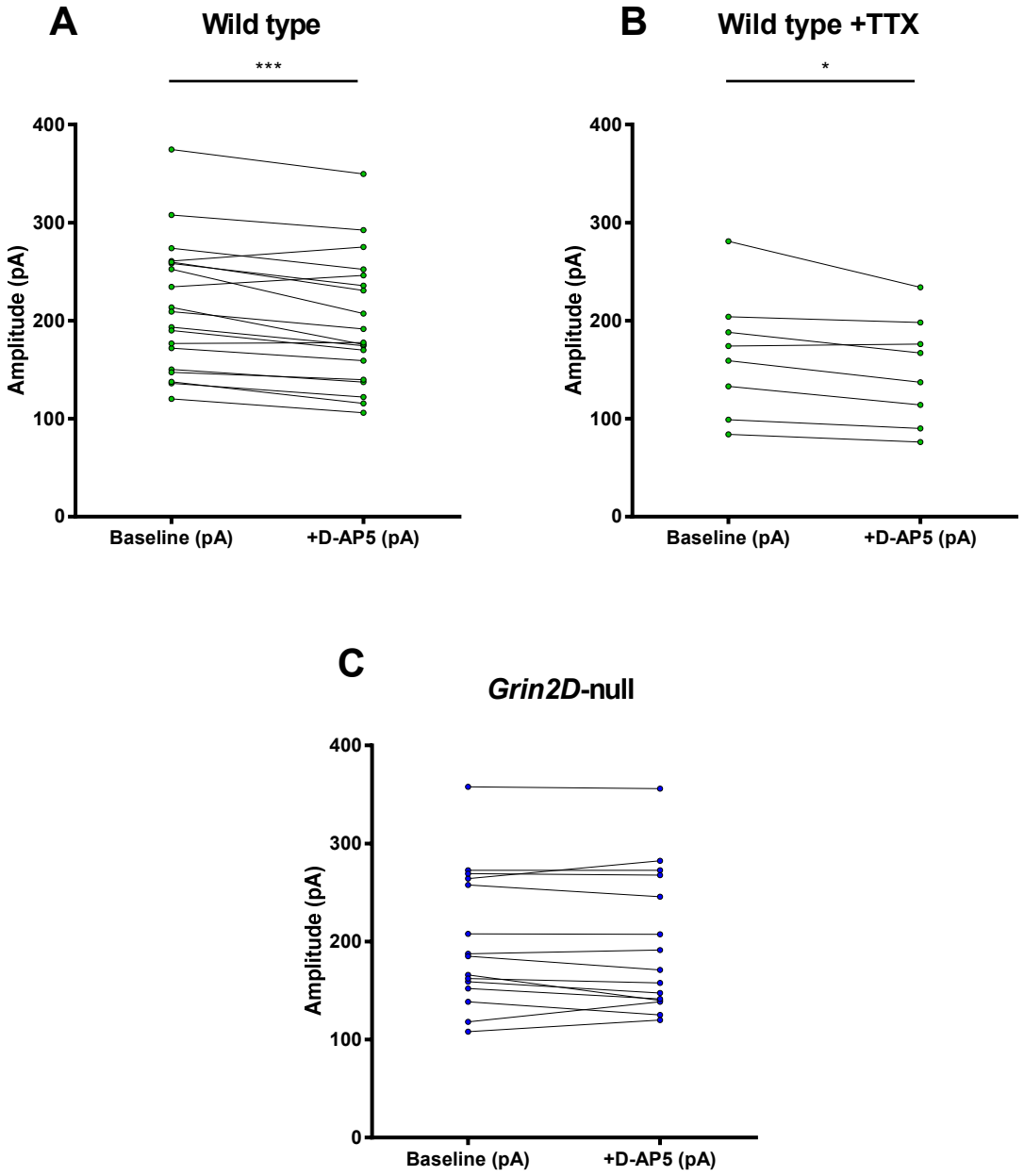

Figure 3.24 – Baseline current is significantly decreased by inhibition of NMDARs in wild type but not *Grin2D*-null mice

Paired data showing baseline currents at -50 mV in SNc-DA neurons, both before and after the addition of 50 µM D-AP5. **A**: Baseline current in D-AP5 was significantly reduced in wild type (C57 and *Grin2D*-WT) mice (p=0.0001***; paired two-tailed t). **B**: Baseline current in D-AP5 was also significantly reduced in C57 mice in the presence of voltage-gated sodium channel blocker TTX (p=0.0180*; paired two-tailed t). **C**: Baseline current in D-AP5 was not altered in *Grin2D*-null mice.

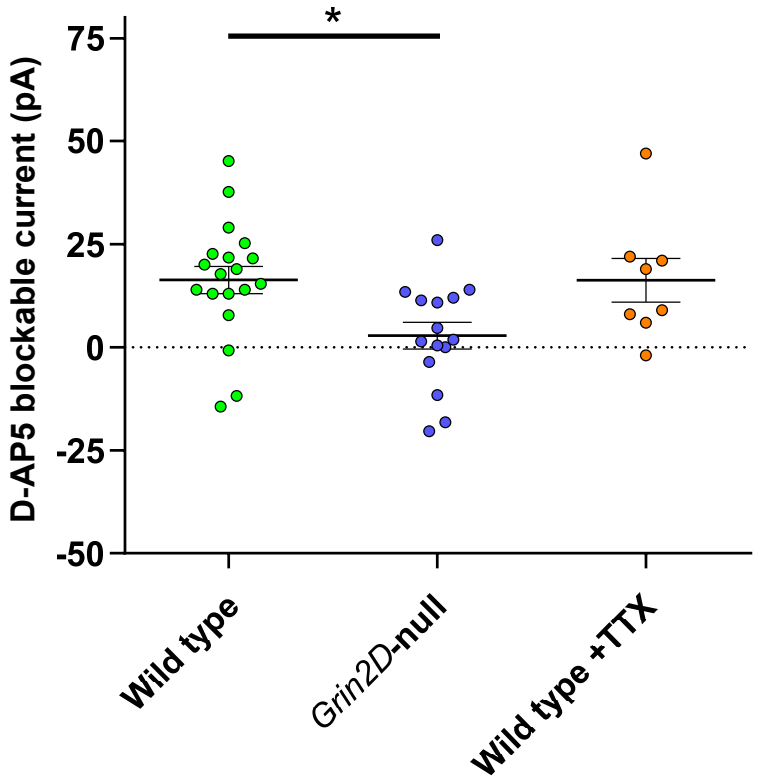

Figure 3.25 – D-AP5-sensitive current is significantly reduced in mice lacking GluN2D

Scatter plot showing the amplitudes of D-AP5-sensitive currents measured in wild type mice (both with and without TTX) and *Grin2D*-null mice. The mean D-AP5-sensitive current was significantly lower in *Grin2D*-null (n=15) in comparison to wild type mice (n=10; C57 and *Grin2D*-WT; p=0.0148*, ANOVA, Dunnett post-hoc). There was no difference between the D-AP5 sensitive current with (n=8) vs. without TTX.

3.3.2 Ambient glutamate in the SNc is regulated by glutamate reuptake transporters

Further experiments were performed in order to evaluate the role of glutamate reuptake in regulating tonic NMDAR activity: here a fast perfusion was applied to the slice, obtaining a stable baseline current in picrotoxin (50 μM) and glycine (10 μM), before applying the competitive glutamate transporter blocker TBOA (30 μM; Herman and Jahr 2007). In order to isolate the effects of transporter dysfunction only, the group II metabotropic glutamate receptor antagonist LY 341495 ('LY'; 200 nM) was applied along with TBOA, in order to prevent modulation of presynaptic glutamate release in response to altered extracellular concentration (Wang et al. 2005; Wild et al., 2015). Following the deflection in current arising from TBOA+LY application, and once a plateau had been reached, the NMDAR blocker D-AP5 (50 μM) was then applied in the presence of TBOA+LY (Example wild type traces shown in **Figure 3.26A**).

In wild type mice, Friedman analysis found there to be a significant difference between the current at baseline, with TBOA+LY, and then with D-AP5 (**Figure 3.27A**; $p<0.0001$****; n=26 [C57 n=10, *Grin2D*-WT n=5]). Application of TBOA+LY significantly increased the median baseline current (in picrotoxin and glycine) from 144.0 to 191.2 pA ($p<0.0001$****; Dunn post-hoc): the currents elicited by application of TBOA+LY were highly variable, and did not follow a normal distribution. Addition of D-AP5 then significantly reduced this current to 153.1 pA ($p<0.001$***; Dunn post-hoc). The baseline current did not significantly differ from the TBOA+LY+D-AP5 final current.

TBOA and LY were also applied in *Grin2D*-null mice, as above (Example trace shown in **Figure 3.26B**). Here, ANOVA found there to be a significant difference between the current at baseline, that with TBOA+LY, and that with D-AP5 (**Figure 3.27B**; $p=0.0072$**; n=15). Application of TBOA+LY significantly increased the baseline current from 195.8 ± 16.3 to 215.5 ± 18.3 pA ($p<0.05$*; Tukey post-hoc): here, the currents elicited by application of TBOA+LY were much less variable than those in those in wild type animals. The addition of D-AP5 then significantly reduced this current to 197.3 ± 16.23 pA ($p<0.05$*; Tukey post-hoc). The baseline current did not significantly differ from the TBOA+LY+D-AP5 final current.

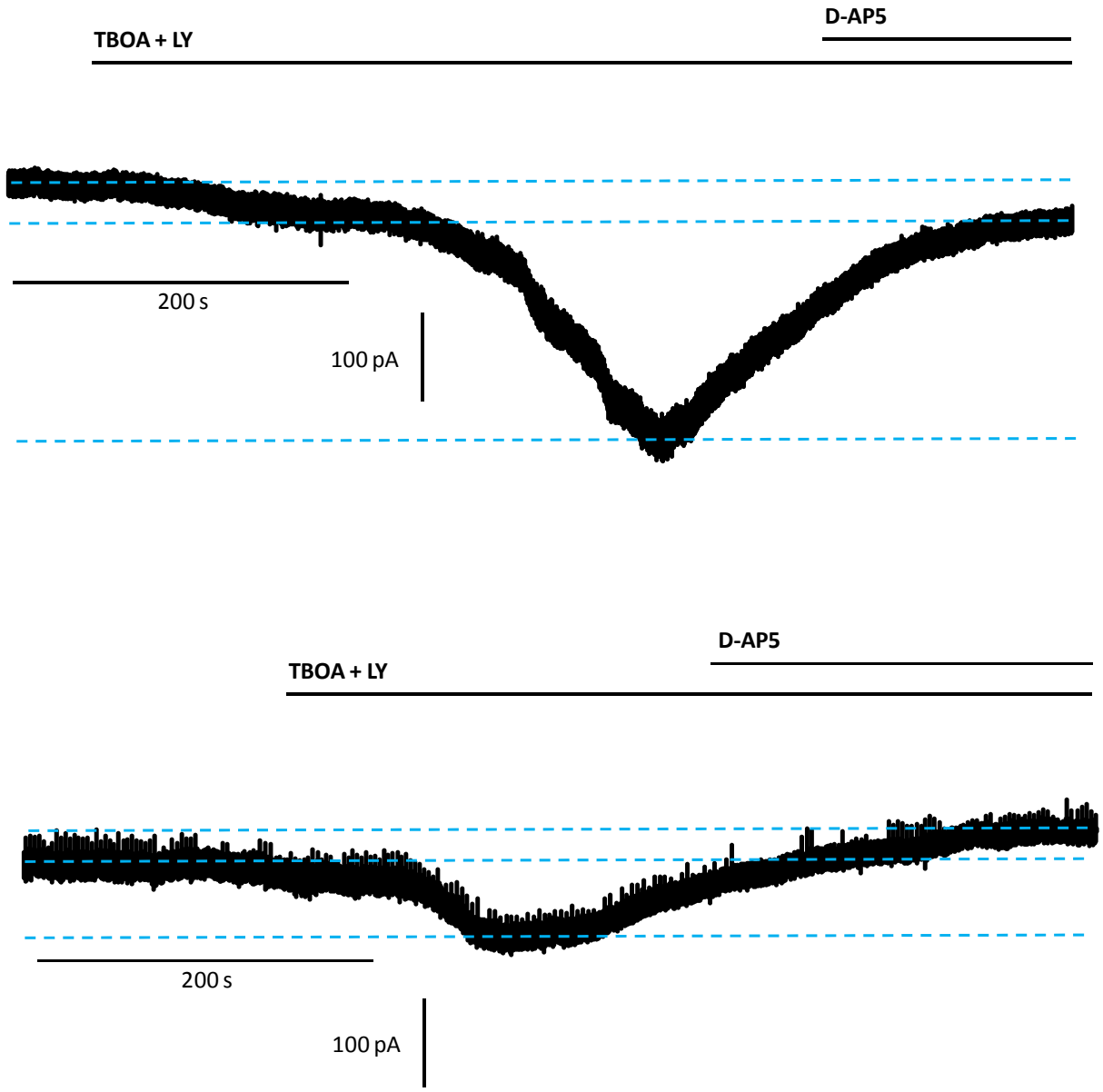

Figure 3.26 – Example traces showing the effect of glutamate transporter blockade on baseline current in wild type and *Grin2D*-null mice

Example traces from SNc-DA neurons held at -50 mV, showing an alteration in baseline current resulting from the addition of competitive glutamate transporter blocker TBOA (30 µM) and group II metabotropic glutamate receptor antagonist LY 341495 (200 nM), before blocking NMDARs by application of D-AP5 (50 µM). Desensitisation is not measured in these examples, hence the fast addition of DAP5. Trace **A** is from a P20 *Grin2D*-WT mouse, and trace **B** is from a P19 *Grin2D*-null mouse.

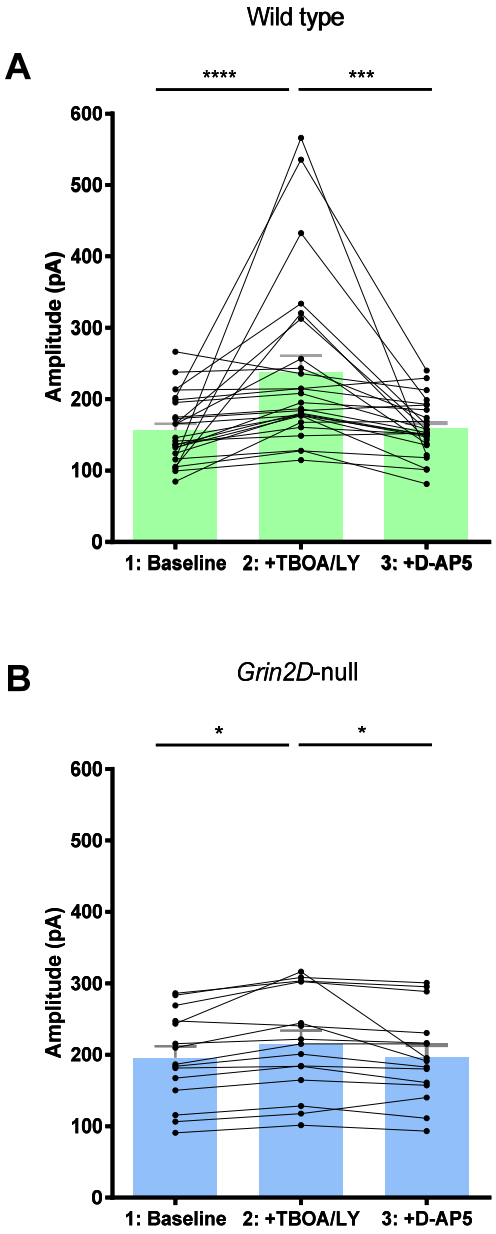

Figure 3.27 – Baseline current is significantly increased by addition of TBOA and LY in both wild type and *Grin2D*-null mice

Paired data showing baseline currents at -50 mV in SNc-DA neurons, at three time points: (1) baseline (picrotoxin and glycine only); (2) peak current following addition of competitive glutamate transporter blocker TBOA (30 µM) and group II metabotropic glutamate receptor antagonist LY 341495 (200 nM); and then (3) after addition of D-AP5 (50 µM). **A**: There was a highly significant difference between groups 1-2 ($p<0.0001$****) and 2-3 ($p<0.001$***; Friedman, Dunn post-hoc) in wild type mice (n=26; C57 and *Grin2D*-WT). **B**: There was also a significant difference between groups 1-2 ($p=0.0072$**) and 2-3 ($p<0.05$*; ANOVA, Tukey post-hoc) in *Grin2D*-null mice (n=15).

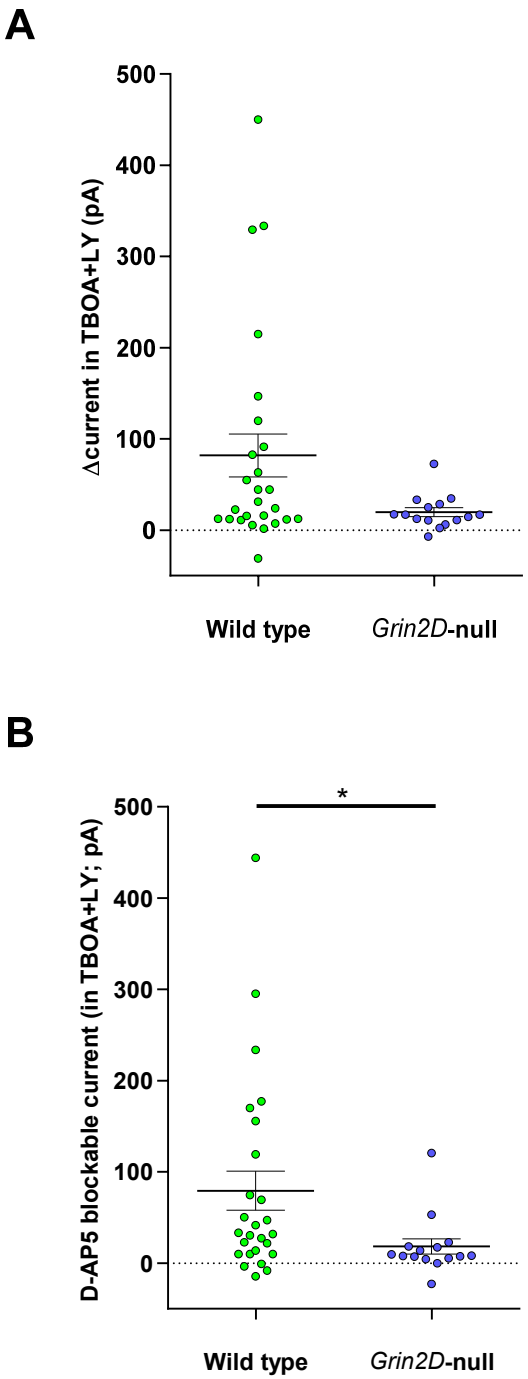

Figure 3.28 – The D-AP5-sensitive element of TBOA/LY-induced current is significantly reduced in mice lacking GluN2D

A: Scatter plot showing the peak amplitudes of TBOA/LY-elicited increases in current in both wild type (n=26; C57 and *Grin2D*-WT) and *Grin2D*-null mice (n=15). There was no significant difference between the two groups. **B**: Scatter plot showing the D-AP5-sensitive portions of the currents plotted in A. In this case there was a significant difference between wild type and *Grin2D*-null mice (p=0.0104*; two-tailed Mann-Whitney U).

The deflection in baseline current induced by the addition of TBOA+LY (current in TBOA+LY, minus baseline current) can be compared between wild type and *Grin2D*-null mice: there was no difference in this current (**Figure 3.28A**; p=0.119, two-tailed Mann-Whitney U), with 27.6 pA in wild type and 17.0 pA in *Grin2D*-null. Additionally, a comparison was performed within the wild type group: the TBOA+LY-induced deflection in current did not significantly differ based on the breeding background of the animals (p=0.892, two-tailed Mann-Whitney U).

We can also compare the D-AP5-blockable (IE NMDAR-mediated) portion of the total current in TBOA+LY, between genotypes. Here, in wild type mice, the median D-AP5-blockable portion of total current in TBOA+LY was 32.6 pA (n=26), significantly higher than the 8.2 pA observed in *Grin2D*-null mice (n=15) (**Figure 3.28B**; p=0.0104*; two-tailed Mann-Whitney U). Additionally, a comparison was performed within the wild type group: the TBOA+LY-induced deflection in current did not significantly differ based on the breeding background of the animals (p= 0.85, two-tailed Mann-Whitney U).

3.4 Bath application of NMDA elicits larger currents in *Grin2D*-null mice in comparison to wild type at very high concentrations only

Here, dose-response data were obtained by applying NMDA to the bath perfusion, in order to evaluate the current amplitudes elicited by wild type and *Grin2D*-null mice. A fast perfusion was applied to the slice, obtaining a stable baseline current in picrotoxin (50 μM) glycine (10 μM), and TTX (100 nM) before applying NMDA at one of several concentrations: 0.001, 0.01, 0.0316, 0.1, 1, or 10 mM; example responses are shown in **Figure 3.29**.

Resulting peak current values were subtracted from baseline and normalised to cell capacitance. Nonlinear regression was used to analyse the dose-response data in wild type (total n=23 [C57 n=4, *Grin2D*-WT n=19] from 22 different animals; age range P18-21) and *Grin2D*-null mice (total n=37; age range P17-21). The data were plotted using a logarithmic *x* axis, and the least squares (ordinary) fit method used in Graphpad Prism 7.03 to fit an

[agonist] vs response curve to each dataset (**Figure 3.30**). The curves clearly separated at the high concentrations, and therefore the extra sum-of-squares F test was next used in order to compare the upper curve plateaus, as well concurrently comparing the EC50 values: the analysis returned the result both parameters were significantly different (**Figure 3.30**; p=0.0374*). The top of the wild-type curve peaked at 52.82 ± 4.15 pA/pF, whereas the top of the *Grin2D*-null curve peaked at 68.64 ± 4.45 pA/pF. The wild-type EC50 value was 0.091 ± 0.037 mM, whereas the *Grin2D*-null EC50 value was 0.178 ± 0.057 mM.

With agonist application, a peak inward current will be reached, followed by a period of NMDAR desensitisation (Colquhoun et al. 1992; Meyerson et al. 2014), which can be measured once a plateau is reached (**Figure 3.31A**). NMDAR desensitisation was recorded from the experiments above where the highest 10 mM concentration of NMDA was applied: in *Grin2D*-WT mice, mean desensitisation was 55.2 ± 3.2 % of peak current, significantly less than the 72.4 ± 3.10 % desensitisation recorded in *Grin2D*-null mice (**Figure 3.31B**; p=0.0068**; two-tailed t-test).

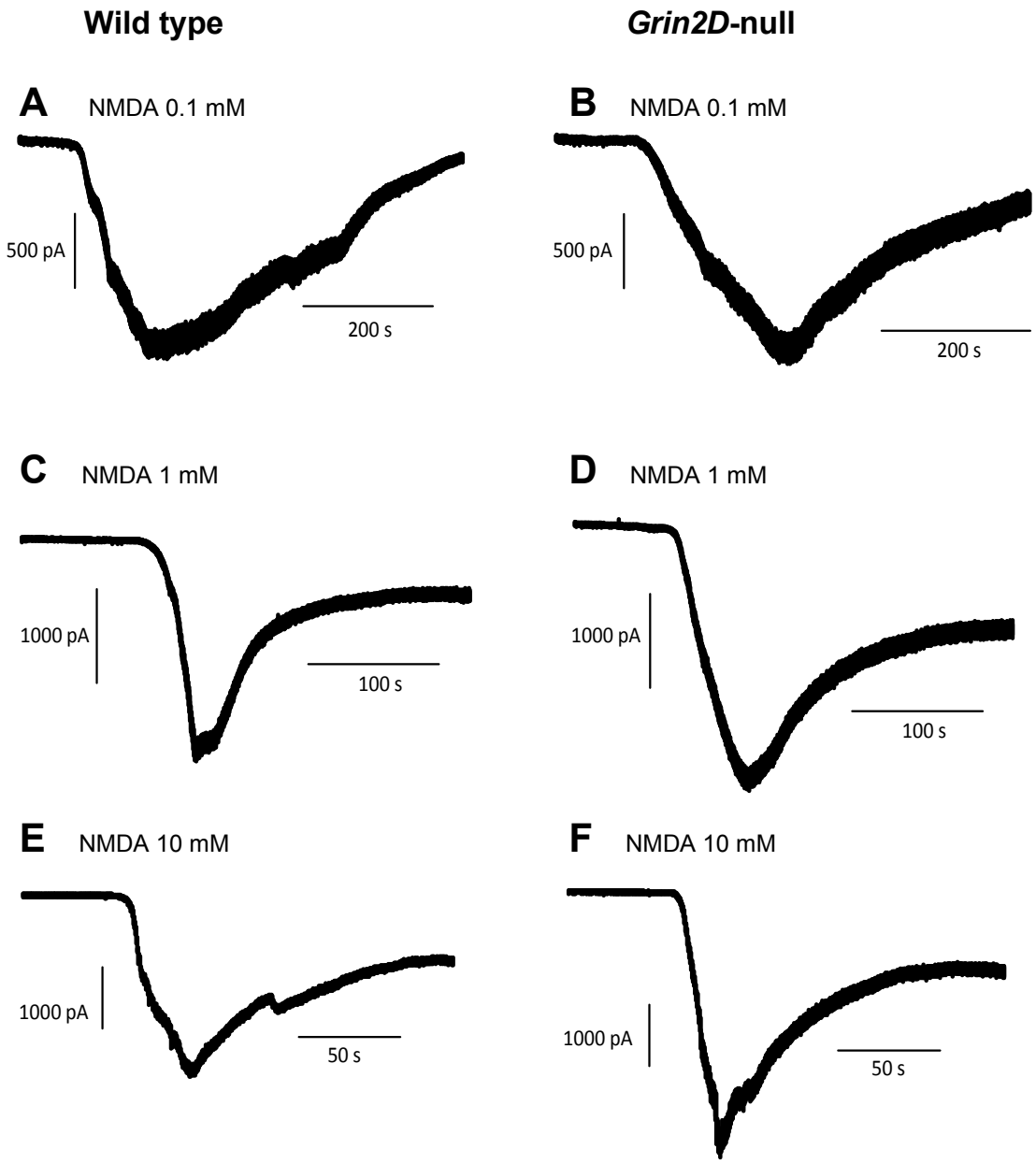

Figure 3.29 – Example traces showing currents elicited by bath applications of NMDA in wild type and *Grin2D*-null mice

Example traces from SNc-DA neurons from approximately three week-old mice, showing typical alterations in baseline current resulting from the addition of NMDA at 0.1, 1, and 10 mM concentrations. Scales matched for comparison based on genotype; note the difference in scale bars based on [NMDA]. **A**: Grin2D-WT, 0.1 mM NMDA; **B**: *Grin2D*-null, 0.1 mM NMDA. **C**: C57, 1 mM NMDA; **D**: *Grin2D*-null, 1 mM NMDA. **E**: Grin2D-WT, 10 mM NMDA; **F**: *Grin2D*-null, 10 mM NMDA.

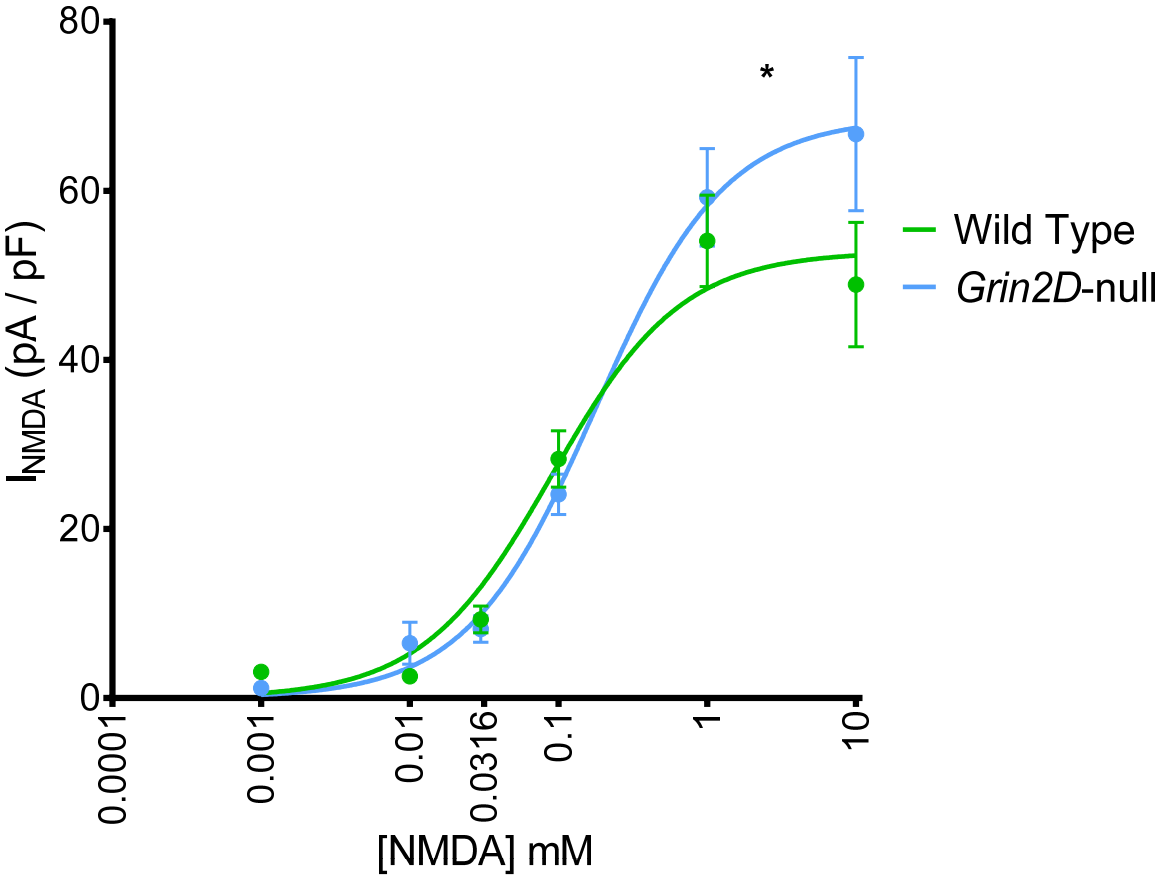

Figure 3.30 – Currents elicited by application of saturating concentrations of NMDA are significantly larger in mice lacking GluN2D

[Agonist] vs response curves showing data obtained at various NMDA concentrations increasing along a logarithmic scale from 1 µM to 10 mM, from wild type (total n=23 [C57 n=4, *Grin2D*-WT n=19] from 22 different animals) and *Grin2D*-null mice (total n=37). The tops of the curves separated, with significantly larger currents elicited at peak agonist concentrations in *Grin2D*-null mice in comparison to wild type, as well as a higher resulting EC50 value in *Grin2D*-null mice (p=0.0374*; extra sum-of-squares F test; both parameters concurrently analysed).

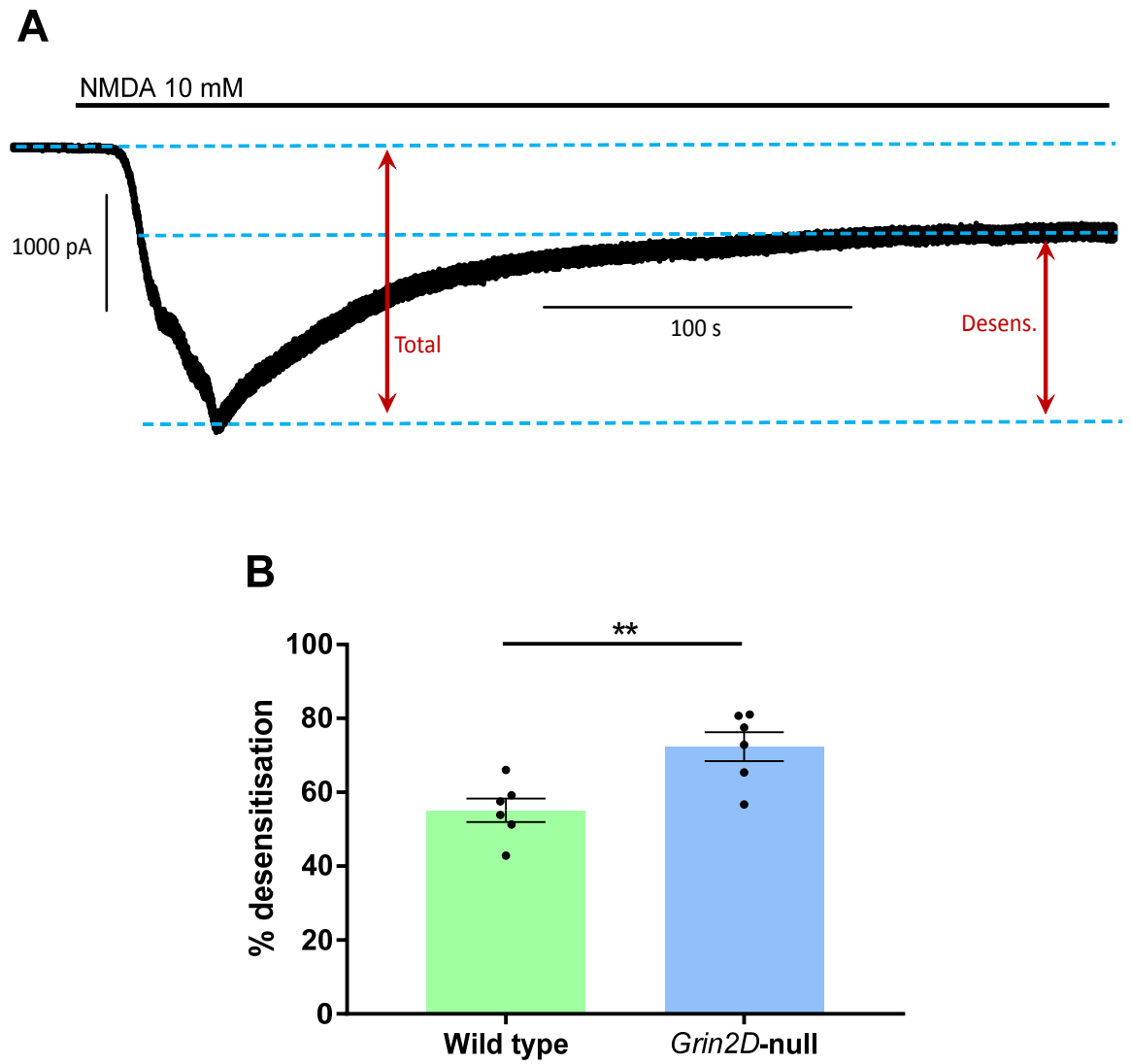

Figure 3.31 – NDMAR desensitisation is significantly increased in mice lacking GluN2D

A: Example trace from a P21 *Grin2D*-WT mouse showing NMDAR desensitisation with sustained application of 10 mM NMDA. Here, D-AP5 was not applied until a stable plateau was reached. **B**: Scatter plot showing desensitisation as a percentage of total NMDA-elicited current, which was significantly higher in *Grin2D*-null mice in comparison to *Grin2D*-WT mice (p=0.0068**; two-tailed t-test).

3.5 Hypoxic conditions cause significant but comparable cell death in both wild type and *Grin2D*-null mice

As above, NMDA-evoked currents were larger in *Grin2D*-null mice only at very high agonist concentrations, indicating that GluN2D limits cation influx at maximum NMDAR saturation. This was interesting because under conditions of hypoxia, the open probability of GluN2D-containing NMDARs has been shown to decrease, thereby also reducing total current flow (Bickler et al. 2003). The presence of whole-cell currents being altered in SNc-DA neurons by removal of the GluN2D subunit may indicate that a practical hypoxia resistance could be conferred by the presence of GluN2D, and an assay was therefore developed to explore cellular viability in acute slices from mice aged P28-48 in combination with fluorescent staining of dopaminergic neurons.

Horizontal slices through the substantia nigra region were carefully made at a thickness of 100 μm. For each slice produced, a cut was made along the midline and one hemisphere randomly assigned to a high oxygen (normoxic) treatment group, and one to a hypoxic treatment group. Following a 40 minute recovery in normoxic conditions (gassed with 95% O_2 / 5% CO_2) slices in both groups were transferred to new Gibb chambers for a 40 minute treatment period: the normoxic group to a new chamber gassed again with 95% O_2 / 5% CO_2, and the hypoxic group to a chamber gassed with 15% O_2 / 80% N_2 / 5% CO_2. The slices in both groups were then carefully transferred back to their original, separate normoxic chambers, and fluorescent nuclear stain propidium iodide (PI; 20 mM) added to the chamber. PI is actively removed from living cells (Lossi 2009; Tasca et al. 2015). After 20 minutes, all slices were briefly and gently washed twice in Krebs buffer, before being stored in darkness in glass vials containing 4% paraformaldehyde (PFA) in phosphate-buffered saline (PBS). After subsequent washing and blocking / permeation stages, all slices were fluorescently labeled for tyrosine hyrdoxylase (TH) in order to visualize dopaminergic cells (**Figure 3.32**). To obtain the data, the SNc region was visually identified by proximity to MT, and the whole region scanned systematically in order to count all TH+ cells. For each TH+ cell observed, the wavelength of the light was switched to the excitation frequency of PI, in order that the PI status of each cell could be recorded.

Each animal contributed an *n* of 1 to each of the normoxic and hypoxic groups (and therefore allowed the data to be paired). Each *n* consists of the percentage value of TH+ cells which are co-stained with PI from all the TH+ cells within the slice hemispheres of that group, for that animal. In C57 mice (n=7; mean age P41.0), and applying the normoxic treatment, 50.9 ± 6.9 % of TH+ cells were stained with PI. In hypoxia-treated slices from the same animals, this value was 79.3 ± 3.6 %. In *Grin2D*-null animals (n=7; mean age P35.1), applying the normoxic treatment, 54.2 ± 2.3 % of TH+ cells were stained with PI. In hypoxia-treated slices, this value was 73.1 ± 3.3 %.

A repeated measures 2-way ANOVA was performed on all the data, comparing the interactions between genotype and oxygenation status, and pairing the normoxic and hypoxic result from each animal. The effect of oxygenation status was found to be highly significant (**Figure 3.32A**; overall p<0.0001****: post-hoc reports p<0.0001**** in WT (C57), and p<0.01** in *Grin2D*-null, Sidak) whereas there was no effect resulting from genotype (p=0.789). The mean number of TH+ cells recorded within the SNc region of each 100 μm slice was also analysed. There was a mean of 12.0 ± 2.7 TH+ cells per slice in normoxic conditions (n=14), and 11.8 ± 0.82 per slice in hypoxic conditions (n=14), as shown in **Figure 3.32B**. A repeated measures 2-way ANOVA was performed on the data: there were no interactions affecting TH+ cells per slice based on either oxygen status (p=0.88) or genotype (10.1 ± 0.9 per slice for WT (C57), and 13.6 ± 1.3 for *Grin2D*-null; p=0.068).

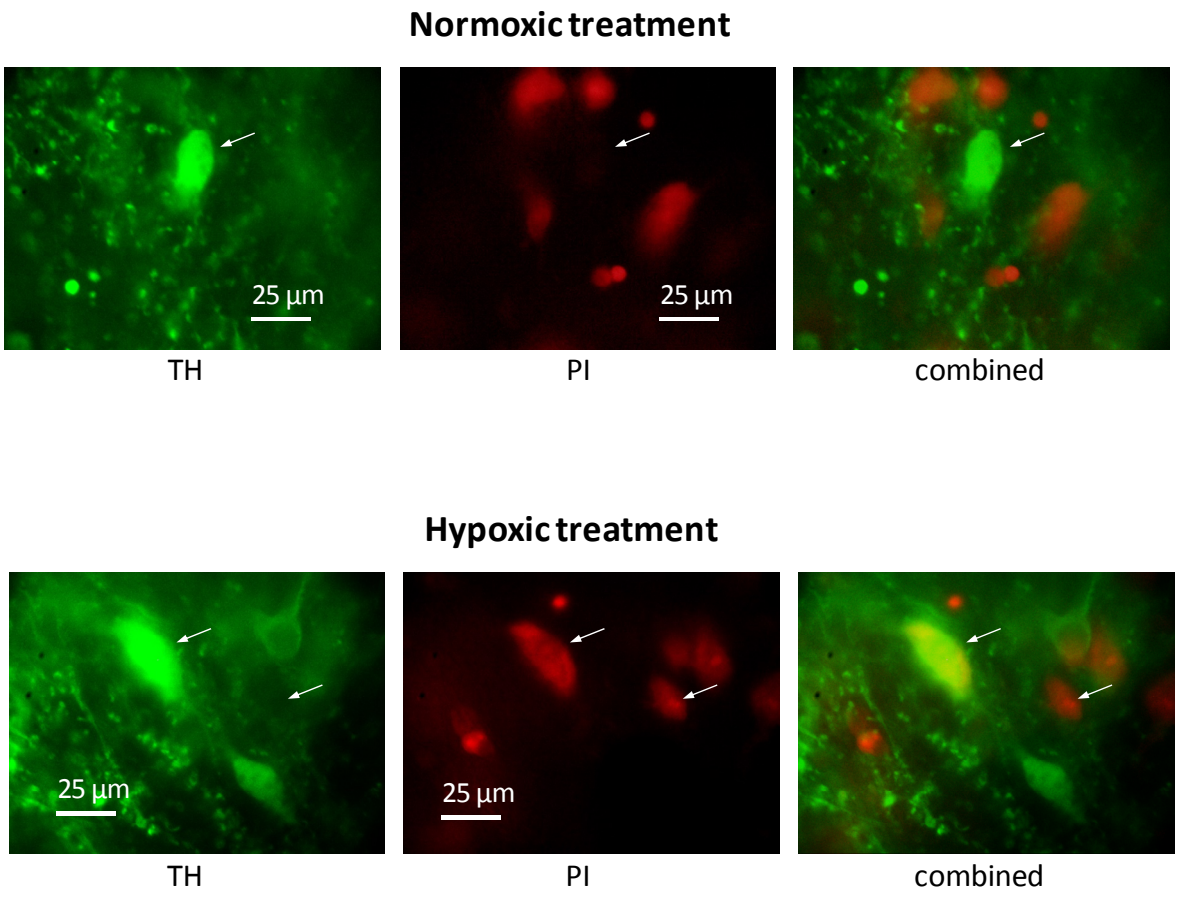

Figure 3.32 – Example fluorescent images from mouse brain slices after high and low oxygen incubations

Example immunofluorescence images showing tyrosine hydroxylase (TH) staining, green; and propidium iodide (PI) viability assay staining, red; in both 'normoxic' (95% O_2 / 5% CO_2, for 40 minutes; above) and 'hypoxic' (15% O_2 / 5% CO_2 / 80% N_2, for 40 minutes; below) treatment groups. Arrows indicate example cells which together demonstrate the specificity of the labeling.

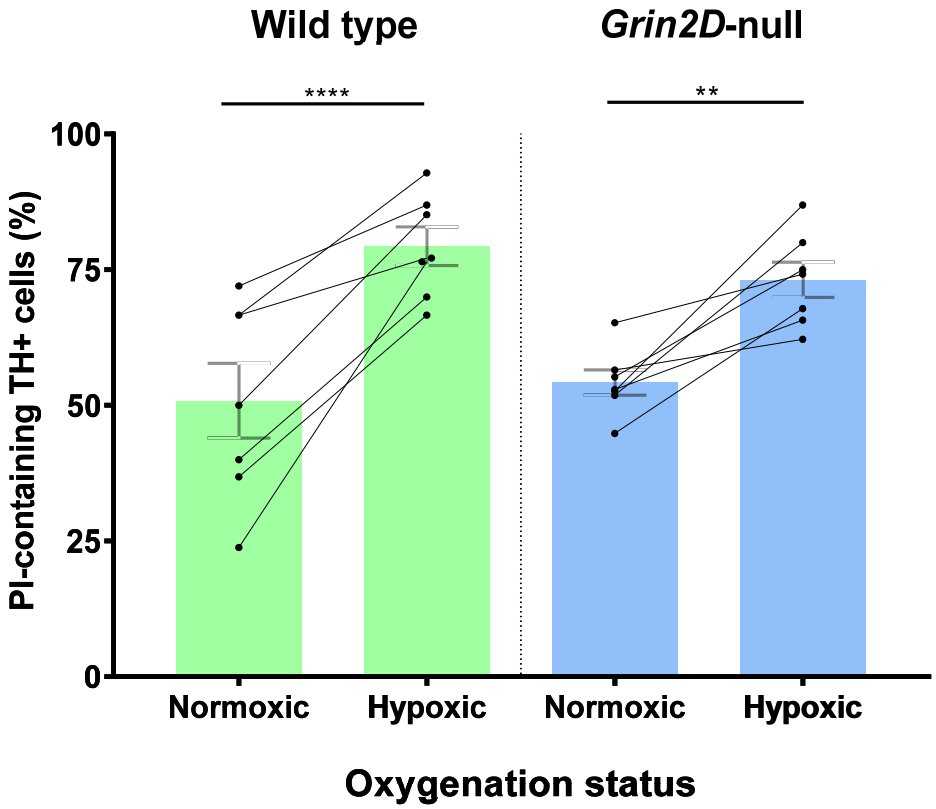

Figure 3.32 – Hypoxic conditions cause significant but comparable cell death in both wild type and *Grin2D*-null mice

Paired scatter plots showing the percentage of tyrosine hydroxylase-positive (TH+) cells which were also positive for cell death marker propidium iodide (PI) in both 'normoxic' (95% O_2 / 5% CO_2, for 40 minutes; above) and 'hypoxic' (15% O2 / 5% CO2 / 80% N_2, for 40 minutes; below) treatment groups. The effect of oxygenation status was highly significant ($p<0.0001$****, two factor ANOVA), but there was no difference based on genotype.

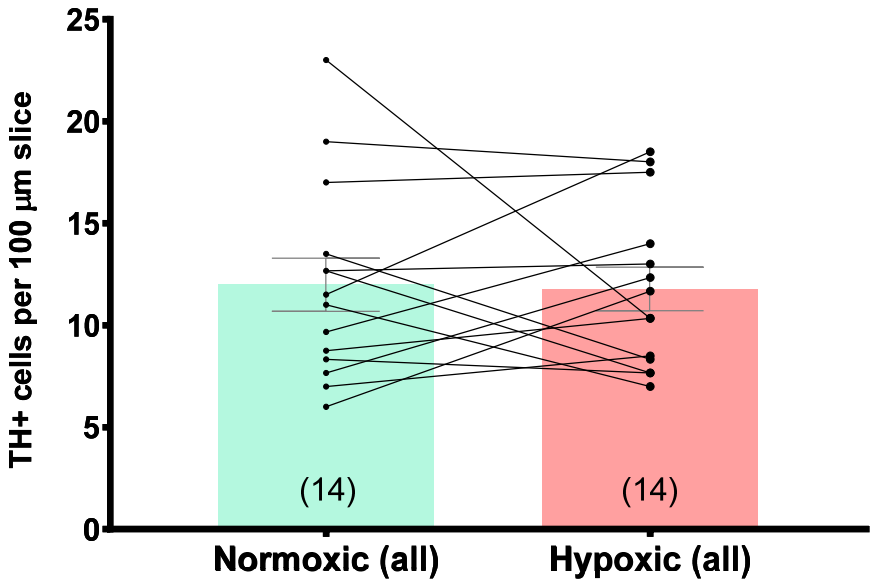

Figure 3.33 – The hypoxic treatment does not cause a change in the number of detectable TH^+ neurons

Scatter plot (WT and *Grin2D*-null data combined) showing the number of tyrosine hydroxylase-positive (TH+) cells observable within the SNc region of each 100 µM-thick slice: there were no differences based on either oxygen status or genotype. There was a mean of 12.0 ± 2.7 TH^+ cells per slice following normoxic treatment (n=14), and a mean of 11.8 ± 0.82 TH^+ cells per slice following hypoxic treatment (n=14).

CHAPTER 4

DISCUSSION

4 Discussion

The focus of this thesis was to investigate the expression of functional NMDARs in SNc-DA neurons, as well as how the GluN2D subunit within NMDARs expressed either synaptically or across the neuronal surface may allow the neuron to react to various potentially excitotoxic conditions such as inhibited glutamate reuptake, increased excitatory burst input, and hypoxia-ischemia. To achieve this, whole-cell patch clamp electrophysiology was used in acute mouse brain slices, as well as cell viability assaying and immunofluorescent staining.

The role of GluN2D has not been extensively studied, and as expression of this subunit can be removed with only relatively minor phenotypic effects, its role in SNc-DA neurons was able to be explored by comparing data from wild type and *Grin2D*-null animals. Firstly, functional synaptic NMDAR expression was examined using presynaptic stimulation along with pharmacological intervention.

4.1 Characterisation of synaptic NMDARs in SNc-DA neurons of *Grin2D*-null mice

Results from pharmacological intervention into glutamatergic synaptic transmission onto SNc-DA neurons showed that genetically engineered mice lacking expression of the GluN2D subunit likely had a different synaptic NMDAR subunit profile to wild type animals. The data, discussed below, suggested that wild type animals had a lower proportion of NMDAR current mediated by GluN2B, as well as a higher proportion mediated by GluN2D, in comparison to the *Grin2D*-null animals, highlighting a functional role of GluN2D at glutamatergic synapses onto SNc-DA neurons.

4.1.1 Constitutive NMDAR expression at Grin2D-null synapses

Removal of the GluN2D subunit is a useful tool for exploring its role in SNc-DA neurons. In order to evaluate whether overall synaptic NMDAR expression is altered in the genetically modified animals, AMPAR/NMDAR current ratios (A/N ratios) were measured. The A/N ratio is appropriate as it is not possible to elucidate the number of synapses activated by the stimulating electrode, and of course this will differ in each experiment. Therefore, the

amplitude of the current through NMDARs compared to AMPARs is much more useful, as the expression of AMPARs should not be altered in *Grin2D*-null mice.

Development during the age ranges tested is not a basic consistent alteration of either NMDAR or AMPAR number: rather, both are altered concurrently over time (Wu et al. 1996; Petralia et al. 1999). There is therefore no linear relationship between A/N and age, and only results within the same age group can be compared by genotype. However, across the ages, genotype did not have an effect on the A/N ratio value, which indicates that removal of the GluN2D subunit does not alter the amplitude of the current passing through synaptic NMDARs, and it is therefore likely that constitutive expression at the synapse remained unaltered in *Grin2D*-null mice. This result initially suggests that GluN2D is either being replaced by another GluN2 subunit within the receptor, or is not present at the synapse (or is present only in small numbers). To investigate this further, subunit-specific pharmacological inhibition was applied to synaptic NMDAR-EPSCs.

4.1.2 Altered properties of synaptic NMDARs in Grin2D-null mice

Pharmacological inhibition data was obtained using GluN2B-preferring inhibitor ifenprodil and measuring its effect on synaptic NMDAR-EPSCs. Ifenprodil is an ideal compound to use in SNc-DA neurons in which the only present GluN2 subunits are likely to be GluN2B and GluN2D (Brothwell et al. 2008), as its affinity for GluN2D is the lowest of any of the subunits with an IC50 of 76 μM, whereas the IC50 for GluN2B is just 0.1 μM (Hess et al. 1998). Results showed that in both P7 and P21 mice there was a significantly greater percentage inhibition of NMDAR-EPSCs in *Grin2D*-null mice in comparison to wild type: this suggests that in mice lacking the GluN2D subunit, GluN2D is replaced by GluN2B within the NMDAR. If triheteromeric GluN1/GluN2B/GluN2D NMDARs are expressed at synapses onto SNc-DA neurons in wild type mice, it appears likely that they are replaced with diheteromeric GluN1/GluN2B receptors in *Grin2D*-null mice. The increase in ifenprodil inhibition in *Grin2D*-null mice compared to wild type was approximately 16 % at both age groups, and it is possible that this difference accounts for the proportion of GluN2D-mediated synaptic current in wild type animals.

There was a trend of decreasing inhibition of GluN2B by ifenprodil in the two P21 age groups, in comparison to those at P7. This suggests that there is a smaller percentage of GluN2B at the synapse in the older mice, consistent with earlier reports of a developmental decrease in diheteromeric GluN1/GluN2B NMDARs in SNc-DA neurons and potentially moving to the triheteromeric GluN1/GluN2B/GluN2D configuration with development (Brothwell et al. 2008): ifenprodil may have a less powerful inhibitory effect on triheteromeric NMDARs which also contain GluN2D, in comparison to GluN1/GluN2B diheteromers.

Application of GluN2D-preferring inhibitor DQP-1105 gave a small inhibition which was significantly larger in both P7 and P21 wild type in comparison to *Grin2D*-null animals. This suggests that GluN2D is present at the synapse at both age groups. However, the comparisons based on genotype were close to the p=0.05 threshold for significance: because the inhibition by DQP is low (as a percentage of the total NMDAR-mediated current) this makes it more difficult to detect a difference in inhibition based on genotype, especially considering the inherent variability in EPSC amplitudes. However, the differences in inhibition based on genotype were around 15 % at P7 and 9 % at P21, close to the 16 % difference based on genotype in the ifenprodil experiments above. As argued above, the smaller percentage inhibition at P21 may be caused by DQP having a less powerful inhibitory effect on triheteromeric NMDARs which also contain GluN2B, in comparison to GluN1/GluN2D diheteromers.

Overall, in the mice lacking GluN2D, there was significantly *less* inhibition by DQP, and significantly *more* inhibition of GluN2B by ifenprodil: together this suggests that GluN2D is present at the synapse in wild type mice, and that in *Grin2D*-null animals the GluN2D subunit is replaced by GluN2B within synaptic NMDARs.

NMDAR-EPSC decay time constants did not differ between genotypes which may imply that GluN2D does not make up a large proportion of synaptic NMDAR currents under the above conditions; something which is supported by the relatively small but concrete difference in ifenprodil sensitivities.

4.2 Activity-dependent regulation of NMDA receptors

The effects of burst firing of glutamatergic afferents onto SNc-DA neurons were explored in this thesis: in summary, results showed a downregulation of NMDAR-mediated synaptic currents. This downregulation, discussed in detail below, only occurred if the burst protocol was applied at a holding potential of -20 mV, and only if the stimulation was applied whilst holding at this potential. The downregulation may possibly have a Ca^{2+}-dependent component, as holding at +40 mV to dissuade cation influx prevented the effect, whilst Ca^{2+} chelation did not. Summated NMDAR-mediated currents, which may also include perisynaptic or extrasynaptic receptors, were depressed in a similar fashion, though significantly less so, potentially indicating differential regulation of these NMDAR populations, or a presynaptic effect. The GluN2D subunit appears not to have any key role in the observed regulation, as *Grin2D*-null animals displayed a matching effect.

4.2.1 Reduction in NMDA-EPSC amplitude in response to high frequency burst firing of excitatory afferents

Glutamatergic synapses in general can be potentiated or depressed by various presynaptic stimulation patterns, often through NMDAR-mediated alteration of synaptic AMPARs (Montgomery et al. 2005). However, both long-term potentiation (LTP) and long-term depression (LTD) of NMDAR-mediated currents can also be induced by presynaptic activity (Montgomery et al. 2005; Harnett et al. 2009; Hunt and Castillo 2012). A paradigm was used which is similar to another previously applied to neurons in the calyx of held synapse (Joshi et al. 2007), where it elicited downregulation of NMDAR-EPSC amplitudes. The paradigm, stimulating glutamatergic afferents onto SNc-DA neurons, was one of high frequency burst firing (100 Hz x 3, every 1 s for 60 s). These afferents originating from the STN increase their firing in PD, and burst firing frequency is close to 100 Hz, and so was logical paradigm to adopt to apply to SNc-DA neurons which are characteristically lost in this disease, and indeed to measure any changes in NMDAR-mediated currents. Excessive Ca^{2+} influx through NMDARs is implicated in excitotoxicity through activation of cell death signalling pathways (Choi 1987; Hardingham and Bading 2010; Surmeier et al. 2010, 2011), and the increased

NMDAR activity occurring as a result of increased burst firing input may also promote cell death (Dong et al. 2009).

The 20-25 minute timeframe (1200-1500 s) was originally selected as being enough for longer term modulatory effects to take place: in the large auditory synapse, depression of NMDAR-EPSCs was pronounced at 20 minutes (Joshi et al. 2007). The results presented in this thesis showed that there was a significant reduction in NMDAR-EPSC amplitudes 1200-1500 s following the IP in wild type animals. No such downregulation was observed in the control group in which the holding current was switched to -20 mV (as it is in the treatment group) but no stimulation applied, and indeed NMDAR-EPSC amplitudes following the IP in the wild type treatment group were significantly depressed in comparison to this control group, indicating that the observed reduction is in response to the stimulation provided within the IP at -20 mV. This downregulation is a process which may occur by the binding of regulatory molecules to one or more subunits, and as the above synaptic pharmacology data supports the presence of GluN2D at synapses on SNc-DA neurons its potential role of in this regulation was next explored.

Mice lacking the GluN2D subunit displayed a similar reduction in NMDAR-EPSC amplitude in response to the IP: the lack of the GluN2D subunit did not affect this form of activity-dependent regulation, as there was no difference between the data in wild type and *Grin2D*-null animals. Therefore the GluN2D subunit is unlikely to be involved in the mechanism by which activity-dependent regulation takes place at glutamatergic synapses on SNc-DA neurons.

A holding potential of +40 mV was chosen for recording the assaying pulses in all experiments where afferent fibres were activated using a stimulating electrode, as there is a decreased NMDAR magnesium blockade at this potential. Additionally, the driving force on Ca^{2+} ions is reduced and there is therefore less likelihood of activating Ca^{2+}-dependent regulatory mechanisms. In the activity dependent regulation experiments it was deemed sensible to also perform a control in which the IP was applied as in the regular treatment group, except that the holding potential remained +40 mV, rather than moving to -20 mV. In this group there was no significant downregulation, suggesting that Ca^{2+} influx is reduced enough at +40 mV to prevent a significant effect on NMDAR regulation: indeed, the assaying pulses are applied at a lower frequency; a single pulse every 10 s or a 50 Hz burst every 20 s,

as opposed to a 100 Hz burst every 1 s. Therefore applying assaying pulses where the postsynaptic cell is held at +40 mV are unlikely to lead to significant NMDAR regulation.

A specific Ca^{2+} influx profile can be essential for plasticity to occur: high frequency burst firing activity has previously been found in the hippocampus to induce either LTP or LTD of NMDAR-EPSCs, depending on intracellular Ca^{2+} conditions (Harney and Anwyl 2012). Low Ca^{2+} buffering allowed NMDAR-LTP to occur using 200 Hz HFS, whereas increasing this buffering caused depression of NMDAR-EPSCs. The results in this thesis showed that in SNc-DA neurons where the IP was applied at -20 mV along with a high concentration of fast Ca^{2+} chelator BAPTA (10 mM) present in the patch pipette, there was a significant downregulation of NMDAR-EPSCs similar to that observed in the normal wild type IP treatment group. The equilibrium potential of Ca^{2+} is +150 mV, and therefore a much stronger inhibition of Ca^{2+} activity may be expected by BAPTA than by simply holding at +40 mV; yet as above, holding at +40 whilst applying the IP appeared to inhibit the activity dependent reduction in NMDAR-EPSC amplitude. One reason BAPTA may fail to reduce the effect of the IP because it does not diffuse far enough away from the soma to effectively buffer Ca^{2+} at more distal synapses. Additionally, the reason that holding at +40 mV during the IP inhibits downregulation may be due to a consequent reduction in the initial spike in Ca^{2+} concentration required by low affinity kinases to effect synaptic plasticity, though high transient spikes in $[Ca^{2+}]$ most often lead to potentiation, rather than depression (Lüscher and Malenka 2012). The initial spike in $[Ca^{2+}]$ will be higher at -20 mV, and it is possible that BAPTA is not fast enough at chelating the Ca^{2+} moving into the cell to prevent a high initial peak: some, but not all of it is likely to be chelated quickly, but that which does not come into contact with BAPTA immediately may still bind to its target molecule. To make a final conclusion on the role of Ca^{2+} in the activity-dependent NMDAR regulation observed here, it may be prudent to repeat the WT IP -20 mV treatment group with Ba^{2+} replacing Ca^{2+} in the perfused Ringer solution, as well as the intracellular solution, in order to inhibit calcium-dependent regulatory processes; or potentially using an increased BAPTA concentration.

Intracellular BAPTA (10 mM) caused a change in the mean potential of the neurons at which there was zero net current (V_{Izero}) of 19.55 mV; from -8.25 to +11.3 mV. A decrease in intracellular $[Ca^{2+}]$ may cause an increase in overall V_{Izero} due to a combination of an increase in the Ca^{2+} reversal potential, and an inhibition of the persistent inward Na^{+} current (I_{NaP}) at

depolarised potentials: I_{NaP} is involved in the generation of natural rhythmic burst firing activity in STN neurons (Darbon et al. 2004), and is mediated via TTX-sensitive voltage-gated sodium channels (though I_{NaP}–mediating channels are distinct from those underlying the upward stroke of the action potential). Previous work has shown that I_{NaP} channels require a minimum concentration of intracellular Ca^{2+} in order to properly function, and that the currents mediated by them are therefore eliminated by high BAPTA in neocortical neurons (Schwindt et al. 1992). Altering I_{NaP} and therefore excitability is unlikely to affect the data obtained here in those recordings made with BAPTA, as the purpose was to limit intracellular Ca^{2+} and measure NMDAR regulation, rather than measure neuronal excitability or firing; and in any case a distinct effect on NMDAR regulation was not observed with the addition of BAPTA.

The paradigm used in this thesis is similar to another previously applied to neurons in the calyx of held synapse (Joshi et al. 2007), where it elicited a reduction in NMDAR-EPSC amplitude, likely through a mechanism whereby NMDARs are removed from the postsynaptic membrane in order to increase temporal fidelity at this synapse, thereby enabling functional auditory signal processing. Whilst NMDAR-EPSCs are similarly depressed by high frequency stimulation in SNc-DA neurons as shown here, the reason for downregulation is likely to differ from that applicable in the calyx of held. One reason is neuroprotection: a downregulation in NMDAR activity in response to an upward shift in input burst firing activity would be a mechanism for limiting the amount of Ca^{2+} influx such that it does not lead to toxicity. Another similar but distinct 'motive' for downregulation of NMDAR activity in this scenario is to limit excitability of SNc-DA neurons such that they do not modulate into their burst firing phase for too long in response to sustained high frequency input.

Other paradigms similar to that used in this thesis (IE stimulation of glutamatergic afferents at 100 Hz in some configuration) have also been shown to cause depression of synaptic NMDAR activity in neurons of the nucleus accumbens (GluN2A-mediated; Chergui, 2011; Kombian and Malenka, 1994); and, conversely, potentiation of synaptic NMDAR activity in neurons of the hippocampus (Scaffer-CA1; Bashir et al. 1991; Berretta et al. 1991; Grosshans et al. 2002) and amygdala (Gean et al. 1993; Hunt and Castillo 2012), demonstrating that the effect of high intensity glutamatergic input is highly dependent on tissue type, as well as

various other factors such as NMDAR subunit profile, mGluR activation, and downstream signalling profile which may be distinct by neuron type (Hunt and Castillo 2012).

Other work in SNc-DA and VTA neurons found that high frequency presynaptic stimulation (70 stimuli at 50 Hz) can result in LTP of synaptic NMDAR-EPSCs when applied with burst firing in the postsynaptic neuron (five APs at 20 Hz; Harnett et al. 2009a). Conversely, presynaptic stimulation alone caused a small but significant LTD of NMDAR-EPSCs. The authors also found that a larger depression of NMDAR EPSCs was induced when the burst was applied preceding (by 250 ms) the applied synaptic stimulation. However, the authors did not differentiate between VTA and SNc dopaminergic neurons. In the results presented in this thesis, the induction paradigm caused a depression of NMDAR-EPSCs amplitudes which was dependent on the presence of high frequency presynaptic bust firing, and in this case a depolarised holding potential of -20 mV was also required for the depression to occur: whilst postsynaptic firing was not elicited, this depolarised holding potential was applied before (2-5 s) before initiation of high frequency presynaptic burst stimulation, and sustained throughout. Additionally, in the work presented here the assaying NMDAR-EPSCs were elicited using physiological [Mg^{2+}] (1 mM), but at +40 mV to relieve Mg^{2+} block. The Harnett study used low [Mg^{2+}] (0.1 mM) at a resting holding potential of -62 mV, and it is therefore possible that one or more of these factors (along with the different stimulation frequency) may contribute to a different response.

It would be of interest to ascertain whether the form of synaptic NMDAR downregulation observed here is due to internalisation. Both AMPA and NMDA downregulation in the hippocampus have been shown to be due to internalisation via dynamin-dependent endocytosis (Carroll et al. 1999; Lau and Zukin 2007), and NMDAR downregulation in the Calyx of Held is both Ca^{2+}- and dynamin-dependent (Joshi et al. 2007). In SNc-DA neurons, NMDAR 'rundown' elicited by repeated application of NMDA via perfusion has previously been found to be Ca^{2+} and dynamin dependent (Wild et al. 2014): however, there was also rundown in an ifenprodil-insensitive portion of the current, potentially mediated by GluN2D-containg NMDARs, which was not Ca^{2+}-dependent.

The key result here with regards to activity dependent synaptic regulation is that NDMAR-EPSC amplitude was significantly reduced in the wild type and *Grin2D*-null treatment groups in comparison to the control group in which holding potential was moved to -20 mV and no

stimulation applied. Therefore is possible to draw the conclusion that the application of high frequency burst stimulation (at a depolarized potential of -20 mV, as it is here) was the cause of the reduction, and that GluN2D is not involved.

4.2.2 Summated NMDA-EPSC amplitudes were also reduced in response to high frequency burst firing of excitatory afferents

Summated assaying EPSCs were elicited along with single EPSCs within each experiment because some perisynaptic NMDARs are likely to be recruited as a result of trains of stimuli applied to glutamatergic fibres onto SNc-DA neurons (Wild et al. 2015), and this was therefore a method to determine if perisynaptic NMDARs were being differentially regulated compared with synaptic NMDARs, and/or whether significant differences arise due to the removal of GluN2D when perisynaptic NMDARs are additionally stimulated. For example, if there is a difference in the number of GluN2D-containing NMDARs at the synapse vs. the peri/extrasynaptic zones, there may be a difference in regulation if either GluN2B or GluN2D is essential to that regulation. In the Joshi et al. study at the calyx of held, synaptic NMDAR-EPSCs remained stable whilst summated responses were depressed, which may suggest that perisynaptic or extrasynaptic NMDARs activated by glutamate spillover were being preferentially downregulated (Joshi et al. 2007). However, the giant calyx synapse is very different morphologically in comparison to typical small CNS synapses which may lead to different transmitter release and spillover profiles and, an indeed NMDAR configurations and downstream signalling processes.

Overall, summated NMDAR-EPSCs showed a similar pattern of regulation to single EPSCs. However, the proportional changes observed in both single and summated EPSCs were recorded within the same experiment, and so this allows pairing of the data: this led to the observation that there is in fact a small but highly significant difference in regulation between these two measures. The results showed that single (synaptic) EPSCs at the 1200-1500 s time period were smaller, proportionally, than summated EPSCs, when normalised to their pre-IP amplitude. That this difference in proportional regulation is small would be expected given the fact that the same synaptic population of NMARs may compromise much of the peak current (Wild et al. 2015).

There are several possibilities why this occurs. Firstly, it was observed that in post-hoc comparison that there was no difference in this effect between the treatment groups: that is, there is a significant difference between regulation of single and summated responses, but treatment has no significant effect on this difference. This suggests that the overall effect here is not a result of the IP, but some other factor. An interesting result which may explain this was that the NMDAR paired pulse ratio also slightly increased over the course of the experiment, regardless of the treatment group: this means that there is an increase in summation, which could be caused by several factors. Firstly, this would occur if the synaptic population of NMDARs were being preferentially downregulated in comparison to those additionally activated by a second pulse, or indeed trains of stimuli. Secondly, this could also occur if NMDARs were being recruited into the perisynaptic zone. Thirdly, it may be a presynaptic factor: potentially, an increase in the probability of vesicular glutamate release (P_{ves}) at the second (and subsequent) stimulus in the train, which could occur due to a decreased capacity for presynaptic Ca^{2+} clearance (Scullin et al. 2012). Lastly, the increase in PPR and summation may be due to increased glutamate spillover from the synapse over the course of the experiment due to decreased GluT function. The multitude of possibilities for the change in NMDAR-PPR and therefore the difference in normalised single and peak summated NMDAR-EPSCs after 20-25 minutes means that it is not possible to be certain if there is in fact a difference in activity-dependent regulation between the synaptic and peri/extrasynaptic zones, although clearly some activity-dependent regulation is occurring as evidenced by the significant difference between controls performed in these experiments.

Further experiments may clarify some of the above questions: for example, examining activity-dependent regulation of perisynaptic (spillover-activated) NMDARs would be clearer by using an activity-dependent and irreversible NMDAR blocker: application of MK-801 via the perfusion whilst eliciting single NMDAR-EPSCs every 10-20 s would allow blockade of the synaptic population only, and the remainder of the experiment could subsequently (after washout) be performed as described in this thesis. Single EPSCs should remain at zero amplitude whilst any current elicited by applying trains of stimuli are likely to be outside the synapse; activated by glutamate spillover. Subsequently then, any changes in summated, perisynaptic NMDAR-EPSC amplitudes could be examined. Additionally, single assaying stimuli should still be applied throughout the experiment to monitor the status of the pharmacologically blocked synaptic NMDAR population: if the single EPSC were to recover

at all over the course of the experiment then this would indicate either reinsertion of NMDARs at the synapse, or trafficking of NMDARs into the synaptic zone from the perisynaptic zone or elsewhere on the cell surface.

4.3 The role of GluN2D and the NMDAR in responding to ambient glutamate

Extrasynaptic NMDARs in the hippocampus are arranged in high density regions opposing astrocytic processes (Jourdain et al. 2007; Petralia 2012), and glutamate released from these processes may activate them and therefore influence neuronal excitability and network synchrony (Angulo et al. 2004; Fellin et al. 2004). The importance of GluN2D in sensitivity of SNc-DA neurons to ambient extracellular glutamate was explored in wild type and *Grin2D*-null mice under normal conditions; and under conditions where glutamate transport is compromised such as may occur in neurodegenerative disease. Results suggested that small NMDAR-mediated currents are present in SNc-DA neurons in response to ambient glutamate, which is not released in an action-potential-dependent manner. GluN2D is also shown to have a pivotal role in allowing the SNc-DA neurons to respond to this ambient glutamate, or to potentially allow nearby glial cells to modulate their excitability. In addition, inhibition of GluTs caused an increase in excitatory current; almost all of which was mediated by NMDARs; and part of that by GluN2D-containing NMDARs, as evidenced by a significantly smaller amount of this current in *Grin2D*-null mice. Together these data contribute to evidence that GluN2D may be a useful target for pharmacological inhibition in PD.

4.3.1 Ambient extracellular glutamate in the SNc elicits NMDAR-mediated currents in dopamine neurons, which are unaffected by pharmacological inhibition of action potential firing

Work in the hippocampus suggests that extrasynaptic NMDARs are activated by ambient extracellular glutamate in order to maintain a tonic level of excitability (Sah et al. 1989; Angulo et al. 2004; Fellin et al. 2004). As the level of desensitisation in NMDARs is much lower than AMPARs, they are likely to mediate the majority of excitation in response to this ambient glutamate (Iacobucci and Popescu 2017). The effect of NMDAR blocker DAP5 was

investigated on current flow in SNc-DA cells at a holding potential of -50 mV. A small but highly significant decrease in inward current was observed, which persisted when neuronal firing was inhibited using TTX, indicating that NMDARs are being activated by ambient extracellular glutamate which does not have an immediate action potential-dependent origin (Wild et al. 2015). It is possible that some of this glutamate is present as a result of previous firing before application of TTX; though the bath perfusion and the endogenous activity of glutamate reuptake transporters might be expected to reduce this to zero. It is possible that this glutamate may be released from glial cells as has been suggested in the hippocampus (Parpura et al. 1994; Bezzi et al. 1998; Angulo et al. 2004; Fellin et al. 2004), and therefore it may be useful in future to ascertain whether this is the case in the SNc by application of the glial toxin fluoroacetate (Muir et al. 1986; Tremblay et al. 2011). It is also possible that the source of ambient glutamate in the SNc could be presynaptic, but in the form of non-action potential-dependent spontaneous release leading to miniature EPSCs. The vacuolar H+-ATPase pump establishes the proton gradient across the vesicular membrane which drives transmitter uptake into synaptic vesicles (Le Meur et al. 2007): it may be prudent to inhibit H+-ATPase activity using bafilomycin A1 (Drose & Altendorf, 1997) in order to elucidate whether ambient glutamate in SNc-DA neurons is of vesicular origin. Indeed, in the hippocampus this compound had no effect on ambient glutamate, which may again indicate a glial origin (Le Meur et al. 2007).

In mice lacking the GluN2D subunit, there was no significant effect of D-AP5 application, and indeed there was significantly less D-AP5-sensitive tonic current in comparison to wild type mice. This is a novel result, and suggests that specifically GluN2D-containing NMDARs have a role in mediating tonic NMDAR activity in response to ambient glutamate in SNc-DA neurons. The difference in DAP5-blockable current observed between genotypes may suggest that it is the increased glutamate affinity and low Mg^{2+} block characteristics conferred by the presence of GluN2D which allows it to contribute significantly to baseline levels of current in response to low levels of ambient glutamate; a function which has previously been predicted (Wyllie et al. 1998). When GluN2D is removed, potentially replaced with GluN2B, these properties are altered. This sensitivity of GluN2D to ambient glutamate may have a function in maintaining a tonic level of excitability in SNc-DA neurons, and/or in allowing modulation of neuronal excitability by glial cells.

4.3.2 Ambient glutamate in the SNc is regulated by glutamate reuptake transporters

Pharmacological inhibition of glutamate transporter activity using TBOA led to significant increases in inward current in SNc-DA neurons, suggesting that glutamate reuptake is very important under baseline conditions to prevent increased NMDAR activity. The amplitude of the current change elicited by TBOA was highly variable, which indicates that cells are not exposed to similar levels of ambient glutamate, or that they have varying numbers of nearby tonically active GluTs. This variability may also be an artifact of working in slices, where some neurons are more likely to be exposed to surface bath flow (and therefore wash away ambient glutamate) than others deeper in the tissue.

Application of TBOA caused similar increases in inward current in both wild type and *Grin2D*-null mice. Whilst there was no difference based on genotype on the overall change in current based on glutamate transporter blockade, the variability in the data means it was more difficult to detect a difference. Results **Figure 3.28A** suggests that in some neurons, all of which were wild type, there was a much greater influx of current in response to GluT blockage than in others. However, this current included activity from both NMDARs and AMPARs (though as above these rapidly desensitise): in these same experiments there was in fact a significantly lower amount of D-AP5-sensitive current under conditions of GluT inhibition in *Grin2D*-null mice (**Figure 3.28B)**, implying that there in indeed still a difference in NMDAR-mediated currents under these conditions. Therefore, GluN2D-containing NMDARs are mediating cation influx into SNc-DA neurons under conditions of GluT blockade: this is further evidence that GluN2D is a good potential target for inhibition in neurodegenerative illnesses (such as PD) which may include GluT dysfunction as part of their pathophysiology (Lipton 2004; Kotermanski and Johnson 2009; van Marum 2009; Emre et al. 2010; Wild et al. 2013, 2015).

TBOA was always applied with compound LY 341495 (‘LY’), an antagonist of Group II mGluRs: this is because it has been found that increased extracellular glutamate caused by application of TBOA activates these receptors and inhibits presynaptic glutamate release (Wild et al. 2015). This does not occur in response to small events such as that resulting in a single EPSC, as they have been found to be unmodified by LY; but only in conditions where

extracellular glutamate increases dramatically, such as when reuptake is compromised (Wild et al. 2015). Therefore to assess directly the role of glutamate transporters, this presynaptic feedback mechanism was inhibited.

4.4 Bath application of NMDA elicits larger currents in *Grin2D*-null mice in comparison to wild type at very high concentrations only

The dose-response data obtained from bath application of NMDA (**Figure 3.30)** appears to show no difference based on genotype at low or moderate concentrations, which may suggest that numbers of NMDARs across the cell are similar. However, an interesting result here was that as the curves begin to plateau at high concentrations of NMDA the curves separated, with *Grin2D*-null animals displaying larger peak current in response to these concentrations (1-10 mM). If GluN2B is indeed replacing GluN2D within the receptor in these animals, it is likely that due to the larger peak current and shorter timeframe required for GluN2B to become ready to reopen (at peak agonist concentrations where immediate reopening is likely), it confers a capability for greater conductance at the highest levels NMDA/glutamate saturation, despite a lower affinity for NMDA and glutamate (Hess et al. 1998). GluN2D on the other hand has a lower conductance, and also much slower channel kinetics (2000 ms to deactivate, as opposed to 300 ms for GluN2B), meaning that immediate reactivation is not possible. Therefore GluN2D, with its lower Mg^{2+} block and higher glutamate affinity, is ideally suited to maintaining a baseline current flow in response to low levels of ambient glutamate, and its presence in a triheteromeric receptor may = attenuate peak current flow in response to very high agonist concentrations.

The results in P21 mice exploring NMDAR desensitisation response to 10 mM NMDA showed that desensitisation was significantly increased in mice lacking GluN2D (**Figure 3.31)**. This is a good indicator of the presence of GluN2D within NMDARs on SNc-DA neurons, and indeed that they are replaced with diheteromeric GluN1/GluN2B NMDARs in *Grin2D*-null animals, as previous studies have shown that, overall, GluN2B subunits desensitise to a much higher extent than GluN2D (Wyllie et al. 1998; Vance et al. 2011).

4.5 Hypoxic conditions cause significant but comparable cell death in both wild type and *Grin2D*-null mice

Hypoxic conditions, such as may be caused by ischemia, quickly leads to metabolic stress and excitotoxicity in neurons (Lai et al. 2014). Low oxygen availability prevents replenishment of ATP levels, thereby disrupting ionic gradients maintained by ATP-powered Na^+/K^+ pumps and so causes depolarisation. Because of this excitation, glutamate is also released from excitatory neurons leading to increased extracellular glutamate and therefore an increase in NMDAR-mediated Ca^{2+} influx, and consequent neuronal cell death (Dugan and Choi 1999; Lai et al. 2014).

GluN2D-containing NMDARs decrease their P_{open} in response to low O_2 (Bickler et al. 2003), a property which is likely to confer hypoxic resistance in neonates, and also in the naked mole rat, a creature which has evolved to survive in a low oxygen and high CO_2 environment (Larson and Park 2009; Schuhmacher et al. 2015). Therefore, the question of whether its presence in SNc-DA neurons conferred any additional resistance to hypoxia-related excitotoxicity was explored using a previously tested hypoxic treatment protocol in acute slices in both wild type and *Grin2D*-null animals, along with a propidium iodide cell viability assay and anti-tyrosine hydroxylase fluorescent staining in order to identify dopaminergic neurons.

After fixing and labeling, the SNc region was identified as in previous experiments using proximity to MT, and fluorescent imaging clearly identified dopaminergic neurons within. Much thinner slices were used here in order to facilitate counting of all SNc-DA neurons within each slice. A non-stereological method was used as the applied insult was relatively mild (15% O_2 for 40 minutes): instead, for each slice produced, a cut was made along the midline and one hemisphere randomly assigned to the high oxygen treatment group, and one to the hypoxic treatment group. This method prioritised the sensitivity afforded by being able to pair the results above analysis of total SNc volume. Previous research recording whole cell electrophysiological data showed that the hypoxic treatment applied here still allowed 60% of mouse hippocampal neurons to recover, regaining fully functional EPCS transmission after high O_2 is restored (Larson and Park 2009). Importantly then, the results presented in this thesis showed that the hypoxic treatment had no effect on the mean number of SNc-DA

neurons per 100 µm slice, indicating that all neurons affected by the treatment were still available for counting.

Paired two-factor ANOVA analysis revealed that the hypoxic treatment had the desired effect in that it caused a very highly significant yet submaximal increase in the percentage of SNc-DA neurons displaying fluorescent PI nuclear staining (**Figure 3.32)**. The same test also revealed that the presence or absence of GluN2D had no effect on SNc-DA cell survival, which may mean that this subunit confers no practical resistance to these neurons under hypoxic conditions, for example in ischemia. However, there is no data on the precise threshold that oxygen levels must reach in order to alter the P_{open} of GluN2D-containing NMDARs: therefore, it is very possible that by using a relatively mild hypoxic insult P_{open} remained unchanged. When originally demonstrating the effect in NMDARs in *xenopus laevis* oocytes, Bickler et al. saturated the perfusate solution with a very low concentration of oxygen (3 % O2 /estimated 20–25 mm Hg in solution; Bickler et al., 2003), whereas the method used in this thesis was chosen as it had previously been shown to lead to partial recovery in mouse neurons (Larson and Park 2009). It is possible that, whilst the method does begin to cause damage to mouse neurons, 15 % O_2 does not in fact lower the saturation enough to effect a change in the GluN2D subunit. In support of this, a recently performed study has found that SNc-DA cells are surprisingly resistant to episodes of complete anoxia (Karunasinghe et al. 2017), though subunit composition was not a factor examined in this work. Further experiments should be performed using very low or complete anoxia in order to confirm whether a GluN2D-mediated resistance to these conditions is inherent in SNc-DA neurons. It is also possible that GluN2D may be less likely to alter the overall physiological properties of the NMDAR if it is present in a triheteromeric GluN1/GluN2B/GluN2D configuration, which is most likely in SNc-DA neurons of older mice (Brothwell et al. 2008).

In conclusion, the results presented in this thesis have provided evidence that the GluN2D subunit expressed within NMDARs both synaptically and across the neuronal surface, and investigated how they may allow SNc-DA neurons to react to various potentially excitotoxic conditions. A form of synaptic plasticity has been demonstrated in SNc-DA neurons which results in downregulation of NMDARs in response to high frequency excitatory burst input, and in which GluN2D does not play a mechanistic role. GluN2D-containging NMDARs are

shown to have a role in detection of ambient extracellular glutamate, and indeed mediate larger currents in response to reuptake dysfunction. Lastly, a hypoxia study showed that the subunit does not confer a practical resistance to lowered oxygen levels, though further investigation is called for in this area. In summary, NMDARs have diverse roles in SNc-DA neurons which may both serve to maintain normal function and protect the cell in potentially pathological conditions.

References

Abraham WC. Metaplasticity: tuning synapses and networks for plasticity. *Nat Rev Neurosci* 9: 387, 2008.

Acker TM, **Yuan H**, **Hansen KB**, **Vance KM**, **Ogden KK**, **Jensen HS**, **Burger PB**, **Mullasseril P**, **Snyder JP**, **Liotta DC**, **Traynelis SF**. Mechanism for noncompetitive inhibition by novel GluN2C/D N-methyl-D-aspartate receptor subunit-selective modulators. *Mol Pharmacol* 80: 782–795, 2011.

Albin RL, **Young AB**, **Penney JB**. The functional anatomy of basal ganglia disorders. *Trends Neurosci* 12: 366–375, 1989.

Alsaloum M, **Kazi R**, **Gan Q**, **Amin J**, **Wollmuth LP**. A Molecular Determinant of Subtype-Specific Desensitization in Ionotropic Glutamate Receptors. *J Neurosci* 36: 2617–2622, 2016.

Amico-Ruvio SA, **Murthy SE**, **Smith TP**, **Popescu GK**. Zinc Effects on NMDA Receptor Gating Kinetics. *Biophys J* 100: 1910–1918, 2011.

Angulo MC, **Kozlov AS**, **Charpak S**, **Audinat E**. Glutamate released from glial cells synchronizes neuronal activity in the hippocampus. *J Neurosci Off J Soc Neurosci* 24: 6920–6927, 2004.

Ascher P, **Nowak L**. The role of divalent cations in the N-methyl-D-aspartate responses of mouse central neurones in culture. *J Physiol* 399: 247–266, 1988.

Assous M, **Had-Aissouni L**, **Gubellini P**, **Melon C**, **Nafia I**, **Salin P**, **Kerkerian-Le-Goff L**, **Kachidian P**. Progressive Parkinsonism by acute dysfunction of excitatory amino acid transporters in the rat substantia nigra. *Neurobiol Dis* 65: 69–81, 2014.

Asztely F, **Erdemli G**, **Kullmann DM**. Extrasynaptic glutamate spillover in the hippocampus: dependence on temperature and the role of active glutamate uptake. *Neuron* 18: 281–293, 1997.

Band M, **Malik A**, **Joel A**, **Avivi A**. Hypoxia associated NMDA receptor 2 subunit composition: developmental comparison between the hypoxia-tolerant subterranean mole-rat, Spalax, and the hypoxia-sensitive rat. *J Comp Physiol [B]* 182: 961–969, 2012.

Bashir ZI, **Alford S**, **Davies SN**, **Randall AD**, **Collingridge GL**. Long-term potentiation of NMDA receptor-mediated synaptic transmission in the hippocampus. *Nature* 349: 156–158, 1991.

Baucum AJ. Proteomic Analysis of Postsynaptic Protein Complexes Underlying Neuronal Plasticity. *ACS Chem Neurosci* 8: 689–701, 2017.

Benveniste M, **Clements J**, **Vyklický L**, **Mayer ML**. A kinetic analysis of the modulation of N-methyl-D-aspartic acid receptors by glycine in mouse cultured hippocampal neurones. *J Physiol* 428: 333–357, 1990.

Bergman H, **Wichmann T**, **Karmon B**, **DeLong MR**. The primate subthalamic nucleus. II. Neuronal activity in the MPTP model of parkinsonism. *J Neurophysiol* 72: 507–520, 1994.

Berretta N, **Berton F**, **Bianchi R**, **Brunelli M**, **Capogna M**, **Francesconi W**. Long-term Potentiation of NMDA Receptor-mediated EPSP in Guinea-pig Hippocampal Slices. *Eur J Neurosci* 3: 850–854, 1991.

Bettini E, **Sava A**, **Griffante C**, **Carignani C**, **Buson A**, **Capelli AM**, **Negri M**, **Andreetta F**, **Senar-Sancho SA**, **Guiral L**, **Cardullo F**. Identification and characterisation of novel NMDA receptor antagonists selective for NR2A- over NR2B-containing receptors. *J Pharmacol Exp Ther* 335: 636–644, 2010.

Bezzi P, **Carmignoto G**, **Pasti L**, **Vesce S**, **Rossi D**, **Rizzini BL**, **Pozzan T**, **Volterra A**. Prostaglandins stimulate calcium-dependent glutamate release in astrocytes. *Nature* 391: 281–285, 1998.

Bickler PE, **Buck LT**. Adaptations of vertebrate neurons to hypoxia and anoxia: maintaining critical Ca2+ concentrations. *J Exp Biol* 201: 1141–1152, 1998.

Bickler PE, **Donohoe PH**, **Buck LT**. Hypoxia-induced silencing of NMDA receptors in turtle neurons. *J Neurosci Off J Soc Neurosci* 20: 3522–3528, 2000.

Bickler PE, **Fahlman CS**, **Taylor DM**. Oxygen sensitivity of NMDA receptors: relationship to NR2 subunit composition and hypoxia tolerance of neonatal neurons. *Neuroscience* 118: 25–35, 2003.

Bickler PE, **Hansen BM**. Hypoxia-tolerant neonatal CA1 neurons: relationship of survival to evoked glutamate release and glutamate receptor-mediated calcium changes in hippocampal slices. *Brain Res Dev Brain Res* 106: 57–69, 1998.

Blandini F. An update on the potential role of excitotoxicity in the pathogenesis of Parkinson's disease. *Funct Neurol* 25: 65–71, 2010.

Blandini F, **Nappi G**, **Tassorelli C**, **Martignoni E**. Functional changes of the basal ganglia circuitry in Parkinson's disease. *Prog Neurobiol* 62: 63–88, 2000.

Blanke ML, **VanDongen AMJ**. Activation Mechanisms of the NMDA Receptor [Online]. In: *Biology of the NMDA Receptor*, edited by Van Dongen AM. CRC Press/Taylor & Francis http://www.ncbi.nlm.nih.gov/books/NBK5274/.

Blythe SN, **Wokosin D**, **Atherton JF**, **Bevan MD**. Cellular mechanisms underlying burst firing in substantia nigra dopamine neurons. *J Neurosci Off J Soc Neurosci* 29: 15531–15541, 2009.

Bolam JP, **Hanley JJ**, **Booth PA**, **Bevan MD**. Synaptic organisation of the basal ganglia. *J Anat* 196 (Pt 4): 527–542, 2000.

Brickley SG, **Misra C**, **Mok MHS**, **Mishina M**, **Cull-Candy SG**. NR2B and NR2D subunits coassemble in cerebellar Golgi cells to form a distinct NMDA receptor subtype restricted to extrasynaptic sites. *J Neurosci Off J Soc Neurosci* 23: 4958–4966, 2003.

Brothwell SLC, **Barber JL**, **Monaghan DT**, **Jane DE**, **Gibb AJ**, **Jones S**. NR2B- and NR2D-containing synaptic NMDA receptors in developing rat substantia nigra pars compacta dopaminergic neurones. *J Physiol* 586: 739–750, 2008.

Burnashev N, **Schoepfer R**, **Monyer H**, **Ruppersberg JP**, **Günther W**, **Seeburg PH**, **Sakmann B**. Control by asparagine residues of calcium permeability and magnesium blockade in the NMDA receptor. *Science* 257: 1415–1419, 1992.

Carroll RC, **Beattie EC**, **Xia H**, **Lüscher C**, **Altschuler Y**, **Nicoll RA**, **Malenka RC**, **von Zastrow M**. Dynamin-dependent endocytosis of ionotropic glutamate receptors. *Proc Natl Acad Sci U S A* 96: 14112–14117, 1999.

Centonze D, **Picconi B**, **Gubellini P**, **Bernardi G**, **Calabresi P**. Dopaminergic control of synaptic plasticity in the dorsal striatum. *Eur J Neurosci* 13: 1071–1077, 2001.

Charara A, **Smith Y**, **Parent A**. Glutamatergic inputs from the pedunculopontine nucleus to midbrain dopaminergic neurons in primates: Phaseolus vulgaris-leucoagglutinin anterograde labeling combined with postembedding glutamate and GABA immunohistochemistry. *J Comp Neurol* 364: 254–266, 1996.

Chen B-S, **Roche KW**. Regulation of NMDA Receptors by Phosphorylation. *Neuropharmacology* 53: 362–368, 2007.

Chergui K. Dopamine induces a GluN2A-dependent form of long-term depression of NMDA synaptic responses in the nucleus accumbens. *Neuropharmacology* 60: 975–981, 2011.

Choi DW. Ionic dependence of glutamate neurotoxicity. *J Neurosci Off J Soc Neurosci* 7: 369–379, 1987.

Clague MJ, **Urbé S**. Ubiquitin: same molecule, different degradation pathways. *Cell* 143: 682–685, 2010.

Clapham DE. Calcium signaling. *Cell* 131: 1047–1058, 2007.

Clark BA, **Cull-Candy SG**. Activity-dependent recruitment of extrasynaptic NMDA receptor activation at an AMPA receptor-only synapse. *J Neurosci Off J Soc Neurosci* 22: 4428–4436, 2002.

Clements JD. Transmitter timecourse in the synaptic cleft: its role in central synaptic function. *Trends Neurosci* 19: 163–171, 1996.

Collins MO, **Husi H**, **Yu L**, **Brandon JM**, **Anderson CNG**, **Blackstock WP**, **Choudhary JS**, **Grant SGN**. Molecular characterisation and comparison of the components and multiprotein complexes in the postsynaptic proteome. *J Neurochem* 97: 16–23, 2006.

Colquhoun D, **Jonas P**, **Sakmann B**. Action of brief pulses of glutamate on AMPA/kainate receptors in patches from different neurones of rat hippocampal slices. *J Physiol* 458: 261–287, 1992.

Costa BM, **Feng B**, **Tsintsadze TS**, **Morley RM**, **Irvine MW**, **Tsintsadze V**, **Lozovaya NA**, **Jane DE**, **Monaghan DT**. N-methyl-D-aspartate (NMDA) receptor NR2 subunit selectivity of a series of novel piperazine-2,3-dicarboxylate derivatives: preferential blockade of extrasynaptic NMDA receptors in the rat hippocampal CA3-CA1 synapse. *J Pharmacol Exp Ther* 331: 618–626, 2009.

Darbon P, **Yvon C**, **Legrand J-C**, **Streit J**. INaP underlies intrinsic spiking and rhythm generation in networks of cultured rat spinal cord neurons. *Eur J Neurosci* 20: 976–988, 2004.

Davies J, **Watkins JC**. Actions of D and L forms of 2-amino-5-phosphonovalerate and 2-amino-4-phosphonobutyrate in the cat spinal cord. *Brain Res* 235: 378–386, 1982.

DeLong MR, **Wichmann T**. Circuits and Circuit Disorders of the Basal Ganglia. *Arch Neurol* 64: 20–24, 2007.

Diamond JS, **Jahr CE**. Transporters Buffer Synaptically Released Glutamate on a Submillisecond Time Scale. *J Neurosci* 17: 4672–4687, 1997.

Dingledine R, **Borges K**, **Bowie D**, **Traynelis SF**. The Glutamate Receptor Ion Channels. *Pharmacol Rev* 51: 7–62, 1999a.

Dingledine R, **Borges K**, **Bowie D**, **Traynelis SF**. The glutamate receptor ion channels. *Pharmacol Rev* 51: 7–61, 1999b.

Dong X, **Wang Y**, **Qin Z**. Molecular mechanisms of excitotoxicity and their relevance to pathogenesis of neurodegenerative diseases. *Acta Pharmacol Sin* 30: 379–387, 2009.

Dravid SM, **Erreger K**, **Yuan H**, **Nicholson K**, **Le P**, **Lyuboslavsky P**, **Almonte A**, **Murray E**, **Mosely C**, **Barber J**, **French A**, **Balster R**, **Murray TF**, **Traynelis SF**. Subunit-specific mechanisms and proton sensitivity of NMDA receptor channel block. *J Physiol* 581: 107–128, 2007.

Dubois CJ, **Lachamp PM**, **Sun L**, **Mishina M**, **Liu SJ**. Presynaptic GluN2D receptors detect glutamate spillover and regulate cerebellar GABA release. *J Neurophysiol* 115: 271–285, 2016.

Dugan LL, **Choi DW**. Excitotoxic injury in Hypoxia-Ischemia [Online]. https://www.ncbi.nlm.nih.gov/books/NBK27972/ [2 Sep. 2017].

Dupuis JP, **Ladépêche L**, **Seth H**, **Bard L**, **Varela J**, **Mikasova L**, **Bouchet D**, **Rogemond V**, **Honnorat J**, **Hanse E**, **Groc L**. Surface dynamics of GluN2B-NMDA receptors controls plasticity of maturing glutamate synapses. *EMBO J* 33: 842–861, 2014.

Dzubay JA, **Jahr CE**. The Concentration of Synaptically Released Glutamate Outside of the Climbing Fiber–Purkinje Cell Synaptic Cleft. *J Neurosci* 19: 5265–5274, 1999.

Ehlers MD, **Zhang S**, **Bernhardt JP**, **Huganir RL**. Inactivation of NMDA Receptors by Direct Interaction of Calmodulin with the NR1 Subunit. *Cell* 84: 745–755, 1996.

Emre M, **Tsolaki M**, **Bonuccelli U**, **Destée A**, **Tolosa E**, **Kutzelnigg A**, **Ceballos-Baumann A**, **Zdravkovic S**, **Bladström A**, **Jones R**, **11018 Study Investigators**. Memantine for patients with Parkinson's disease dementia or dementia with Lewy bodies: a randomised, double-blind, placebo-controlled trial. *Lancet Neurol* 9: 969–977, 2010.

von Engelhardt J, **Bocklisch C**, **Tönges L**, **Herb A**, **Mishina M**, **Monyer H**. GluN2D-containing NMDA receptors-mediate synaptic currents in hippocampal interneurons and pyramidal cells in juvenile mice. *Front Cell Neurosci* 9: 95, 2015.

Evans RH, **Francis AA**, **Jones AW**, **Smith DA**, **Watkins JC**. The effects of a series of omega-phosphonic alpha-carboxylic amino acids on electrically evoked and excitant amino acid-induced responses in isolated spinal cord preparations. *Br J Pharmacol* 75: 65–75, 1982.

Fellin T, **Pascual O**, **Gobbo S**, **Pozzan T**, **Haydon PG**, **Carmignoto G**. Neuronal synchrony mediated by astrocytic glutamate through activation of extrasynaptic NMDA receptors. *Neuron* 43: 729–743, 2004.

Feng B, **Morley RM**, **Jane DE**, **Monaghan DT**. The effect of competitive antagonist chain length on NMDA receptor subunit selectivity. *Neuropharmacology* 48: 354–359, 2005.

Feng B, **Tse HW**, **Skifter DA**, **Morley R**, **Jane DE**, **Monaghan DT**. Structure-activity analysis of a novel NR2C/NR2D-preferring NMDA receptor antagonist: 1-(phenanthrene-2-carbonyl) piperazine-2,3-dicarboxylic acid. *Br J Pharmacol* 141: 508–516, 2004.

Flavell SW, **Greenberg ME**. Signaling mechanisms linking neuronal activity to gene expression and plasticity of the nervous system. *Annu Rev Neurosci* 31: 563–590, 2008.

Foster TC, **Sharrow KM**, **Masse JR**, **Norris CM**, **Kumar A**. Calcineurin Links Ca2+ Dysregulation with Brain Aging. *J Neurosci Off J Soc Neurosci* 21: 4066–4073, 2001.

Furukawa H, **Gouaux E**. Mechanisms of activation, inhibition and specificity: crystal structures of the NMDA receptor NR1 ligand-binding core. *EMBO J* 22: 2873–2885, 2003.

Furukawa H, **Singh SK**, **Mancusso R**, **Gouaux E**. Subunit arrangement and function in NMDA receptors. *Nature* 438: 185–192, 2005.

Futai K, **Okada M**, **Matsuyama K**, **Takahashi T**. High-Fidelity Transmission Acquired via a Developmental Decrease in NMDA Receptor Expression at an Auditory Synapse. *J Neurosci* 21: 3342–3349, 2001.

Gallagher MJ, **Huang H**, **Pritchett DB**, **Lynch DR**. Interactions between ifenprodil and the NR2B subunit of the N-methyl-D-aspartate receptor. *J Biol Chem* 271: 9603–9611, 1996.

Galvan A, **Devergnas A**, **Wichmann T**. Alterations in neuronal activity in basal ganglia-thalamocortical circuits in the parkinsonian state. *Front Neuroanat* 9, 2015.

Gautam V, **Trinidad JC**, **Rimerman RA**, **Costa BM**, **Burlingame AL**, **Monaghan DT**. Nedd4 is a Specific E3 Ubiquitin Ligase for the NMDA Receptor Subunit GluN2D. *Neuropharmacology* 74, 2013.

Gean PW, **Chang FC**, **Huang CC**, **Lin JH**, **Way LJ**. Long-term enhancement of EPSP and NMDA receptor-mediated synaptic transmission in the amygdala. *Brain Res Bull* 31: 7–11, 1993.

Graybiel AM, **Aosaki T**, **Flaherty AW**, **Kimura M**. The basal ganglia and adaptive motor control. *Science* 265: 1826–1831, 1994.

Groc L, **Bard L**, **Choquet D**. Surface trafficking of N-methyl-d-aspartate receptors: Physiological and pathological perspectives. *Neuroscience* 158: 4–18, 2009.

Groc L, **Heine M**, **Cousins SL**, **Stephenson FA**, **Lounis B**, **Cognet L**, **Choquet D**. NMDA receptor surface mobility depends on NR2A-2B subunits. *Proc Natl Acad Sci U S A* 103: 18769–18774, 2006.

Grosshans DR, **Clayton DA**, **Coultrap SJ**, **Browning MD**. LTP leads to rapid surface expression of NMDA but not AMPA receptors in adult rat CA1. *Nat Neurosci* 5: 27–33, 2002.

Grubbs FE. Sample Criteria for Testing Outlying Observations. *Ann Math Stat* 21: 27–58, 1950.

Hage TA, **Sun Y**, **Khaliq ZM**. Electrical and Ca(2+) signaling in dendritic spines of substantia nigra dopaminergic neurons. *eLife* 5, 2016.

Hammond C, **Bergman H**, **Brown P**. Pathological synchronization in Parkinson's disease: networks, models and treatments. *Trends Neurosci* 30: 357–364, 2007.

Hardingham GE, **Bading H**. Synaptic versus extrasynaptic NMDA receptor signalling: implications for neurodegenerative disorders. *Nat Rev Neurosci* 11: 682–696, 2010.

Harnett MT, **Bernier BE**, **Ahn K-C**, **Morikawa H**. Burst-Timing-Dependent Plasticity of NMDA Receptor-Mediated Transmission in Midbrain Dopamine Neurons. *Neuron* 62: 826–838, 2009.

Harney SC, **Anwyl R**. Plasticity of NMDA receptor-mediated excitatory postsynaptic currents at perforant path inputs to dendrite-targeting interneurons. *J Physiol* 590: 3771–3786, 2012.

Harney SC, **Jane DE**, **Anwyl R**. Extrasynaptic NR2D-Containing NMDARs Are Recruited to the Synapse during LTP of NMDAR-EPSCs. *J Neurosci* 28: 11685–11694, 2008.

Harney SC, **Rowan M**, **Anwyl R**. Long-term depression of NMDA receptor-mediated synaptic transmission is dependent on activation of metabotropic glutamate receptors and is altered to long-term potentiation by low intracellular calcium buffering. *J Neurosci Off J Soc Neurosci* 26: 1128–1132, 2006.

Harris AZ, **Pettit DL**. Extrasynaptic and synaptic NMDA receptors form stable and uniform pools in rat hippocampal slices. *J Physiol* 584: 509–519, 2007.

Harris AZ, **Pettit DL**. Recruiting Extrasynaptic NMDA Receptors Augments Synaptic Signaling. *J Neurophysiol* 99: 524–533, 2008.

Häusser MA, **de Weille JR**, **Lazdunski M**. Activation by cromakalim of pre- and post-synaptic ATP-sensitive K+ channels in substantia nigra. *Biochem Biophys Res Commun* 174: 909–914, 1991.

Hayes D, **Wiessner M**, **Rauen T**, **McBean GJ**. Transport of L-[14C]cystine and L-[14C]cysteine by subtypes of high affinity glutamate transporters over-expressed in HEK cells. *Neurochem Int* 46: 585–594, 2005.

Hebb DO. *The Organization of Behavior: A Neuropsychological Theory*. Psychology Press, 1949.

Herman MA, **Jahr CE**. Extracellular glutamate concentration in hippocampal slice. *J Neurosci Off J Soc Neurosci* 27: 9736–9741, 2007.

Herron CE, **Lester RA**, **Coan EJ**, **Collingridge GL**. Frequency-dependent involvement of NMDA receptors in the hippocampus: a novel synaptic mechanism. *Nature* 322: 265–268, 1986.

Hess SD, **Daggett LP**, **Deal C**, **Lu C-C**, **Johnson EC**, **Veliçelebi G**. Functional Characterisation of Human N-Methyl-d-Aspartate Subtype 1A/2D Receptors. *J Neurochem* 70: 1269–1279, 1998.

Hrabetova S, **Serrano P**, **Blace N**, **Tse HW**, **Skifter DA**, **Jane DE**, **Monaghan DT**, **Sacktor TC**. Distinct NMDA receptor subpopulations contribute to long-term potentiation and long-term depression induction. *J Neurosci Off J Soc Neurosci* 20: RC81, 2000.

Hu B, **Zheng F**. Molecular determinants of glycine-independent desensitization of NR1/NR2A receptors. *J Pharmacol Exp Ther* 313: 563–569, 2005.

Huang Z, **Gibb AJ**. Mg2+ block properties of triheteromeric GluN1-GluN2B-GluN2D NMDA receptors on neonatal rat substantia nigra pars compacta dopaminergic neurones. *J Physiol* 592: 2059–2078, 2014.

Hunt DL, **Castillo PE**. Synaptic plasticity of NMDA receptors: mechanisms and functional implications. *Curr Opin Neurobiol* 22: 496–508, 2012.

Iacobucci GJ, **Popescu GK**. NMDA receptors: linking physiological output to biophysical operation. *Nat Rev Neurosci* 18: 236–249, 2017.

Iino M, **Ozawa S**, **Tsuzuki K**. Permeation of calcium through excitatory amino acid receptor channels in cultured rat hippocampal neurones. *J Physiol* 424: 151–165, 1990.

Ikeda K, **Araki K**, **Takayama C**, **Inoue Y**, **Yagi T**, **Aizawa S**, **Mishina M**. Reduced spontaneous activity of mice defective in the epsilon 4 subunit of the NMDA receptor channel. *Brain Res Mol Brain Res* 33: 61–71, 1995.

Jamur MC, **Oliver C**. Permeabilization of cell membranes. *Methods Mol Biol Clifton NJ* 588: 63–66, 2010.

Jang M, **Um KB**, **Jang J**, **Kim HJ**, **Cho H**, **Chung S**, **Park MK**. Coexistence of glutamatergic spine synapses and shaft synapses in substantia nigra dopamine neurons. *Sci Rep* 5: 14773, 2015.

Jensen AA, **Fahlke C**, **Bjørn-Yoshimoto WE**, **Bunch L**. Excitatory amino acid transporters: recent insights into molecular mechanisms, novel modes of modulation and new therapeutic possibilities. *Curr Opin Pharmacol* 20: 116–123, 2015.

Jespersen A, **Tajima N**, **Fernandez-Cuervo G**, **Garnier-Amblard EC**, **Furukawa H**. Structural insights into competitive antagonism in NMDA receptors. *Neuron* 81: 366–378, 2014.

Jones MV, **Westbrook GL**. The impact of receptor desensitization on fast synaptic transmission. *Trends Neurosci* 19: 96–101, 1996.

Jones S, **Gibb AJ**. Functional NR2B- and NR2D-containing NMDA receptor channels in rat substantia nigra dopaminergic neurones. *J Physiol* 569: 209–221, 2005.

Joshi I, **Yang Y-M**, **Wang L-Y**. Coincident activation of metabotropic glutamate receptors and NMDA receptors (NMDARs) downregulates perisynaptic/extrasynaptic NMDARs and enhances high-fidelity neurotransmission at the developing calyx of Held synapse. *J Neurosci Off J Soc Neurosci* 27: 9989–9999, 2007.

Jourdain P, **Bergersen LH**, **Bhaukaurally K**, **Bezzi P**, **Santello M**, **Domercq M**, **Matute C**, **Tonello F**, **Gundersen V**, **Volterra A**. Glutamate exocytosis from astrocytes controls synaptic strength. *Nat Neurosci* 10: 331–339, 2007.

Karakas E, **Simorowski N**, **Furukawa H**. Subunit arrangement and phenylethanolamine binding in GluN1/GluN2B NMDA receptors. *Nature* 475: 249–253, 2011.

Karunasinghe RN, **Grey AC**, **Telang R**, **Vlajkovic SM**, **Lipski J**. Differential spread of anoxic depolarization contributes to the pattern of neuronal injury after oxygen and glucose deprivation (OGD) in the Substantia Nigra in rat brain slices. *Neuroscience* 340: 359–372, 2017.

Kennedy MB. Signal-processing machines at the postsynaptic density. *Science* 290: 750–754, 2000.

Kharazia VN, **Weinberg RJ**. Immunogold localization of AMPA and NMDA receptors in somatic sensory cortex of albino rat. *J Comp Neurol* 412: 292–302, 1999.

Kita H, **Kitai ST**. Efferent projections of the subthalamic nucleus in the rat: light and electron microscopic analysis with the PHA-L method. *J Comp Neurol* 260: 435–452, 1987.

Kombian SB, **Malenka RC**. Simultaneous LTP of non-NMDA- and LTD of NMDA-receptor-mediated responses in the nucleus accumbens. *Nature* 368: 242–246, 1994.

Kopell BH, **Rezai AR**, **Chang JW**, **Vitek JL**. Anatomy and physiology of the basal ganglia: implications for deep brain stimulation for Parkinson's disease. *Mov Disord Off J Mov Disord Soc* 21 Suppl 14: S238-246, 2006.

Kotecha SA, **Jackson MF**, **Al-Mahrouki A**, **Roder JC**, **Orser BA**, **MacDonald JF**. Co-stimulation of mGluR5 and N-methyl-D-aspartate receptors is required for potentiation of excitatory synaptic transmission in hippocampal neurons. *J Biol Chem* 278: 27742–27749, 2003.

Kotermanski SE, **Johnson JW**. Mg2+ imparts NMDA receptor subtype selectivity to the Alzheimer's drug memantine. *J Neurosci Off J Soc Neurosci* 29: 2774–2779, 2009.

Koutsilieri E, **Riederer P**. Excitotoxicity and new antiglutamatergic strategies in Parkinson's disease and Alzheimer's disease. *Parkinsonism Relat Disord* 13 Suppl 3: S329-331, 2007.

Krupp JJ, **Vissel B**, **Heinemann SF**, **Westbrook GL**. Calcium-dependent inactivation of recombinant N-methyl-D-aspartate receptors is NR2 subunit specific. *Mol Pharmacol* 50: 1680–1688, 1996.

Krupp JJ, **Vissel B**, **Heinemann SF**, **Westbrook GL**. N-terminal domains in the NR2 subunit control desensitization of NMDA receptors. *Neuron* 20: 317–327, 1998.

Kwon H-B, **Castillo PE**. Long-term potentiation selectively expressed by NMDA receptors at hippocampal mossy fiber synapses. *Neuron* 57: 108–120, 2008.

Lai TW, **Zhang S**, **Wang YT**. Excitotoxicity and stroke: Identifying novel targets for neuroprotection. *Prog Neurobiol* 115: 157–188, 2014.

Larkum ME, **Nevian T**. Synaptic clustering by dendritic signalling mechanisms. *Curr Opin Neurobiol* 18: 321–331, 2008.

Larson J, **Park TJ**. Extreme hypoxia tolerance of naked mole-rat brain. *Neuroreport* 20: 1634–1637, 2009.

Lau CG, **Zukin RS**. NMDA receptor trafficking in synaptic plasticity and neuropsychiatric disorders. *Nat Rev Neurosci* 8: 413–426, 2007.

LaVinka PC, **Brand A**, **Landau VJ**, **Wirtshafter D**, **Park TJ**. Extreme tolerance to ammonia fumes in African naked mole-rats: animals that naturally lack neuropeptides from trigeminal chemosensory nerve fibers. *J Comp Physiol A Neuroethol Sens Neural Behav Physiol* 195: 419–427, 2009.

Le Meur K, **Galante M**, **Angulo MC**, **Audinat E**. Tonic activation of NMDA receptors by ambient glutamate of non-synaptic origin in the rat hippocampus. *J Physiol* 580: 373–383, 2007.

Lee C-H, **Lü W**, **Michel JC**, **Goehring A**, **Du J**, **Song X**, **Gouaux E**. NMDA receptor structures reveal subunit arrangement and pore architecture. *Nature* 511: 191–197, 2014.

Lee H-K. Synaptic plasticity and phosphorylation. *Pharmacol Ther* 112: 810–832, 2006.

Lin Y, **Jover-Mengual T**, **Wong J**, **Bennett MVL**, **Zukin RS**. PSD-95 and PKC converge in regulating NMDA receptor trafficking and gating. *Proc Natl Acad Sci* 103: 19902–19907, 2006.

Lipton SA. Paradigm shift in NMDA receptor antagonist drug development: molecular mechanism of uncompetitive inhibition by memantine in the treatment of Alzheimer's disease and other neurologic disorders. *J Alzheimers Dis JAD* 6: S61-74, 2004.

Lissin DV, **Gomperts SN**, **Carroll RC**, **Christine CW**, **Kalman D**, **Kitamura M**, **Hardy S**, **Nicoll RA**, **Malenka RC**, **von Zastrow M**. Activity differentially regulates the surface expression of synaptic AMPA and NMDA glutamate receptors. *Proc Natl Acad Sci U S A* 95: 7097–7102, 1998.

Liu Y, **Wong TP**, **Aarts M**, **Rooyakkers A**, **Liu L**, **Lai TW**, **Wu DC**, **Lu J**, **Tymianski M**, **Craig AM**, **Wang YT**. NMDA receptor subunits have differential roles in mediating excitotoxic neuronal death both in vitro and in vivo. *J Neurosci Off J Soc Neurosci* 27: 2846–2857, 2007.

Logan SM, **Partridge JG**, **Matta JA**, **Buonanno A**, **Vicini S**. Long-lasting NMDA receptor-mediated EPSCs in mouse striatal medium spiny neurons. *J Neurophysiol* 98: 2693–2704, 2007.

Lossi SAL. Cell death and proliferation in acute slices and organotypic cultures of mammalian CNS. *Prog Neurobiol* 88: 221–45, 2009.

Lozovaya NA, **Grebenyuk SE**, **Tsintsadze TS**, **Feng B**, **Monaghan DT**, **Krishtal OA**. Extrasynaptic NR2B and NR2D subunits of NMDA receptors shape "superslow" afterburst EPSC in rat hippocampus. *J Physiol* 558: 451–463, 2004.

Lüscher C, **Malenka RC**. NMDA Receptor-Dependent Long-Term Potentiation and Long-Term Depression (LTP/LTD). *Cold Spring Harb Perspect Biol* 4, 2012.

Magnin M, **Morel A**, **Jeanmonod D**. Single-unit analysis of the pallidum, thalamus and subthalamic nucleus in parkinsonian patients. *Neuroscience* 96: 549–564, 2000.

Maki BA, **Popescu GK**. Extracellular Ca2+ ions reduce NMDA receptor conductance and gating. *J Gen Physiol* 144: 379–392, 2014.

Martel M-A, **Ryan TJ**, **Bell KFS**, **Fowler JH**, **McMahon A**, **Al-Mubarak B**, **Komiyama NH**, **Horsburgh K**, **Kind PC**, **Grant SGN**, **Wyllie DJA**, **Hardingham GE**. The subtype of GluN2 C-terminal domain determines the response to excitotoxic insults. *Neuron* 74: 543–556, 2012.

van Marum RJ. Update on the use of memantine in Alzheimer's disease. *Neuropsychiatr Dis Treat* 5: 237–247, 2009.

Mayer ML, **Westbrook GL**, **Guthrie PB**. Voltage-dependent block by Mg2+ of NMDA responses in spinal cord neurones. *Nature* 309: 261–263, 1984.

McCullumsmith RE, **Sanacora G**. Regulation of Extrasynaptic Glutamate Levels as a Pathophysiological Mechanism in Disorders of Motivation and Addiction. *Neuropsychopharmacology* 40: 254–255, 2015.

Mesbahi-Vasey S, **Veras L**, **Yonkunas M**, **Johnson JW**, **Kurnikova MG**. All atom NMDA receptor transmembrane domain model development and simulations in lipid bilayers and water. *PLOS ONE* 12: e0177686, 2017.

Meyerson JR, **Kumar J**, **Chittori S**, **Rao P**, **Pierson J**, **Bartesaghi A**, **Mayer ML**, **Subramaniam S**. Structural mechanism of glutamate receptor activation and desensitization. *Nature* 514: 328–334, 2014.

Misra C, **Brickley SG**, **Farrant M**, **Cull-Candy SG**. Identification of subunits contributing to synaptic and extrasynaptic NMDA receptors in Golgi cells of the rat cerebellum. *J Physiol* 524 Pt 1: 147–162, 2000.

Miyamoto Y, **Yamada K**, **Noda Y**, **Mori H**, **Mishina M**, **Nabeshima T**. Lower sensitivity to stress and altered monoaminergic neuronal function in mice lacking the NMDA receptor epsilon 4 subunit. *J Neurosci Off J Soc Neurosci* 22: 2335–2342, 2002.

Momiyama A. Distinct synaptic and extrasynaptic NMDA receptors identified in dorsal horn neurones of the adult rat spinal cord. *J Physiol* 523 Pt 3: 621–628, 2000.

Momiyama A, **Feldmeyer D**, **Cull-Candy SG**. Identification of a native low-conductance NMDA channel with reduced sensitivity to Mg2+ in rat central neurones. *J Physiol* 494 (Pt 2): 479–492, 1996.

Monaghan DT, **Irvine MW**, **Costa BM**, **Fang G**, **Jane DE**. Pharmacological Modulation of NMDA Receptor Activity and the Advent of Negative and Positive Allosteric Modulators. *Neurochem Int* 61: 581–592, 2012.

Montgomery JM, **Selcher JC**, **Hanson JE**, **Madison DV**. Dynamin-dependent NMDAR endocytosis during LTD and its dependence on synaptic state. *BMC Neurosci* 6: 48, 2005.

Monyer H, **Burnashev N**, **Laurie DJ**, **Sakmann B**, **Seeburg PH**. Developmental and regional expression in the rat brain and functional properties of four NMDA receptors. *Neuron* 12: 529–540, 1994.

Morley RM, **Tse H-W**, **Feng B**, **Miller JC**, **Monaghan DT**, **Jane DE**. Synthesis and pharmacology of N1-substituted piperazine-2,3-dicarboxylic acid derivatives acting as NMDA receptor antagonists. *J Med Chem* 48: 2627–2637, 2005.

Mosley CA, **Acker TM**, **Hansen KB**, **Mullasseril P**, **Andersen KT**, **Le P**, **Vellano KM**, **Bräuner-Osborne H**, **Liotta DC**, **Traynelis SF**. Quinazolin-4-one derivatives: A novel class of noncompetitive NR2C/D subunit-selective N-methyl-D-aspartate receptor antagonists. *J Med Chem* 53: 5476–5490, 2010.

Moussawi K, **Riegel A**, **Nair S**, **Kalivas PW**. Extracellular Glutamate: Functional Compartments Operate in Different Concentration Ranges. *Front Syst Neurosci* 5, 2011.

Muir D, **Berl S**, **Clarke DD**. Acetate and fluoroacetate as possible markers for glial metabolism in vivo. *Brain Res* 380: 336–340, 1986.

Mullasseril P, **Hansen KB**, **Vance KM**, **Ogden KK**, **Yuan H**, **Kurtkaya NL**, **Santangelo R**, **Orr AG**, **Le P**, **Vellano KM**, **Liotta DC**, **Traynelis SF**. A subunit-selective potentiator of NR2C- and NR2D-containing NMDA receptors. *Nat Commun* 1: 90, 2010.

Nafia I, **Re DB**, **Masmejean F**, **Melon C**, **Kachidian P**, **Kerkerian-Le Goff L**, **Nieoullon A**, **Had-Aissouni L**. Preferential vulnerability of mesencephalic dopamine neurons to glutamate transporter dysfunction. *J Neurochem* 105: 484–496, 2008.

Nambu A, **Takada M**, **Inase M**, **Tokuno H**. Dual somatotopical representations in the primate subthalamic nucleus: evidence for ordered but reversed body-map transformations from the primary motor cortex and the supplementary motor area. *J Neurosci Off J Soc Neurosci* 16: 2671–2683, 1996.

Nelson AB, **Kreitzer AC**. Reassessing Models of Basal Ganglia Function and Dysfunction. *Annu Rev Neurosci* 37: 117–135, 2014.

Neuhoff H, **Neu A**, **Liss B**, **Roeper J**. Ih Channels Contribute to the Different Functional Properties of Identified Dopaminergic Subpopulations in the Midbrain. *J Neurosci* 22: 1290–1302, 2002.

Nowak L, **Bregestovski P**, **Ascher P**, **Herbet A**, **Prochiantz A**. Magnesium gates glutamate-activated channels in mouse central neurones. *Nature* 307: 462–465, 1984.

Ogden KK, **Traynelis SF**. New advances in NMDA receptor pharmacology. *Trends Pharmacol Sci* 32: 726–733, 2011.

Pál B. Astrocytic Actions on Extrasynaptic Neuronal Currents. *Front Cell Neurosci* 9, 2015.

Paoletti P, **Bellone C**, **Zhou Q**. NMDA receptor subunit diversity: impact on receptor properties, synaptic plasticity and disease. *Nat Rev Neurosci* 14: 383–400, 2013.

Paoletti P, **Neyton J**. NMDA receptor subunits: function and pharmacology. *Curr Opin Pharmacol* 7: 39–47, 2007.

Parent A, **Hazrati LN**. Functional anatomy of the basal ganglia. II. The place of subthalamic nucleus and external pallidum in basal ganglia circuitry. *Brain Res Brain Res Rev* 20: 128–154, 1995.

Park TJ, **Reznick J**, **Peterson BL**, **Blass G**, **Omerbašić D**, **Bennett NC**, **Kuich PHJL**, **Zasada C**, **Browe BM**, **Hamann W**, **Applegate DT**, **Radke MH**, **Kosten T**, **Lutermann H**, **Gavaghan V**, **Eigenbrod O**, **Bégay V**, **Amoroso VG**, **Govind V**, **Minshall RD**, **Smith ESJ**, **Larson J**, **Gotthardt M**, **Kempa S**, **Lewin GR**. Fructose-driven glycolysis supports anoxia resistance in the naked mole-rat. *Science* 356: 307–311, 2017.

Parpura V, **Basarsky TA**, **Liu F**, **Jeftinija K**, **Jeftinija S**, **Haydon PG**. Glutamate-mediated astrocyte-neuron signalling. *Nature* 369: 744–747, 1994.

Parsons MP, **Raymond LA**. Extrasynaptic NMDA Receptor Involvement in Central Nervous System Disorders. *Neuron* 82: 279–293, 2014.

Patt S, **Gertz HJ**, **Gerhard L**, **Cervós-Navarro J**. Pathological changes in dendrites of substantia nigra neurons in Parkinson's disease: A Golgi study. *Histol Histopathol* 6: 373–380, 1991.

Pearlstein E, **gouty-colomer laurie-anne**, **Michel FJ**, **Cloarec R**, **Hammond C**. Glutamatergic synaptic currents of nigral dopaminergic neurons follow a postnatal developmental sequence. *Front Cell Neurosci* 9: 210, 2015.

Pérez-Otaño I, **Larsen RS**, **Wesseling JF**. Emerging roles of GluN3-containing NMDA receptors in the CNS. *Nat Rev Neurosci* 17: 623–635, 2016.

Pérez-Otaño I, **Luján R**, **Tavalin SJ**, **Plomann M**, **Modregger J**, **Liu X-B**, **Jones EG**, **Heinemann SF**, **Lo DC**, **Ehlers MD**. Endocytosis and synaptic removal of NR3A-containing NMDA receptors by PACSIN1/syndapin1. *Nat Neurosci* 9: 611–621, 2006.

Perszyk RE, **DiRaddo JO**, **Strong KL**, **Low C-M**, **Ogden KK**, **Khatri A**, **Vargish GA**, **Pelkey KA**, **Tricoire L**, **Liotta DC**, **Smith Y**, **McBain CJ**, **Traynelis SF**. GluN2D-Containing N-methyl-d-Aspartate Receptors Mediate Synaptic Transmission in Hippocampal Interneurons and Regulate Interneuron Activity. *Mol Pharmacol* 90: 689–702, 2016.

Peterson BL, **Park TJ**, **Larson J**. Adult naked mole-rat brain retains the NMDA receptor subunit GluN2D associated with hypoxia tolerance in neonatal mammals. *Neurosci Lett* 506: 342–345, 2012.

Petralia RS. Distribution of Extrasynaptic NMDA Receptors on Neurons. *Sci World J* 2012: e267120, 2012.

Petralia RS, **Al-Hallaq RA**, **Wenthold RJ**. Trafficking and Targeting of NMDA Receptors [Online]. In: *Biology of the NMDA Receptor*, edited by Van Dongen AM. CRC Press/Taylor & Francis http://www.ncbi.nlm.nih.gov/books/NBK5290/ [24 Aug. 2017].

Petralia RS, **Esteban JA**, **Wang YX**, **Partridge JG**, **Zhao HM**, **Wenthold RJ**, **Malinow R**. Selective acquisition of AMPA receptors over postnatal development suggests a molecular basis for silent synapses. *Nat Neurosci* 2: 31–36, 1999.

Petralia RS, **Wang YX**, **Hua F**, **Yi Z**, **Zhou A**, **Ge L**, **Stephenson FA**, **Wenthold RJ**. Organization of NMDA receptors at extrasynaptic locations. *Neuroscience* 167: 68–87, 2010a.

Petralia RS, **Wang YX**, **Hua F**, **Yi Z**, **Zhou A**, **Ge L**, **Stephenson FA**, **Wenthold RJ**. Organization of NMDA receptors at extrasynaptic locations. *Neuroscience* 167: 68–87, 2010b.

Piallat B, **Polosan M**, **Fraix V**, **Goetz L**, **David O**, **Fenoy A**, **Torres N**, **Quesada J-L**, **Seigneuret E**, **Pollak P**, **Krack P**, **Bougerol T**, **Benabid AL**, **Chabardès S**. Subthalamic neuronal firing in obsessive-compulsive disorder and Parkinson disease. *Ann Neurol* 69: 793–802, 2011.

Pisani A, **Martella G**, **Tscherter A**, **Costa C**, **Mercuri NB**, **Bernardi G**, **Shen J**, **Calabresi P**. Enhanced sensitivity of DJ-1-deficient dopaminergic neurons to energy metabolism impairment: Role of Na+/K+ ATPase. *Neurobiol Dis* 23: 54–60, 2006.

Plested AJR. Structural mechanisms of activation and desensitization in neurotransmitter-gated ion channels. *Nat Struct Mol Biol* 23: 494–502, 2016.

Rebola N, **Lujan R**, **Cunha RA**, **Mulle C**. Adenosine A2A receptors are essential for long-term potentiation of NMDA-EPSCs at hippocampal mossy fiber synapses. *Neuron* 57: 121–134, 2008.

Redgrave P, **Rodriguez M**, **Smith Y**, **Rodriguez-Oroz MC**, **Lehericy S**, **Bergman H**, **Agid Y**, **DeLong MR**, **Obeso JA**. Goal-directed and habitual control in the basal ganglia: implications for Parkinson's disease. *Nat Rev Neurosci* 11: 760–772, 2010.

Reiner A, **Medina L**, **Veenman CL**. Structural and functional evolution of the basal ganglia in vertebrates. *Brain Res Brain Res Rev* 28: 235–285, 1998.

Remple MS, **Bradenham CH**, **Kao CC**, **Charles PD**, **Neimat JS**, **Konrad PE**. Subthalamic nucleus neuronal firing rate increases with Parkinson's disease progression. *Mov Disord* 26: 1657–1662, 2011.

Roeper J, **Hainsworth AH**, **Ashcroft FM**. Tolbutamide reverses membrane hyperpolarisation induced by activation of D2 receptors and GABAB receptors in isolated substantia nigra neurones. *Pflugers Arch* 416: 473–475, 1990.

Röper J, **Ashcroft FM**. Metabolic inhibition and low internal ATP activate K-ATP channels in rat dopaminergic substantia nigra neurones. *Pflugers Arch* 430: 44–54, 1995.

Rosenmund C, **Feltz A**, **Westbrook GL**. Synaptic NMDA receptor channels have a low open probability. *J Neurosci* 15: 2788–2795, 1995.

Sah P, **Hestrin S**, **Nicoll RA**. Tonic activation of NMDA receptors by ambient glutamate enhances excitability of neurons. *Science* 246: 815–818, 1989.

Salter MW, **Dong Y**, **Kalia LV**, **Liu XJ**, **Pitcher G**. Regulation of NMDA Receptors by Kinases and Phosphatases [Online]. In: *Biology of the NMDA Receptor*, edited by Van Dongen AM. CRC Press/Taylor & Francis http://www.ncbi.nlm.nih.gov/books/NBK5288/.

Salussolia CL, **Prodromou ML**, **Borker P**, **Wollmuth LP**. Arrangement of subunits in functional NMDA receptors. *J Neurosci Off J Soc Neurosci* 31: 11295–11304, 2011.

Sandoval R, **González A**, **Caviedes A**, **Pancetti F**, **Smalla K-H**, **Kaehne T**, **Michea L**, **Gundelfinger ED**, **Wyneken U**. Homeostatic NMDA receptor down-regulation via brain derived neurotrophic factor and nitric oxide-dependent signalling in cortical but not in hippocampal neurons. *J Neurochem* 118: 760–772, 2011.

Sather W, **Dieudonné S**, **MacDonald JF**, **Ascher P**. Activation and desensitization of N-methyl-D-aspartate receptors in nucleated outside-out patches from mouse neurones. *J Physiol* 450: 643–672, 1992.

Sato H, **Arawaka S**, **Hara S**, **Fukushima S**, **Koga K**, **Koyama S**, **Kato T**. Authentically Phosphorylated α-Synuclein at Ser129 Accelerates Neurodegeneration in a Rat Model of Familial Parkinson's Disease. *J Neurosci* 31: 16884–16894, 2011.

Schneggenburger R. Simultaneous measurement of Ca2+ influx and reversal potentials in recombinant N-methyl-D-aspartate receptor channels. *Biophys J* 70: 2165–2174, 1996.

Schneggenburger R. Altered voltage dependence of fractional Ca2+ current in N-methyl-D-aspartate channel pore mutants with a decreased Ca2+ permeability. *Biophys J* 74: 1790–1794, 1998.

Schuhmacher L-N, **Husson Z**, **Smith ESJ**. The naked mole-rat as an animal model in biomedical research: current perspectives. *Open Access Anim. Physiol.* 2015.

Schwindt PC, **Spain WJ**, **Crill WE**. Effects of intracellular calcium chelation on voltage-dependent and calcium-dependent currents in cat neocortical neurons. *Neuroscience* 47: 571–578, 1992.

Scullin CS, **Tafoya LC**, **Wilson MC**, **Partridge LD**. Presynaptic residual calcium and synaptic facilitation at hippocampal synapses of mice with altered expression of SNAP-25. *Brain Res* 1431: 1–12, 2012.

Semerdjieva S, **Abdul-Razak HH**, **Salim SS**, **Yáñez-Muñoz RJ**, **Chen PE**, **Tarabykin V**, **Alifragis P**. Activation of EphA Receptors Mediates the Recruitment of the Adaptor Protein Slap, Contributing to the Downregulation of N-Methyl-d-Aspartate Receptors. *Mol Cell Biol* 33: 1442–1455, 2013.

Sheldon AL, **Robinson MB**. The Role of Glutamate Transporters in Neurodegenerative Diseases and Potential Opportunities for Intervention. *Neurochem Int* 51: 333–355, 2007.

Shen W, **Flajolet M**, **Greengard P**, **Surmeier DJ**. Dichotomous dopaminergic control of striatal synaptic plasticity. *Science* 321: 848–851, 2008.

Shimamoto K, **Lebrun B**, **Yasuda-Kamatani Y**, **Sakaitani M**, **Shigeri Y**, **Yumoto N**, **Nakajima T**. DL-threo-beta-benzyloxyaspartate, a potent blocker of excitatory amino acid transporters. *Mol Pharmacol* 53: 195–201, 1998.

Shulman JM, **De Jager PL**, **Feany MB**. Parkinson's disease: genetics and pathogenesis. *Annu Rev Pathol* 6: 193–222, 2011.

Siegler Retchless B, **Gao W**, **Johnson JW**. A single GluN2 subunit residue controls NMDA receptor channel properties via intersubunit interaction. *Nat Neurosci* 15: 406–413, S1-2, 2012.

Singh V, **Carman M**, **Roeper J**, **Bonci A**. Brief ischemia causes long-term depression in midbrain dopamine neurons. *Eur J Neurosci* 26: 1489–1499, 2007.

Sornarajah L, **Vasuta OC**, **Zhang L**, **Sutton C**, **Li B**, **El-Husseini A**, **Raymond LA**. NMDA receptor desensitization regulated by direct binding to PDZ1-2 domains of PSD-95. *J Neurophysiol* 99: 3052–3062, 2008.

Standaert DG, **Testa CM**, **Young AB**, **Penney JB**. Organization of N-methyl-D-aspartate glutamate receptor gene expression in the basal ganglia of the rat. *J Comp Neurol* 343: 1–16, 1994.

Steigerwald F, **Pötter M**, **Herzog J**, **Pinsker M**, **Kopper F**, **Mehdorn H**, **Deuschl G**, **Volkmann J**. Neuronal Activity of the Human Subthalamic Nucleus in the Parkinsonian and Nonparkinsonian State. *J Neurophysiol* 100: 2515–2524, 2008.

Stephenson-Jones M, **Ericsson J**, **Robertson B**, **Grillner S**. Evolution of the basal ganglia: dual-output pathways conserved throughout vertebrate phylogeny. *J Comp Neurol* 520: 2957–2973, 2012.

Stocca G, **Vicini S**. Increased contribution of NR2A subunit to synaptic NMDA receptors in developing rat cortical neurons. *J Physiol* 507 (Pt 1): 13–24, 1998.

Suárez F, **Zhao Q**, **Monaghan DT**, **Jane DE**, **Jones S**, **Gibb AJ**. Functional heterogeneity of NMDA receptors in rat substantia nigra pars compacta and reticulata neurones. *Eur J Neurosci* 32: 359–367, 2010.

Sugihara H, **Moriyoshi K**, **Ishii T**, **Masu M**, **Nakanishi S**. Structures and properties of seven isoforms of the NMDA receptor generated by alternative splicing. *Biochem Biophys Res Commun* 185: 826–832, 1992.

Sun H, **Feng Z**. Neuroprotective role of ATP-sensitive potassium channels in cerebral ischemia. *Acta Pharmacol Sin* 34: 24–32, 2013.

Surmeier DJ, **Guzman JN**, **Sanchez-Padilla J**. Calcium, cellular aging, and selective neuronal vulnerability in Parkinson's disease. *Cell Calcium* 47: 175–182, 2010.

Surmeier DJ, **Guzman JN**, **Sanchez-Padilla J**, **Schumacker PT**. The role of calcium and mitochondrial oxidant stress in the loss of substantia nigra pars compacta dopaminergic neurons in Parkinson's disease. *Neuroscience* 198: 221–231, 2011.

Surmeier DJ, **Mercer JN**, **Chan CS**. Autonomous pacemakers in the basal ganglia: who needs excitatory synapses anyway? *Curr Opin Neurobiol* 15: 312–318, 2005.

Surmeier DJ, **Obeso JA**, **Halliday GM**. Selective neuronal vulnerability in Parkinson disease. *Nat Rev Neurosci* 18: 101–113, 2017.

Swanger SA, **Vance KM**, **Pare J-F**, **Sotty F**, **Fog K**, **Smith Y**, **Traynelis SF**. NMDA Receptors Containing the GluN2D Subunit Control Neuronal Function in the Subthalamic Nucleus. *J Neurosci Off J Soc Neurosci* 35: 15971–15983, 2015.

Tajima N, **Karakas E**, **Grant T**, **Simorowski N**, **Diaz-Avalos R**, **Grigorieff N**, **Furukawa H**. Activation of NMDA receptors and the mechanism of inhibition by ifenprodil. *Nature* 534: 63–68, 2016.

Takei K, **Mundigl O**, **Daniell L**, **Camilli PD**. The synaptic vesicle cycle: a single vesicle budding step involving clathrin and dynamin. *J Cell Biol* 133: 1237–1250, 1996.

Takumi Y, **Ramírez-León V**, **Laake P**, **Rinvik E**, **Ottersen OP**. Different modes of expression of AMPA and NMDA receptors in hippocampal synapses. *Nat Neurosci* 2: 618–624, 1999.

Tasca CI, **Dal-Cim T**, **Cimarosti H**. In vitro oxygen-glucose deprivation to study ischemic cell death. *Methods Mol Biol Clifton NJ* 1254: 197–210, 2015.

Tepper JM, **Damlama M**, **Trent F**. Postnatal changes in the distribution and morphology of rat substantia nigra dopaminergic neurons. *Neuroscience* 60: 469–477, 1994.

Tingley WG, **Ehlers MD**, **Kameyama K**, **Doherty C**, **Ptak JB**, **Riley CT**, **Huganir RL**. Characterisation of protein kinase A and protein kinase C phosphorylation of the N-methyl-D-aspartate receptor NR1 subunit using phosphorylation site-specific antibodies. *J Biol Chem* 272: 5157–5166, 1997.

Tomitori H, **Suganami A**, **Saiki R**, **Mizuno S**, **Yoshizawa Y**, **Masuko T**, **Tamura Y**, **Nishimura K**, **Toida T**, **Williams K**, **Kashiwagi K**, **Igarashi K**. Structural changes of regulatory domain heterodimer of N-methyl-D-aspartate receptor subunits GluN1 and GluN2B through the binding of spermine and ifenprodil. *J Pharmacol Exp Ther* 343: 82–90, 2012.

Tong ZY, **Overton PG**, **Clark D**. Antagonism of NMDA receptors but not AMPA/kainate receptors blocks bursting in dopaminergic neurons induced by electrical stimulation of the prefrontal cortex. *J Neural Transm Vienna Austria 1996* 103: 889–904, 1996.

Tovar KR, **Westbrook GL**. The incorporation of NMDA receptors with a distinct subunit composition at nascent hippocampal synapses in vitro. *J Neurosci Off J Soc Neurosci* 19: 4180–4188, 1999.

Traynelis SF, **Wollmuth LP**, **McBain CJ**, **Menniti FS**, **Vance KM**, **Ogden KK**, **Hansen KB**, **Yuan H**, **Myers SJ**, **Dingledine R**. Glutamate receptor ion channels: structure, regulation, and function. *Pharmacol Rev* 62: 405–496, 2010.

Tremblay M-È, **Stevens B**, **Sierra A**, **Wake H**, **Bessis A**, **Nimmerjahn A**. The Role of Microglia in the Healthy Brain. *J Neurosci* 31: 16064–16069, 2011.

Vance KM, **Simorowski N**, **Traynelis SF**, **Furukawa H**. Ligand-specific deactivation time course of GluN1/GluN2D NMDA receptors. *Nat Commun* 2: 294, 2011.

Villarroel A, **Regalado MP**, **Lerma J**. Glycine-independent NMDA receptor desensitization: localization of structural determinants. *Neuron* 20: 329–339, 1998.

Wang L, **Kitai ST**, **Xiang Z**. Modulation of excitatory synaptic transmission by endogenous glutamate acting on presynaptic group II mGluRs in rat substantia nigra compacta. *J Neurosci Res* 82: 778–787, 2005.

Watabe-Uchida M, **Zhu L**, **Ogawa SK**, **Vamanrao A**, **Uchida N**. Whole-Brain Mapping of Direct Inputs to Midbrain Dopamine Neurons. *Neuron* 74: 858–873, 2012.

Watanabe M, **Inoue Y**, **Sakimura K**, **Mishina M**. Developmental changes in distribution of NMDA receptor channel subunit mRNAs. *NeuroReport* 3: 1138–1140, 1992.

Watanabe M, **Inoue Y**, **Sakimura K**, **Mishina M**. Distinct distributions of five N-methyl-D-aspartate receptor channel subunit mRNAs in the forebrain. *J Comp Neurol* 338: 377–390, 1993.

Watanabe M, **Mishina M**, **Inoue Y**. Distinct distributions of five NMDA receptor channel subunit mRNAs in the brainstem. *J Comp Neurol* 343: 520–531, 1994.

Wenzel A, **Fritschy JM**, **Mohler H**, **Benke D**. NMDA receptor heterogeneity during postnatal development of the rat brain: differential expression of the NR2A, NR2B, and NR2C subunit proteins. *J Neurochem* 68: 469–478, 1997.

Wenzel A, **Scheurer L**, **Künzi R**, **Fritschy JM**, **Mohler H**, **Benke D**. Distribution of NMDA receptor subunit proteins NR2A, 2B, 2C and 2D in rat brain. *Neuroreport* 7: 45–48, 1995.

Wild AR, **Akyol E**, **Brothwell SLC**, **Kimkool P**, **Skepper JN**, **Gibb AJ**, **Jones S**. Memantine block depends on agonist presentation at the NMDA receptor in substantia nigra pars compacta dopamine neurones. *Neuropharmacology* 73: 138–146, 2013.

Wild AR, **Bollands M**, **Morris PG**, **Jones S**. Mechanisms regulating spill-over of synaptic glutamate to extrasynaptic NMDA receptors in mouse substantia nigra dopaminergic neurons. *Eur J Neurosci* 42: 2633–2643, 2015.

Wild AR, **Jones S**, **Gibb AJ**. Activity-dependent regulation of NMDA receptors in substantia nigra dopaminergic neurones. *J Physiol* 592: 653–668, 2014.

Wilson CJ, **Young SJ**, **Groves PM**. Statistical properties of neuronal spike trains in the substantia nigra: Cell types and their interactions. *Brain Res* 136: 243–260, 1977.

Wollmuth LP, **Kuner T**, **Sakmann B**. Intracellular Mg2+ interacts with structural determinants of the narrow constriction contributed by the NR1-subunit in the NMDA receptor channel. *J Physiol* 506 (Pt 1): 33–52, 1998a.

Wollmuth LP, **Kuner T**, **Sakmann B**. Adjacent asparagines in the NR2-subunit of the NMDA receptor channel control the voltage-dependent block by extracellular Mg2+. *J Physiol* 506: 13–32, 1998b.

Wu G, **Malinow R**, **Cline HT**. Maturation of a central glutamatergic synapse. *Science* 274: 972–976, 1996.

Wyllie DJ, **Béhé P**, **Colquhoun D**. Single-channel activations and concentration jumps: comparison of recombinant NR1a/NR2A and NR1a/NR2D NMDA receptors. *J Physiol* 510 (Pt 1): 1–18, 1998.

Wyllie DJ, **Béhé P**, **Nassar M**, **Schoepfer R**, **Colquhoun D**. Single-channel currents from recombinant NMDA NR1a/NR2D receptors expressed in Xenopus oocytes. *Proc Biol Sci* 263: 1079–1086, 1996.

Wyllie DJA, **Livesey MR**, **Hardingham GE**. Influence of GluN2 subunit identity on NMDA receptor function. *Neuropharmacology* 74: 4–17, 2013.

Yamamoto H, **Kamegaya E**, **Hagino Y**, **Takamatsu Y**, **Sawada W**, **Matsuzawa M**, **Ide S**, **Yamamoto T**, **Mishina M**, **Ikeda K**. Loss of GluN2D subunit results in social recognition deficit, social stress, 5-HT2C receptor dysfunction, and anhedonia in mice. *Neuropharmacology* 112: 188–197, 2017.

Yi Z, **Petralia RS**, **Fu Z**, **Swanwick CC**, **Wang Y-X**, **Prybylowski K**, **Sans N**, **Vicini S**, **Wenthold RJ**. The role of the PDZ protein GIPC in regulating NMDA receptor trafficking. *J Neurosci Off J Soc Neurosci* 27: 11663–11675, 2007.

Yuan H, **Hansen KB**, **Vance KM**, **Ogden KK**, **Traynelis SF**. Control of N-methyl-D-aspartate Receptor Function by the NR2 Subunit Amino-Terminal Domain. *J Neurosci Off J Soc Neurosci* 29: 12045–12058, 2009.

Zhang J, **Diamond JS**. Distinct perisynaptic and synaptic localization of NMDA and AMPA receptors on ganglion cells in rat retina. *J Comp Neurol* 498: 810–820, 2006.

Zheng F, **Erreger K**, **Low CM**, **Banke T**, **Lee CJ**, **Conn PJ**, **Traynelis SF**. Allosteric interaction between the amino terminal domain and the ligand binding domain of NR2A. *Nat Neurosci* 4: 894–901, 2001.

Zhou X, **Hollern D**, **Liao J**, **Andrechek E**, **Wang H**. NMDA receptor-mediated excitotoxicity depends on the coactivation of synaptic and extrasynaptic receptors. *Cell Death Dis* 4: e560, 2013.

Zilberter Y, **Uteshev V**, **Sokolova S**, **Khodorov B**. Desensitization of N-methyl-D-aspartate receptors in neurons dissociated from adult rat hippocampus. *Mol Pharmacol* 40: 337–341, 1991.

Zorumski CF, **Thio LL**, **Clark GD**, **Clifford DB**. Blockade of desensitization augments quisqualate excitotoxicity in hippocampal neurons. *Neuron* 5: 61–66, 1990.